UNIVERSIDAD DE CHILE

FACULTAD DE CIENCIAS FÍSICAS Y MATEMÁTICAS

DEPARTAMENTO DE INGENIERÍA DE MINAS

STUDY OF THE GRAVITY FLOW MECHANISMS AT GOLDEX BY MEANS OF A PHYSICAL MODEL

TESIS PARA OPTAR AL GRADO DE MAGISTER EN MINERIA.

MEMORIA PARA OPTAR AL TÍTULO DE INGENIERO CIVIL DE MINAS

MONTSERRAT FERNANDA PINEDA TAPIA

PROFESOR GUÍA:
RAÚL CASTRO RUIZ

MIEMBROS DE LA COMISIÓN:
JAVIER VALLEJOS MASSA
MATTHEW PIERCE
ALDO TAMBURRINO TAVANTZIS

SANTIAGO DE CHILE

DICIEMBRE DE 2012

RESUMEN EJECUTIVO

Por más de un siglo se ha llevado a cabo investigación referente al campo del flujo gravitacional a través de variadas herramientas. De hecho, casi todas las minas operadas por métodos basados en hundimiento o explotadas por métodos fundamentados en flujo gravitacional han sido objeto de diversas experiencias de modelamiento con modelos numéricos, modelos físicos y pruebas a escala mina, las que han llevado a lograr un importante avance en el entendimiento de los principales mecanismos que gobiernan el flujo gravitacional. En este contexto, los modelos físicos se presentan como una herramienta de ingeniería que tiene la ventaja de ser el enfoque de menor costo, evitando las dificultades propias de la experimentación a escala mina – como las complicaciones de obtener mediciones in-situ- siendo además de larga data y muy costosas. Sin embargo, con el fin de validar los modelos físicos, es fundamental desarrollar una metodología apropiada teniendo en cuenta los efectos de escala y las limitaciones propias derivadas de estos modelos.

Este trabajo de tesis, tiene como propósito establecer una metodología para el estudio del flujo gravitacional para un caso en particular, la Mina Goldex (Agnico –Eagle, Canadá). El caserón Primario Este, en Goldex, presenta un novedoso método de explotación: el mineral es perforado y tronado como en un SLS pero el nivel de producción corresponde al de una operación de hundimiento por bloques. La mayor preocupación radica en el hecho de que el Nivel de Producción es menor que la proyección vertical del cuerpo mineralizado, generando interrogantes acerca de la movilidad del material ubicado en la pared yacente del caserón. El principal objetivo de esta investigación, es por lo tanto, el estudio de los mecanismos que conducen el flujo gravitacional para el Caserón Primario Este, con el fin de apoyar el diseño ingenieril y para ser utilizado como herramienta para la estimación de reservas y para la estimación de la entrada de la dilución.

Los experimentos se realizan en un modelo axisimétrico a escala 1:200. En una primera etapa se desarrolla un test de prueba de IMZ (zona de movimiento aislado) a modo de determinar la geometría de la zona de movimiento. El segundo experimento consiste en determinar la potencial falla del mineral localizado en la pared yacente, mediante una extracción de múltiples puntos. Dado que el mineral situado fuera de la proyección vertical del nivel de producción no se moviliza, es propuesto un nuevo nivel de extracción. El modelo físico se modifica con este nuevo nivel (Nivel 76) y se realizan experimentos mediante la extracción de ambos niveles de producción. Finalmente se conduce un experimento simulando la continua entrada de dilución desde el techo del caserón; el objetivo es determinar los mecanismos de entrada de dilución, así como la recuperación minera y los principales mecanismos que rigen la entrada de la dilución para un hipotético caso inestable.

En una etapa final, y utilizando el conocimiento adquirido a partir de los resultados experimentales se lleva a cabo modelación numérica de los experimentos utilizando REBOPv3.1. Los modelos numéricos y los resultados físicos sólo pueden compararse cuando el mecanismo de flujo por gravedad es identificado, con el fin de calibrar adecuadamente el software. Una vez que REBOP que ha sido calibrado, hay evidencia de que las simulaciones del software presentan una buena concordancia con los resultados experimentales para los casos estables, sin embargo, para los casos inestables cuando el mecanismo que rige la entrada de la dilución es el movimiento lateral de la roca quebrada, REBOP no es capaz de reproducir los mecanismos y por lo tanto la entrada de dilución a nivel cuantitativo.

ABSTRACT

For over a century research has been conducted regarding to the gravity flow field through different tools. In fact, nearly all mines operated by caving or exploited by a mining method based on the gravity flow phenomena have been subject of several modeling experiences with numerical models, physical models and mine scale tests, which have led to remarkable progress in understanding the principal mechanisms governing the phenomena. In this context, physical models are presented as an engineering tool presenting the advantage of being the lowest cost approach, avoiding the difficulties from full scale trials such as complications associated with obtaining in situ measurements, being at the same time very time consuming and expensive. However, in order to validate physical modeling is fundamental to develope an appropriate methodology considering the scale effects and the limitations derived from these models.

This thesis work aims to set a methodology of study for gravity flow for a specific case of study, Goldex Mine. The Eastern Primary Stope at Goldex Mine presents a novel extraction method: the ore is blasted as in a SLS but the production level layout corresponds to a Block Caving operation. The major concern lies in the fact that the footprint is smaller than the projection of the ore body, generating questions regarding to the mobility of the ore located at the footwall of the stope. The main objective of this research is therefore, to study the draw mechanisms that would drive the gravity flow for the Eastern Primary Stope, to support the engineering design and to be used for the estimation of ore recovery and dilution entry.

The experiments are conducted in an axysimetrical model at a defined scale (1:200). In a first stage an IMZ (Isolated Movement Zone) test is conducted to determine the geometry of the movement zone. The second experiment consists in a uniform multiple drawpoint extraction to determine the potential failure of the broken rock located at the footwall of the stope. Since the ore located outside the projection of the production level the material did not fail, a new extraction level is proposed, based on the IMZ test results. The physical model is modified and the experiment is conducted to quantify primary ore recovery when drawing from level 76 and from the proposed new level 73.Finally is performed an experiment simulating dilution entry from the top of the stope. The aim is to quantify potential dilution entry mechanism and ore recovery, as well as the governing mechanism for dilution entry for an unstable case. For the unstable case, the addition of the new level increases ore recovery in a 14%.

In a final stage, and using the knowledge gained from the experimental results is conducted numerical modeling using REBOP v3.1. Numerical models and physical results can only be compared when the gravity flow mechanism are identified in order to calibrate properly the software. Once REBOP it's been calibrated, the numerical software simulations presents a good match with the experimental results for the stable cases, nevertheless for the unstable cases when the mechanism governing flow is the lateral movement of the broken rock , REBOP is not able to reproduce the mechanisms and therefore dilution entry.

AGRADECIMIENTOS

Más allá de los éxitos o los fracasos, a la batalla de mi madre por criarme.

A mis amigos y familia, a quienes les manifiesto recíproco amor y lealtad inquebrantables.

Al tiempo, perseguidor y hostil.

No cabe poder gozar sin poder sufrir, y la facultad de goce es la misma que la del dolor. El que no sufre tampoco goza, como no siente calor el que no siente frío.

Miguel de Unamuno.

Del sentimiento trágico de la vida.

TABLE OF CONTENTS

LIST OF FIGURES

LIST OF TABLES

TERMS AND ABREVIATIONS

h_W	Lifshitz- Van der Waals constant
Bo_G	Bond number
D_{TA}	Isolated Draw Diameter
F_{B_C}	Bond Number for the Electrostatic Force
F_{B_H}	Bond Number for the Van der Waals Force
F_{B_M}	Bond Number for the Magnetic Force
F_{B_VdW}	Bond Number for the Van der Waals Force
F_G	Gravity force
F_H	Capillarity
F_M	Magnetic Force
F_{VdW}	Van de Waals force
F_c	Electrostatic force
P_A	Thrust on the wedge for the passive case
P_P	Thrust on the wedge for the active case
d_P	Particle diameter
δ_0	Distance between molecules
ε_0	Permittivity of vacuum
$\lambda_{tan(\phi)}$	Friction angle scale factor
λ_L	Geometrical scale factor
λ_T	Time scale factor
λ_V	Velocity scale Factor
ρ_P	Density of the particle
c	Cohesion
IEZ	Isolated Extraction Zone
IMZ	Isolated Movement Zone
N	Normal stress in failure plane
S	Shear stress in the failure plane
γ	Surface tension
δ	Friction angle between the broken rock and the stope walls
φ	Angle of flow at the base of the IMZ.
ϕ	Friction angle

CHAPTER 1

INTRODUCTION

This chapter describes the background and the motivation for the development of the research. It also includes the antecedents for the case of study, Goldex Mine of the Agnico-Eagle Mines Limited.

The introduction in addition presents the main objectives, the justification of the research, the methodology to be conducted and the thesis outline.

1.1. Background

Gravity flow is the process by which a granular material moves from its initial position due to gravity (Castro, 2006) , the phenomenon as the mechanism ruling flow will have a large impact on ore recovery and the final content of dilution.

The economic impact and the importance of the phenomenon of gravity flow itself justifies this research. In fact, nearly all mines operated by caving or exploited by a mining method based on the gravity flow phenomena have been subject of several modeling experiences using numerical models, physical models and mine scale tests; these have led to remarkable progress in understanding the phenomenon.

In this context lies Goldex Mine; Goldex is part of the chain of operations and properties that Agnico-Eagle owns .The Goldex Mine is a gold mine located 4 km west of the town of Val-d'Or in the Abitibi region of northwest Quebec.

The mining method is called "Primary/Secondary Long Hole Blasting". The orebody is divided in 3 stopes each consisting of sublevels about 80m apart. Each sublevel is drilled and blasted in a sequence where the stopes located at the extremes are blasted first and a central stope is mined at a later stage (Hudyma *et* al., 2010). The mining method combines the effectiveness of a Sublevel Stoping mine with the high production rates of a Block Caving operation. This method achieves approximately the same rate of production as the estimated maximum rate for the block caving method but with drilling and blasting of long production holes.

Goldex Mine commercial production was achieved in 2008. In 2011 Goldex Mine operation processed about 8,000 tonnes of ore per day and was on track to produce about 184,000 ounces of gold. However, production was suspended in October 2011 due to a water inflow and ground stability issue. The situation is being investigated and remediation is taking place at the time (Agnico-Eagle Mines Limited, 2011).

At the request of the Agnico-Eagle Mines Limited Goldex Project management, in March of 2011 it was asked to provide physical modeling in order to understand the flow

mechanism governing muck flow at the Eastern Primary Stope to improve ore recovery and minimize dilution. Since the footprint is slimmer than the ore body to be extracted, there's no notion of the predominant phenomena ruling the flow and the mixing profile due to extraction for an important mineral zone, compromising about the 40% of ore reserves with high economic interest.

1.2. Research Objectives

The main objective of this research is to study the draw mechanisms that govern the gravity flow for blasted rock at the Eastern Primary Stope –at Goldex Mine- by means of a physical model, to support the engineering design and to be used for estimating ore recovery and potential dilution entry.

The knowledge gained from the experimental study of the physical model will be used as validation tool for numerical modeling.

The main tasks to be developed to achieve the objectives previously mentioned are:

- By means of a limit equilibrium approach analyze the mobility of the ore reserves located at the footwall of the Eastern Primary Stope for Goldex Mine, in order to identify the critical section to be modeled.
- Design and build an axisymmetric physical model (scale 1:200) for a critical section of the Eastern Primary Stope considering the current mine conditions. Geometric conditions and the preponderant forces dominating the gravity flow will be scaled in the model.
- Test the scaled prototype with the purpose of understanding the draw mechanisms of gravity flow for broken rock in Goldex such as rilling or lateral flow.
- In the physical model simulate different draw scenarios and designs at a defined scale (1:200) with the purpose of establishing the failure mechanism of the footwall for the Eastern primary stope using a multiple drawpoint extraction.
- Improve knowledge of similitude analysis and the scalability for physical models, in order to validate them as a design tool for engineering support and to use them for validating numerical simulations of gravity flow.
- Perform numerical modeling of the blasted rock in order to establish a match with the experimental results from physical modeling.

1.3. Scope of the research

The development of this research aims to replicate in the most appropriate possible form, the gravity flow of a two-dimensional section at Goldex Mine.

The scope of this investigation is therefore define from the use of a physical model of reduced scale (1:200) the mechanism of failure and potential ore recovery for the Eastern Primary Stope at Goldex Mine (Agnico Eagle, Quebec, Canada) using different draw scenarios and designs strategies.

It is not possible under the experimental conditions replicate all the dynamics that occur inside a stope of these conditions, in particular the stress conditions and the secondary fragmentation while the material is flowing.

Therefore, in order to reproduce the gravity flow phenomena in the most accurate way, only the preponderant forces will be replicated in the model.

1.4. Research Justification

Even though the great amount of mining operations that are currently operated by caving methods, the knowledge of the governing mechanisms of gravity flow and dilution entry are quite limited, despite the large impact on ore recovery.

The gravity flow has been studied through a variety of tools over time, such as physical modeling, numerical modeling and empirical observation at mine scale, with the purpose to understand the main mechanisms governing the phenomena. However, the incorporation of the knowledge gained from these physical models as a design tool for extraction layouts, using computer models and simulations, is an unfinished task, due to the lack of validation of these numerical tools.

The development of physical models using gravel has been considered by some authors as the most suitable way for studying the flow of coarse granular material (Peters, 1984 and Power, 2003), however it also has been stated that sand (Susaeta, 2004) can be utilized to represent the behaviour of fines fragmentation as the case of study. In this context various physical models have been built with the aim of studying and comprehending the mechanisms of gravity flow. Castro (2010) , investigated through a scale model of 3.3 m x 2.4 m and height 3.4 conducting several experiments in order to understand the isolated gravity flow, interactive gravity flow and the fines migration phenomena in caved rock. To date this has been one of the most completes research's developed, since beside the scope of the results it was used as a validation tool for the calibration of numerical models (REBOP).

Based on physical modeling and with the aim to validate a numerical tool as a design and planning tool, it will be developed this research with the aim to link both methodologies, developing a guide to estimate ore recovery and dilution entry mechanism for a particular case, using these results as a validation tool for future numerical simulations.

The case of study to be used is the Eastern Primary Stope at Goldex Mine, which presents a novel extraction method named *Primary/Secondary Long Hole Blasting with 3 Stopes*. The ore is blasted as in a SLS but the production level layout corresponds to a Block Caving. The principal concerns lies in the fact that the footprint is slimmer than the projection of the ore body, generating concerns regarding the mobility of the ore located at the footwall of the stope.

1.5. Research Methodology

The proposed methodology is intended to achieve the general and specific objectives of the research. The following stages are proposed to accomplish the abovementioned objectives:

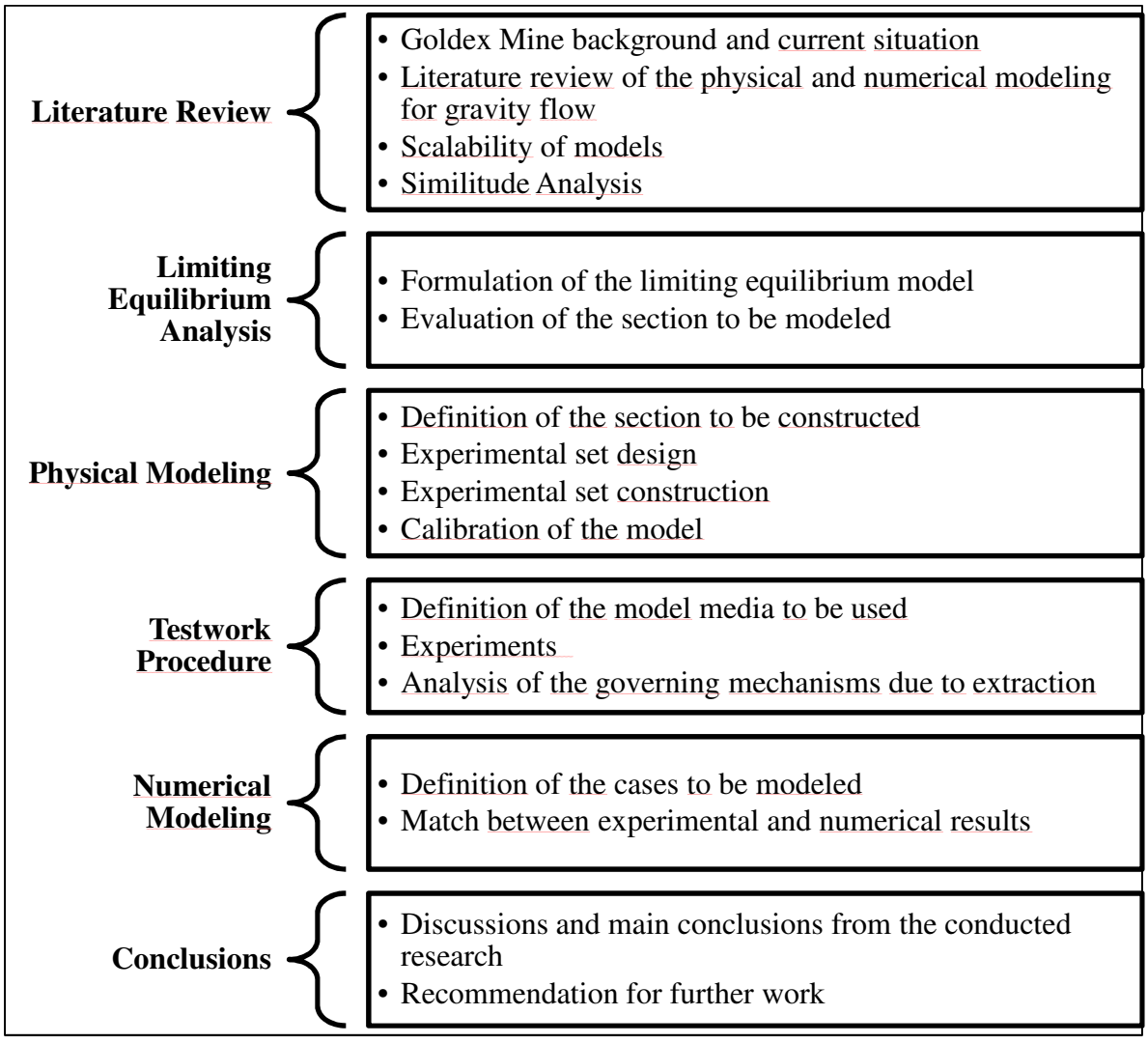

1.6. Thesis Outline

The results of this research are discussed in the following chapters:

Chapter 1: Contains the introduction of the thesis topic, the background, the justification of the research and the thesis outline

Chapter 2: Contains a review of the current situation at Goldex Mine, in order to understand the problem to be solved as the antecedents from previous work and research conducted regarding to the case of study.

Chapter 3: Contains and describes a review of the state of the art for physical modeling in caving operations as the dominant forces affecting flow.

Chapter 4: Contains and describes the basis and formulation of limit equilibrium analyses for the different sections of the Eastern Primary Stope in order to conduct the experiments in a critical section, able to represent the problem to be solved.

Chapter 5: Contains the experimental methodology for the development of the physical modeling, based on a limiting equilibrium analysis, a similitude analysis and the experimental set up to be used.

Chapter 6: Contains the results and analysis of each experiment conducted in the physical model. It includes the results of an Isolated Draw Zone test, as the results from the experiments carried out performing the extraction from multiple drawpoints in the axysimmetrical model for different drawing and design strategies evaluated. It is analyzed and discussed the effects on ore recovery of the different flow mechanisms observed and the dilution entry mechanism for a hypothetical unstable case.

Chapter 7: Contains the results of the numerical modeling for gravity flow carried out in REBOP, and the main discussions and analysis of the match between experimental and numerical analysis.

Chapter 8: Contains the main conclusions and recommendations of the study.

Chapter 9: Contains the references used in order to contextualize and enhance the knowledge derived from the research.

CHAPTER 2

BACKGROUND AT GOLDEX MINE

This chapter describes the background and the information for the current conditions at Goldex Mine. It includes a description of the main antecedents of the regional geology, geotechnical issues, the exploitation method, ventilation system and the monitoring system.

The chapter also introduces a description of the problem to be investigated in this thesis work as some antecedents from previous work related to the case of study.

2.1. Agnico Eagle Limited

As declared by the company "*Agnico-Eagle is a long established, Canadian headquartered, gold producer with operations located in Canada, Finland and Mexico, and exploration and development activities in Canada, Finland, Mexico and the United States"*[1]. The operations owned and operated by Agnico-Eagle at the time are LaRonde, Goldex, Lapa and Meadowbank in Canada, Kittila in Finland and Pinos Altos in Mexico.

2.2. Goldex Division

2.2.1. Location

Goldex is located within the limits of the municipality of Val d'Or in the Province of Quebec, Canada[2] .The Goldex mine site is located on the south side of Highway 117 near the Thompson River (see Figure 2.1), approximately 4 km west from Val d'Or's downtown core. [3]

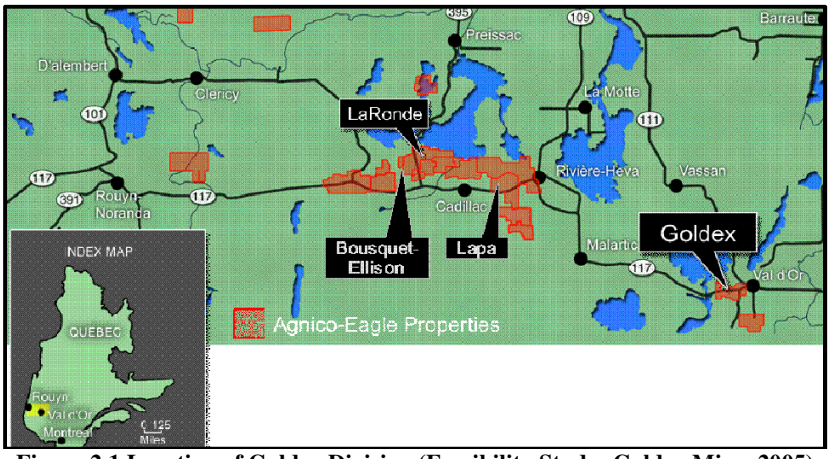

Figure 2.1.Location of Goldex Division (Feasibility Study- Goldex Mine, 2005)

[1] http://www.agnico-eagle.com/
[2] Cited in *Monitoring Open Stope Caving at Goldex Mine* (Hudyma, *et al.*,2010)
[3] Cited in *Feasibility Study- Goldex Mine, 2005, Agnico-Eagle Mines ltd.*

2.2.2. Goldex Geology

Goldex Mine is part the south-eastern portion of the Val d'Or area at the Abitibi Subprovince, a typical granite-greenstone terrane and part of the Superior Province of the Canadian Shield [4].The Abitibi belt is the largest greenstone belt in the world (85,000 km2; Card, 1990) and also one of the richest mining areas[5].

The main geological groups in the Val d'Or area include: the Piché Group, the Cadillac Group, the Malartic Group (or "Malartic Composite Block" described by Desrochers *et al*., 1996; Desrochers and Hubert, 1996), and the Louvicourt Group (the Héva and Val-d'Or formations)[6]. The regional geology is presented in Figure 2.2.

As specified by Frenette (2010):

> *The Goldex deposit is hosted within a quartz diorite sill located in a package of mafic to ultramafic volcanic rocks. The geology is oriented generally N280 and dips 75-85 degrees to the North. The major geological domains are granodiorite, basalt (mafic), mylonite, komatiite (ultramafic) and diabase dykes. The granodiorite hosts the quartz-tourmaline gold bearing veins. The basalt is located both on the north and south of the granodiorite; mylonite and komatiite shears are also located both north and south of the granodiorite and small diabase dykes cut the orebody at an almost perpendicular angle.*

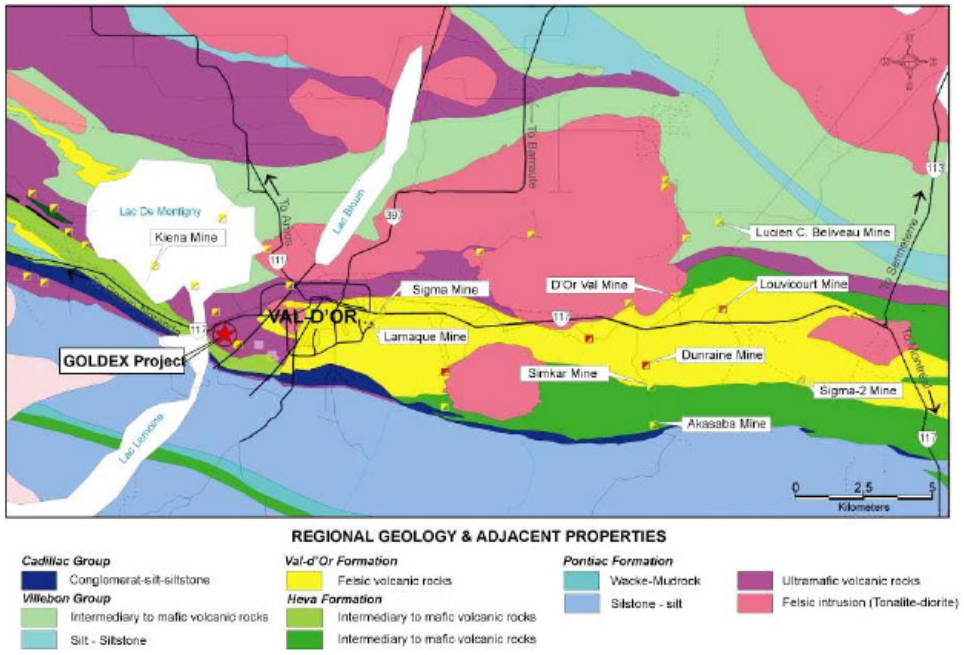

Figure 2.2. Regional geology map with the location of the Val d'Or area (Feasibility Study- Goldex Mine, 2005)

[4]Cited *in Monitoring Open Stope Caving at Goldex Mine* (Hudyma, et al.,2010).
[5] Hodgson and Hamilton, 1989; Poulsen *et al*., 1992, cited in *Feasibility Study- Goldex Mine, 2005, Agnico-Eagle Mines ltd.*
[6]Cited in *Feasibility Study- Goldex Mine, 2005, Agnico-Eagle Mines ltd.*

The Goldex deposit consists of six main mineralized zones: the West Zone, the GEZ (Goldex Extension Zone), the E Zone just east of the GEZ, the S Zone (GEZ Superior), the D Zone (Deep Zone) below the GEZ and the M Zone (Main Zone).The GEZ accounted for 80% of the total reserve tonnage mineral reserves and resources; the M and E zones held the other 20% (in the December 31, 2010).Since the GEZ was perceived as the zone with the highest economic interest, it was chosen to focus a resource estimation analysis and a feasibility study conducted at 2005. It was in this same year when Agnico Eagle decided to put into production the deposit by the implementation of a new extraction method, starting commercial production in August 2008.

The Goldex Extension Zone extends from 480 m to 790 m below surface and it's located in the centre of the quartz diorite sill. The main mineralized zones of the Goldex deposit (GEZ, E Zone, S Zone, D Zone and the M Zone) can be seen in Figure 2.3.

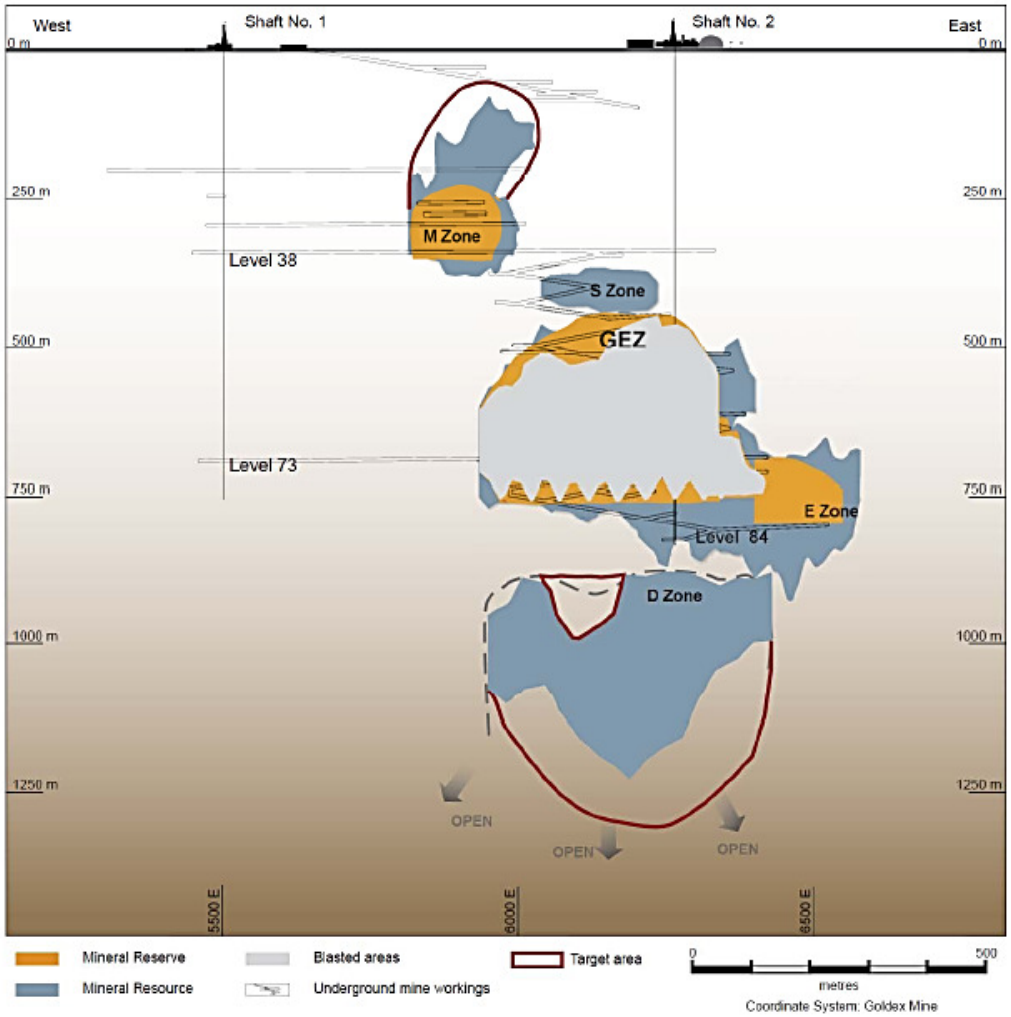

Figure 2.3. Longitudinal view looking north-northeast showing the GEZ, M, E, D and S zones (Goldex Mine Technical Report, 2011)

2.2.3. Resources Estimation

The Goldex project was the object of many exploration programs and resource estimations before it was put into commercial production; exploration phase started at the 1960s and were conducted through several decades until finally the Goldex deposit became a mine in 2005, achieving production in 2008.

Mineral reserves were first estimated at the Goldex project in 2004, and remained part of the mineral inventory until mining was suspended in October 2011, at which time the existing mineral reserves were reclassified as mineral resources. At December 31, 2010, the Goldex mine had proven and probable gold reserves of 27.8 million tonnes grading 1.75 g/t gold (containing 1.6 million ounces of gold).

When mining was suspended in October of 2011, the former ore reserves were downgraded to resources, deducting the ore that had already been processed in 2011 (2.4 million tonnes at a grade of 1.79 g/t gold).

Table 2.1. Resources estimation at December of 2010(Source: Goldex Mine Technical Report, 2011)

Category	Tonnes [Mton]	Gold grade [g/ton]	Gold [Oz]
Proven Reserves	14.8	1.87	890
Probable Reserves	12.99	1.62	676
Total proven plus probable reserves	27.79	1.75	1566
Indicated resources	8.28	1.77	472
Inferred resources	25.81	1.67	1,382

2.2.4. Rock Mechanics

The stress model – that includes stress ratios, orientations and gradients- used for the Goldex assumed that the maximum principal stress σ_1 is sub-horizontal and oriented perpendicular to the orebody (North-South), with a magnitude of 1.9 times the vertical stress (Arjang, 1996)[7].The intermediate principal stress σ_2 is also sub-horizontal, but oriented parallel to the orebody (East-West) with a magnitude of 1.3 times the vertical stress. This is consistent with normal conditions in the Abitibi Region of northwest Quebec.

The ore body (GEZ) extends from 480 m to 790 m below surface with a rock density of 2,7 [ton/m^3]. Therefore, the vertical stress σ_V at the current production level (760m below surface) is 20,72 [MPa]. The values of the principal stresses σ_1, σ_2 and σ_3 are presented in Table 2.2.

[7] Cited in *Feasibility Study- Goldex Mine, 2005, Agnico-Eagle Mines ltd.*

Table 2.2. Principal stresses characterization.

Stress	Value [MPa]
σ_1	39 .4
σ_2	26.9
σ_3	26.9

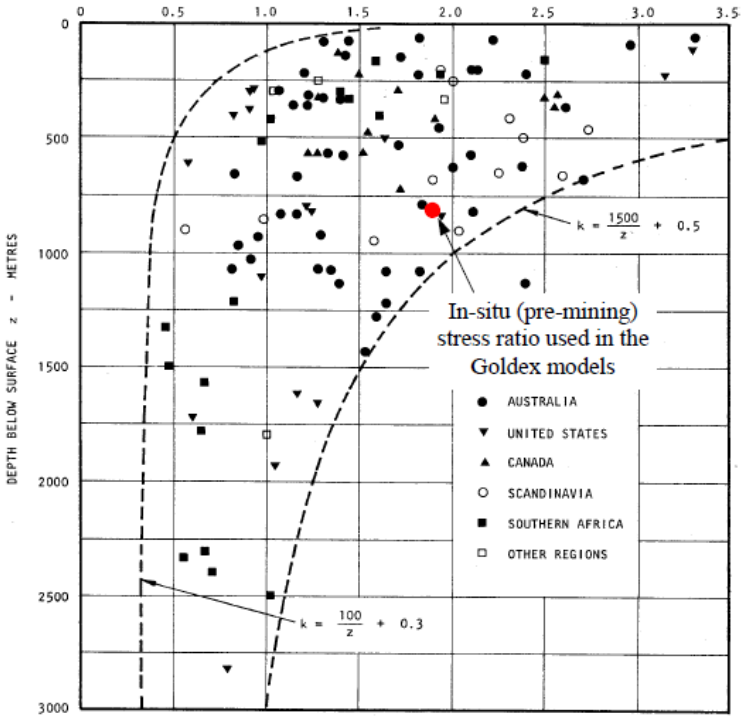

Figure 2.4. Variation of average horizontal-to-vertical stress ratio as function of depth below surface. (Hoek & Brown, 1992)

The rock mass properties can be summarized as shown in Table 2.3.

Table 2.3. Rock mass properties

Index	Unit	Granodiorite mineralized	Granodiorite not mineralized	Milonite
RQD	[%]	50 – 90	75 – 95	20 – 50
UCS	[MPa]	105	154	76
Q'		6.7	5.3	5.5

2.3. Mining

2.3.1. Mining Method

For the selection of the mining method, several mining approaches were modeled including block caving and open stoping methods, but none of them was completely adaptable for the Goldex orebody. Given the low grades of the deposit, block caving mining method was investigated for its low operating cost; however the method was not able to me implemented for three major reasons:

- The ore body size and geometry is at the minimum size limit for the method. The Goldex block cave modeling conducted at the feasibility study concluded that the west sector would not produce a sufficient hydraulic radius or stress to allow the cave to self-propagate and would need blasting assistance.
- The low grade of the orebody and the potential dilution entry could result in an uneconomical situation after the extraction of approximately 70% of the ore envelope.
- The inherent fragmentation could result in major hang-up problems in the drawpoints and consequently would reduce production rates.

Hudyma, *et al*.(2010) described, *"the selected mining method is called Primary/Secondary Long Hole Blasting. The orebody is divided in 3 stopes each consisting of sublevels about 80m apart (see Figure 2.5). Each sublevel is drilled and blasted in a sequence where the extremity stopes are blasted first and a central stope is mined at a later stage*". For stability issues, in the first stages only the swell of the blasted ore is extracted, providing support to the walls. Once the orebody is completely blasted, the ore is removed from the production level using LHD's of high capacity.

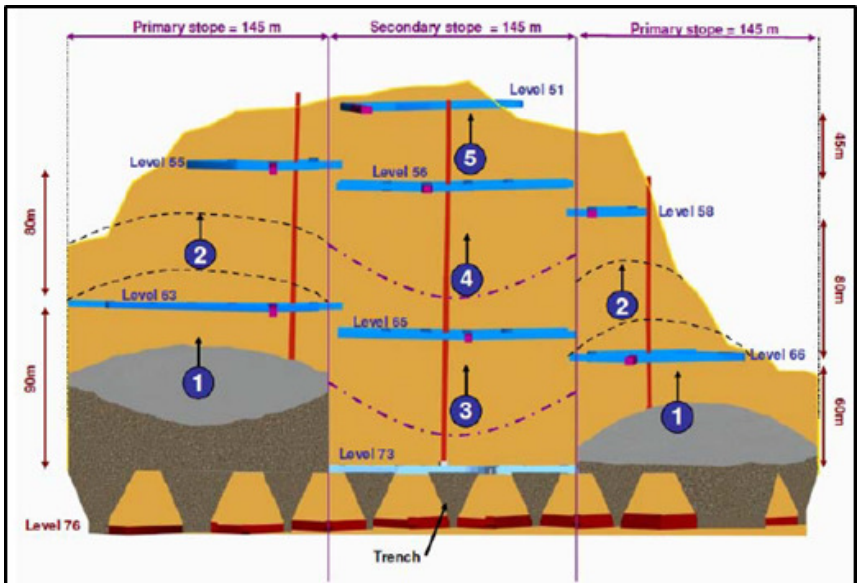

Figure 2.5. Goldex mining method and extraction sequence (Monitoring Open Stope Caving, Hudyma el.al,2010)

This method achieves approximately the same rate of production as the estimated maximum rate for the block caving method but with drilling and blasting of long production holes-this is called assisted blasting-. The production rate is estimated to be 7,500 tons per day to the mill.

This mining method was selected based on the following criteria:

- Minimise development (differed and operation);
- Minimise walls sloughing for very high stopes;
- Achieve productive fragmentation; and
- Design pillars to be easily recoverable (as necessary).

This new mining method uses concepts from different other mining methods such as:

- The high efficiency haulage level of a block cave operation;
- Wall stability of a shrinkage stoping method;
- Fragmentation of a long hole stoping method; and
- Large blast and mucking flexibility of a vertical crater retreat (VCR) method. [8]

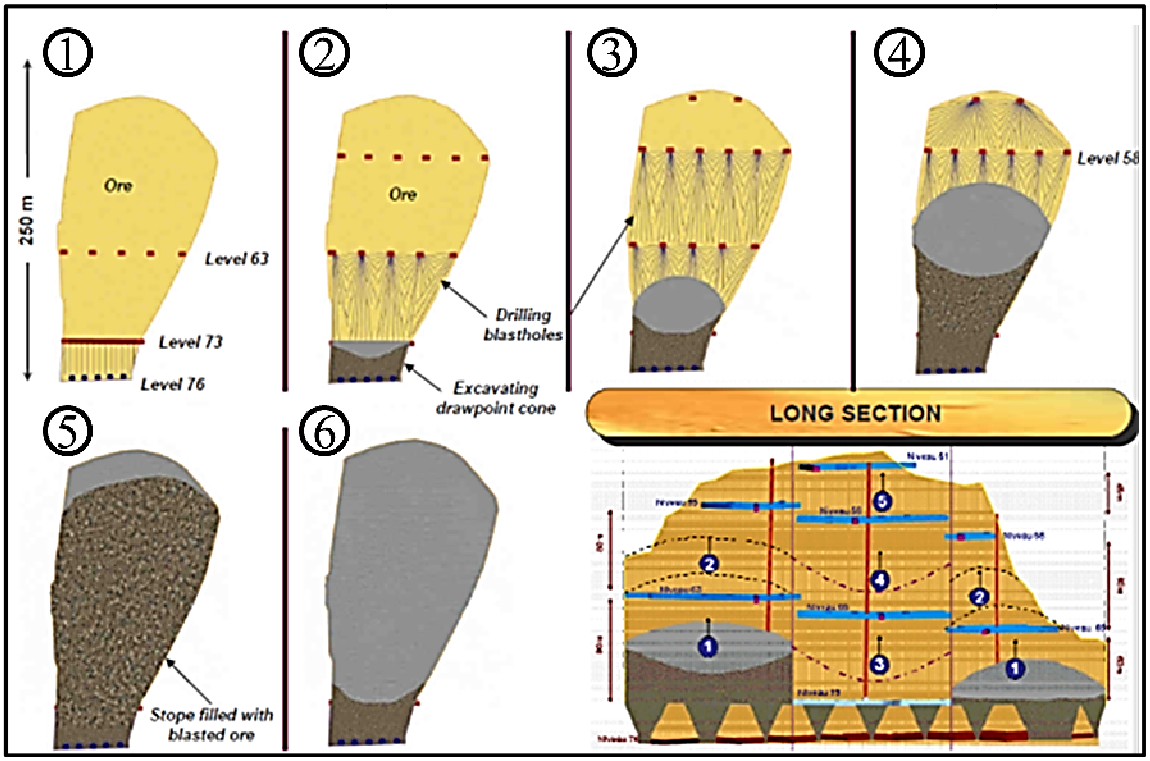

Figure 2.6. Blasting sequence for the GEZ(Monitoring Open Stope Caving, Hudyma el.al,2010)

[8] Monitoring Open Stope Caving (Hudyma, *et. al*, 2010)

2.3.2. Material Handling System

The handling of the ore from the drawpoints is based on a Block Cave operation system. The ore is transported from the drawpoints through LHD equipment and discharched to grizzly of dimensions 1[m] x 1[m]. Afterwards, the ore is received by a crusher and reduced to 7" in order to be transported through a belt conveyor to a silo. The ore stored in the silo is transported in a belt conveyor to a substation where is loaded into a skip that will carry the ore to the surface. The skip is also used for workers transport, ventilation and services supply at the mine.

The LHD equipment use at Goldex is a Caterpillar 2900G XTRA LHD with a shovel capacity of 11.3 [m^3]. The LHD runs an average medium distance of 200 [m] from the drawpoints to the grizzlies.

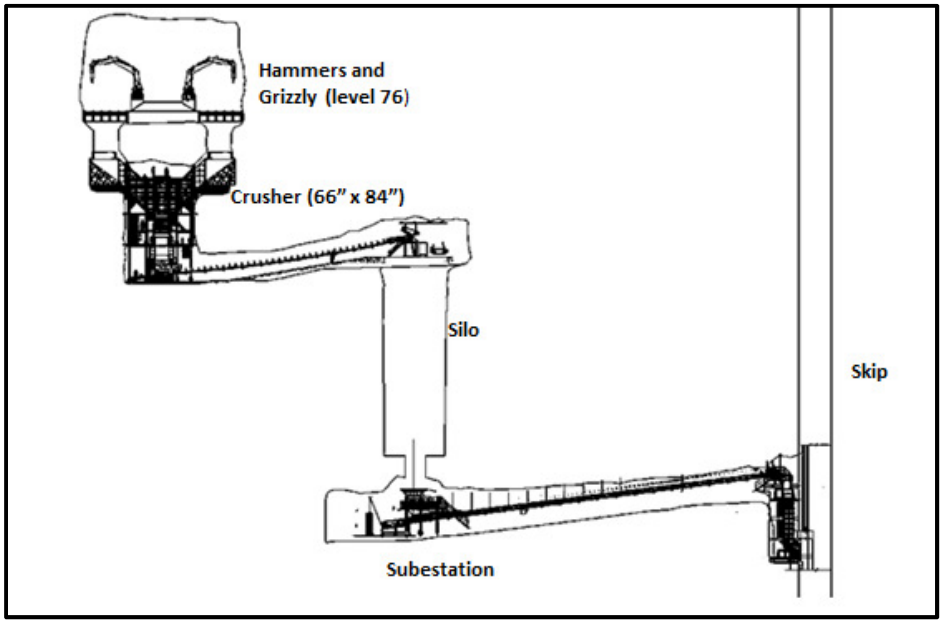

Figure 2.7. Conceptual scheme of the material handling system.

2.3.3. Haulage Level

The haulage level has 56 drawpoints, located and connected through drawbells crossing from north to south the ore body. In Figure 2.8 it can be seen the location of the drawbells in the orebody. It is also indicated the distance between drawpoints as the distance between drawbells through the mayor apex; the figure also presents the main facilities of the haulage level.

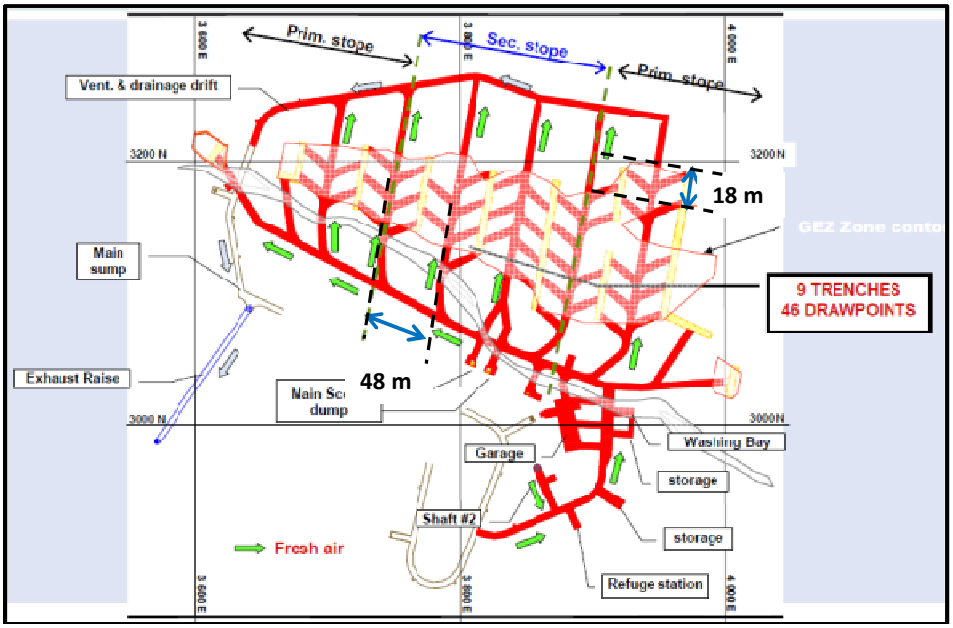

Figure 2.8. Plan view of the Haulage Level 76

2.3.4. Drill sublevel access

The mining method considers the division of the stopes into three horizontal drilling sublevels; each sublevel is between 60m and 90m in height, making drill holes longer than 100m in some cases. There are 5 main drill sublevels located as presented in Figure 2.9 (Level 73, 65, 63, 58 and 53). To achieve the required precision, ITH drilling was selected, using holes of 165mm on an approximate 4m x 4.5m pattern.

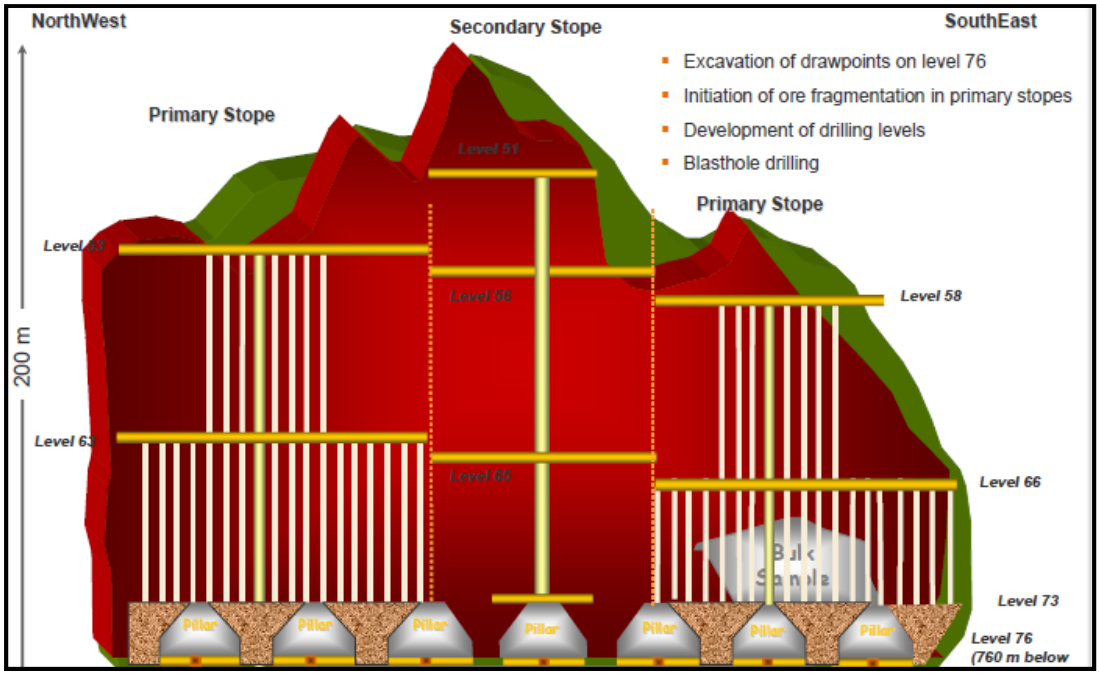

Figure 2.9. Drill sublevels at the GEZ(Ref:Goldex Mining Sequence, Agnico-Eagle)

2.3.5. Ventilation

The main circuit consists in the injection of fresh air through a main shaft (5.55 [m] in diameter) to Level 76; then, the air is distributed through the mine using remotely controlled automatic curtains that will spread the fresh air into the drives as they require.The return air rises to the surface, first to level 38 through a shaft 13 'in diameter and finally, from the level 38 to surface trough two shafts 10' diameter. The ventilation circuit can be seen in Figure 2.10.

The mine has four main fans, two for injection and two for extraction. The extraction system is the extraction being the most important as it also works as a siphon for the entry of fresh air, they are located in the underground due to the proximity of the mine to the town. The injection is used only in winter and its objective is to heat the air at 6 ° C.The mine also counts with 50 auxiliary fans, use to ventilate shelters, parking lots and to assist blasting. Actually ventilation requirements are 300,000 [cfm], with a ventilation rate of 37.5 [cfm/tpd].

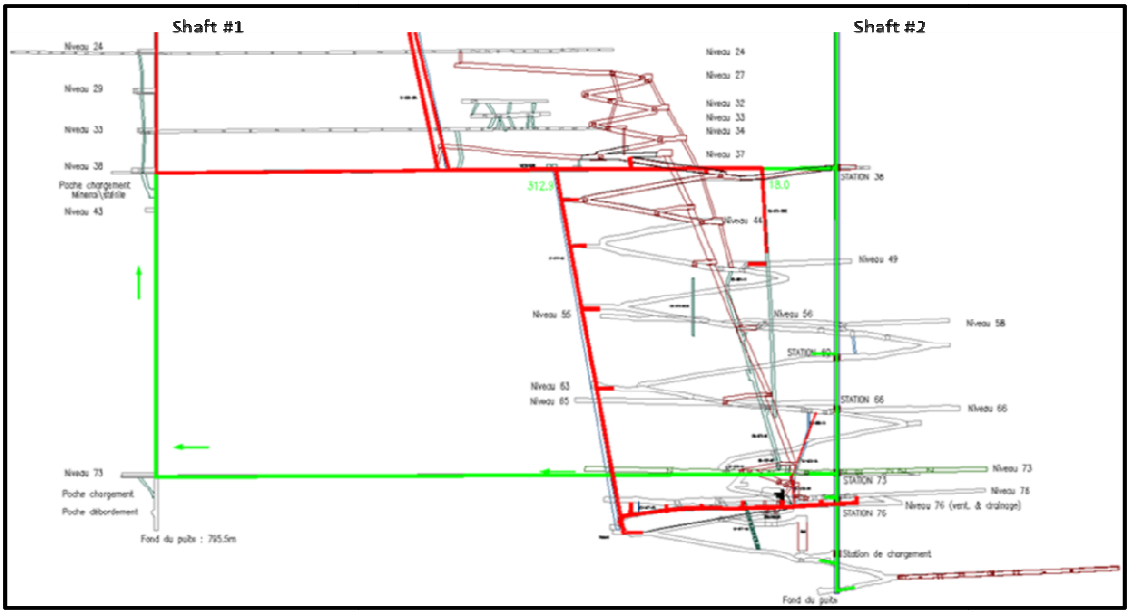

Figure 2.10. Ventilation circuit for Goldex Mine

2.3.6. Monitoring system

In accordance to the novel mining method implemented at Goldex, a microseismic monitoring system was designed to observe the profile of the large stopes and the extent of overbreak around the stopes, with the objective of supervise the rock mass response to mining. The seismic monitoring system at Goldex attends stress changes following mine blasts and identifies the location of the back of the large open stopes (see Figure 2.11) providing real-time information about sloughing around the stopes; also, helps safety of the infrastructure areas of the mine, by quantifying movement or failure, and identifying high stress areas.

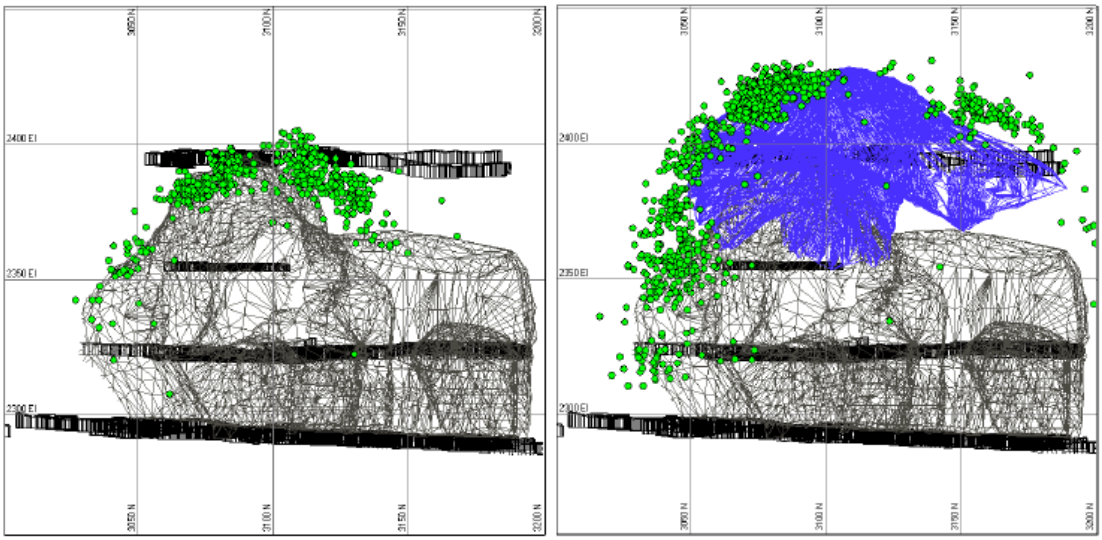

Figure 2.11.Locations of seismic events before and after a production blast, profiling the shape of the East stope (Monitoring Open Stope Caving, Hudyma, *et.al*, 2010)

The Goldex seismic array is composed by uniaxial and triaxial accelerometers. The locations of recorded microseismic event have proven to be very accurate, with errors in the range of only a few meters. This high quality microseismic data provides a rock mass monitoring system identifying important rock mechanics information, including: depth of stope back and stope wall overbreak, areas of stress change, and a differing rock mass response to mining between the West and East stopes.

Nevertheless, the implemented monitoring system, in October 2011, Agnico-Eagle suspended mining operations at Goldex Mine. The decision followed apparent failure of weak volcanic rock in the hanging wall of the Goldex deposit, and important groundwater flow into the mine. While the company's underground instrumentation showed that the volcanic rock mass above the Goldex orebody is stable, it has received an opinion from a rock mechanics consultant that suggests water inflow has negatively impacted the integrity of the rock mass. As a result, the company is undertaking further assessment of the stability of the rock mass and is increasing its efforts to decrease water inflow and the potential negative effects of the water on the rock mass [9].

2.4. Research Questions

Due to the novel mining method implemented at Goldex and to the current configuration of the production level, there is the question of whether the ore located at the footwall will be mobilized; the ore located at the FW represents about a 40% percent of the total reserves for the Eastern Primary Stope (see Figure 2.12) and is also an area of high gold grades. Nevertheless the rock is blasted and therefore these reserves could be mobilized by the rilling mechanism.

The major concerns lies in the fact that the footprint is smaller than the projection of the ore body, generating apprehensions about the mobility of the ore located at the footwall of the stope; in addition there's no notion of the predominant phenomena ruling the flow and the mixing profile due to extraction.

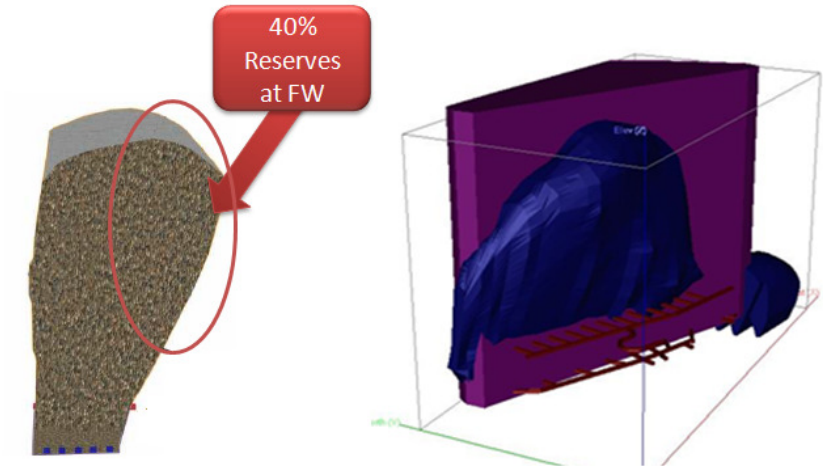

Figure 2.12.(Left) Ore located at the footwall. (Right) 3D view of the stope and the material located beyond the extraction level.

[9] Engineering and Mining Journal (www.e-mj.com)

As an antecedent of the mobility of the FW wedge it was known the research developed by ITASCA, using FLAC3D. This software utilizes an explicit finite difference formulation that can model complex behaviors not readily suited to FEM codes, such as: problems that consist of several stages, large displacements and strains, non-linear material behavior and unstable systems (even cases of yield/failure over large areas, or total collapse).

The study conducted by ITASCA considered the modeling of a 50m thick section as in the physical model, symmetry planes on E and W sides and frictional interface on FW and HW. The draw and extraction was simulated by growing IMZs into the stope manually and incrementally corresponding to average draw rate of 174 tonnes per drawpoint per day. IMZs were grown following Nedderman's equation (Equation 1)[10].

$$r = 4 \times B \times z \times ln\left(\frac{T \times Q \times DensityIMZ}{2 \times b \times \pi \times z^2 \times dP}\right) \qquad \textbf{Equation 1}$$

Where:

r: is the radial distance from the center point to the IMZ limit.
z: IMZ height.
B: is the fragment size (0.35m)
T: is time in seconds (Increments of 172799 seconds were used to grow the IMZ)
Q: is the flow rate in m^3/s (0.0014 m^3/s)
$dP = DensityOreBody - DensityIMZ$

The simulations evaluated were the following cases:

- Uniform draw: Level 76 only, current extraction level
- FW draw rate=2xHW draw rate: Level 76 only
- Uniform draw: Level 76 and Level 72 (25m crosscut spacing)

The main results are shown in Figure 2.13 and Figure 2.14.

[10] The parameters and the formulation of the model were provided by Thierry Lavoie, Itasca Consultant.

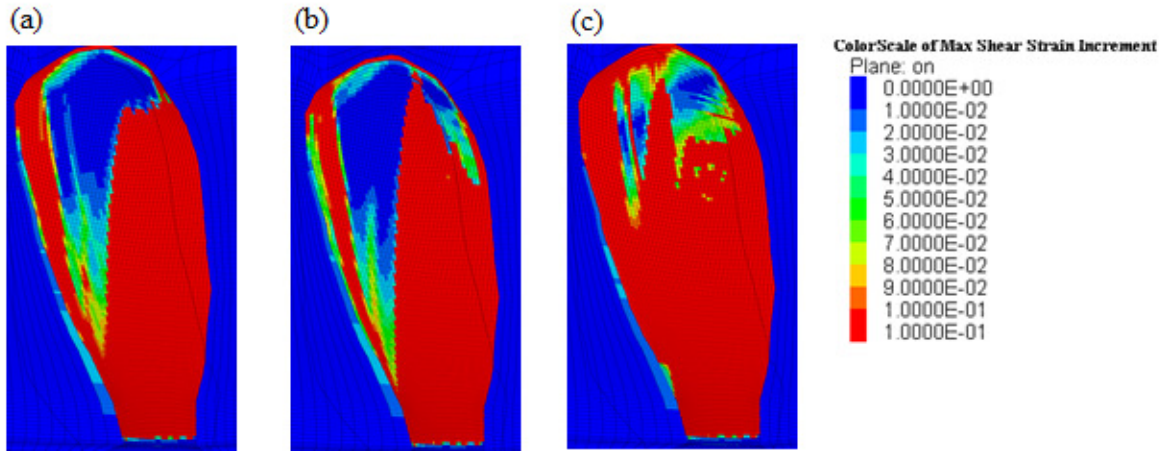

Figure 2.13.(a) Shear-Strain for a extraction of 69,000 drawing only from 76. (b). Shear-Strain for a extraction of 69,000 drawing only from 76 (FW=2HW). (c) Shear-Strain for a extraction of 69,000 drawing from level 76 and 72 (ITASCA).[11]

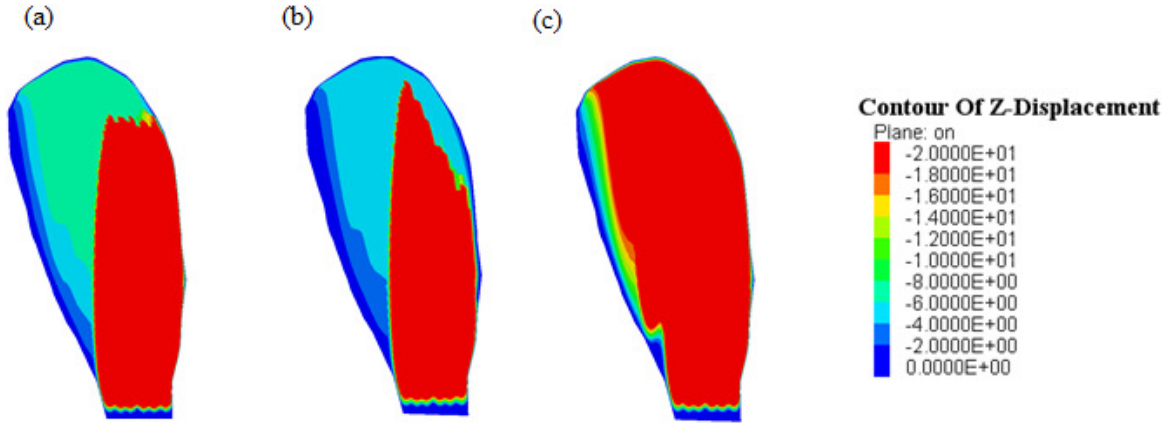

Figure 2.14.(a) Displacements for a extraction of 69,000 drawing only from 76. (b). Displacements for a extraction of 69,000 drawing only from 76 (FW=2HW). (c) Displacements for a extraction of 69,000 drawing from level 76 and 72(ITASCA).[12]

[11] Provided by Thierry Lavoe, Itasca Consultant.
[12] Provided by Thierry Lavoe, Itasca Consultant.

From the numerical modeling conducted in FLAC3D, it was concluded that when drawing only from level 76, the ore located at the FW is mobilized, however the displacements are significantly slower relative to material located above the footprint of the production level. When drawing from both levels there's a higher displacement of the ore located at the FW than in the base case as can be seen in Figure 2.13.

The same behavior is observed for the shear-strain simulations. The numerical model states therefore, that the ore located at the footwall will be mobilized for the base case (extracting from level 76) and for the hypothetical case of including another production level.

Based on the background of numerical modeling, another approach- physical modeling- is proposed in order to understand the mechanism governing gravity flow for the case of study.

2.5. Conclusions

Goldex Division of Agnico Eagle Ltd. operates an underground mine located in the city of Val-d'Or, Québec, Canada. Due to the geometry of the deposit (GEZ Zone) and the low gold grades of the ore body, the mining method considers the exploitation of a large stope using a combination of a Block Caving operation for its low cost and high productivity; Longhole Stoping, looking for an adequate fragmentation and providing suitable flexibility in the operation, and Shrinkage Stoping due to the stability it provides to the walls of the stope. Given the mining method used and considering the current configuration of the production level, there is the question of whether the ore located at the footwall will move due to extraction. The ore located at the FW represents about a 40% percent of the total reserves for the Eastern Primary Stope and is also an area of high gold grades.

The above mentioned reasons motivate the following study. Its main objective is to determine the potential recovery at Goldex Mine and to observe the gravity flow mechanism by means of physical modeling. The next chapter presents the state of the art for physical modeling to contextualize the research

.

CHAPTER 3
GRAVITY FLOW STUDIES FOR PHYSICAL MODELING

This chapter describes a critical review of the state of the art of physical modeling in order to achieve a better understanding of the gravity flow phenomena at reduced scale and the limitations derived from these models.

In addition, is detailed a review of the preponderant forces to be emulated in the physical in order to simplify the phenomena to be represented.

3.1. Introduction

Gravity flow is the process by which a granular material moves from its initial position due to gravity (Castro, 2006), which has a large impact on mineral recovery method and the final content of dilution. The overall understanding of the phenomena associated to gravity flow, requires a great amount of collected data and experimental tests at mine scale, in order to optimize and improve ore recovery and delay dilution entry at the drawpoints, both key for the success of the operation under study. This information is used to determine, for example, how draw rates can affect the intermixing of ore/waste, an optimum design and to enhance draw control strategies and operational practices for extraction.

Despite its importance, the mechanics of the gravity flow of blasted or caved ore is not completely understood. At a fundamental level, the subject has been studied using physical model experiments, by analogy with the flow of other granular materials in bins and bunkers (Kvapil, 1965; Jenike, 1966), by mathematical or numerical modeling using the theory of plasticity (Pariseau and Pfleider, 1968), by numerical modeling using probability theory (Jolley, 1968; Gustafson, 1998) and by mine scale tests based on markers recovery (Janelid and Kvapil, 1966; Just, 1981; Rustan, 2000)[13]. However, in spite of the enormous amount of research in the gravity flow field 3D simulations of ore recovery and waste rock dilution can still not be done for conditions in a specific mine (Rustan, 2000).

As it was detailed in the previous Chapter, Goldex Mine is exploited by a novel method that combines the efficiency of sublevel stoping drilling/blasting and an extraction layout similar to a block cave operation; therefore, the intermixing of the ore column lies in gravity flow mechanisms due to extraction. Supported on this background the main aspects related to the physical modeling regarding to gravity flow will be reviewed.

The chapter is divided in two main sections; the first is an extended review of granular flow research developed to date, including reduced scale models, empirical models and mine

[13] Cited in Brady & Brown, 2005.

scale studies. These studies have been conducted attempting to simulate the process and experience in caving mines. The second part is a review of the similitude analysis conducted in order to determine the applicability of physical modeling to reality, and to determine as well the limitations of the model.

3.2. Gravity flow models

3.2.1. Physical models

Physical modeling is the use of representative small-scale systems for the study of physical phenomena (Langhaar, 1951)[14].Similitude is the critical factor determining the applicability of the physical modeling to reality, and is defined as the degree at which the physical model coincides with the reality represented. It's been suggested that tests on scale models are based on the possibility of changing the scales: length, time and force (weight), without altering the equations describing the mechanics of the system (Mandel, 1963).

To date, the research conducted through physical modeling can be divided into two main categories: large-scale physical models and reduce-scale physical model. The reduce-scale physical modeling has been used to understand the principles governing the granular flow (McCormick, 1968; Castro, 2001).

During the history of physical modeling, two types of materials have been used: sand and gravel. Researchers have used sand as model media, since this material is easy to manipulate. On the other hand, gravel, has been indicated by some authors as the most appropriate way of representing broken rock from the mine (Peters, 1984; Power, 2003)[15].

The physical models are built to achieve two types of functions:

a) To model specific situation at a mine, or
b) To investigate generic rules governing a specific phenomenon.

This section focuses on the most relevant publications regarding to gravity flow physical models, whose results have been applied with the purpose to improve the comprehension of the phenomena governing the mechanism of flow. Hereupon is described the state of the art of physical models and the contribution of various researchers in the field of gravity flow. This gained knowledge should be used as a tool to make progress in the design and draw control strategies for the case of study.

3.2.1.1. Rudolph Kvapil (1965, 1989 and 1992)

Kvapil appears as the first researcher who tried to obtain a quantitative approach to the gravity flow phenomenon. His first research aimed to obtain empirical mathematical

[14]Cited in Castro, 2006.
[15]Cited in Orellana, 2011.

relationships for gravity flow in silos and bins. Kvapil conducted experiments using a physical model consisting of a box filled with sand, with a hole at its base; the experiments showed the existence of two volumes that characterized the granular flow (Kvapil, R, 1965), the first is defined by the original location of the actual material drawn from the drawpoint, and the second defined by the boundary between the material that actually moved and the material that remained in its initial position. The shape of these two volumes fitted with an ellipsoid, characterized by its eccentricity; the volumes were named extraction and movement (or loosening) ellipsoid respectively, and can be seen in Figure 3.1. The author also determined that if extraction is continued, the ellipsoid increases in height as allowed by the column of material, but its diameter is bounded at a certain point from the extraction. Therefore, for high altitudes, the ellipsoid reaches a cylindrical shape, independent of the size of the drawpoint.

Kvapil also noted that the ellipsoid's eccentricity is affected by a number of variables including the particle size and shape, the roughness of the particles, the internal friction angle, the amount of material drawn, and others. These variables combined produce a behavior that can be expressed in terms of mobility of the material. The higher mobility of the material generates a smaller diameter of the ellipsoid than a lower mobility material.

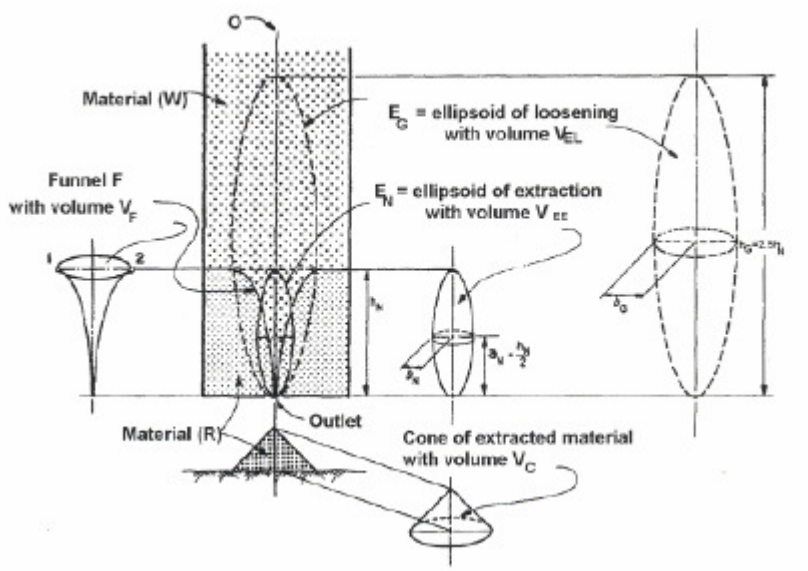

Figure 3.1. Kvapil's Ellipsoid theory (1992)

Kvapil's ellipsoid theory since then has been widely accepted as a design guideline in sublevel caving mines around the world. However, some subsequent researchers found that this theory does not model the flow accurately (Heslop, 1983; Heslop and Laubscher, 1981; Laubscher, 2000; Marano, 1980; McCormick 1968)[16].

[16] Cited in Halim, 2004.

3.2.1.2. Mc Cormick (1968)

Mc Cormick built a two-dimensional physical model with a single drawpoint located at the base; using sand as model media. The variable under study was the maximum size particle and how affected drawzone geometry width. From the conducted experiments the author concluded that the both coarse and fine fragmentation resulted in similar flow behaviors. The author also conducted a single drawpoint experiment varying the drawpoint width, concluding that the drawzone geometry is not influenced by the drawpoint size.

3.2.1.3. Li Yenge (1980)

Yenge used bidimentional model filled with sand as model media, simulating the flow in a Sub Level Caving mine. Based on this model he commented as well that the flow for broken rock in mining is controlled not only by the dimensions of draw opening, but also the pattern of draw across the face of extraction and by the systematic arrangement of draw drifts with respect to the geometry of the ore body. Yenge also concluded that the assumptions made to relate the failure of cohesionless materials (soil mechanics approach) to the yielding behavior of the rock column neglects the interlocking structures upon which the flow pattern is dependent. The flow geometry depends, therefore, upon the packing geometry and the boundary conditions imposed upon the draw.

3.2.1.4. Marano (1980)

Marano conducted his experiments in a three dimensional sand model with the purpose to investigate the behavior of the gravity flow for granular materials at a 1:80 scale. He conducted the experiments by drawing from an isolated drawpoint and from multiple drawpoints. Marano defined that the area of influence of a drawpoint is equivalent to the IMZ width, and concluded that there was a critical distance, for concurrent draw of multiple drawpoints, at which the flowing zones interacted even if they were spaced above the IMZ width value. He also concluded that total similitude cannot be achieved using sand, since the IMZ geometry strongly depends on the material properties.

Just like McCormick, Marano commented about the cylindrical shape due to flow observed in the experiments. Additionally Marano pointed out that the results derived from experiments conducted with a single drawpoint are not extrapolated to a multiple drawpoint extraction.

3.2.1.5. Peters (1984)

In 1984 Peters conducted experiments in the largest bidimensional physical model built at the time; the dimensions of the box where 0.5[m] x6[m] x4.6 [m]. Peters used gravel instead of sand as a model media. This research focused mainly on the effect of particle size on the ellipsoid geometry and the effect of drawpoint spacing for multiple drawpoint extraction. The author concluded that particle size has a small effect on the extraction zone geometry and that the drawpoint width had a more important effect on the drawzone

geometry. The effect the author found on the drawpoint width can be explained since the experiments are considered to be representative of near-field conditions (because of the dimensions of the model and the particle size distribution); under these conditions, the drawpoint width is expected to have a strong impact on IMZ shape. Peters also found that interaction between extraction zones was given at a distance between drawpoints of 1.14 times the IEZ width.

3.2.1.6. Laubscher and Heslop (Heslop, 1983; Heslop and Laubscher, 1981; Laubscher 1994, 2000)

Laubscher and Heslop carried out experiments in a 3D sand model, which was specifically built to investigate the interactive drawing of adjacent drawpoints. The model consisted of a metal box with a size of 760mm long x 760mm wide x 2400mm high. The base contained 50 holes, evenly spaced, with a diameter of 25mm, representing the drawpoints. The scale of the model was 1:80. The block height could be varied by filling the model to the top or only part of it. Drawpoints in this model were drawn simultaneously.

In these experiments the authors found that uniform lowering of the upper markers occurred when the drawpoints were drawn simultaneously as shown in Figure 3.2. From the analysis the authors concluded that the Kvapil's ellipsoid theory does not apply in this situation, which later they termed as interactive flow theory. Later, Laubscher (1994, 2000) based on sand model experiments and the interpretation of stresses around excavations, proposed his interactive flow theory by defining the isolated diameter zone, described as the maximum diameter obtained by drawing from a single drawpoint. The main conclusions of the drawpoint interaction theory stated by Laubscher are connected to the relation between the Isolated Draw Diameter (DTA) and the spacing between drawpoints. When the drawpoints are located at a distance less than 1,5DTA there's interaction among them, and the flow zones are overlapped existing interactive draw. The height of interaction will depend on the particle size distribution, the distance between drawpoints, the draw strategy and the draw rate.

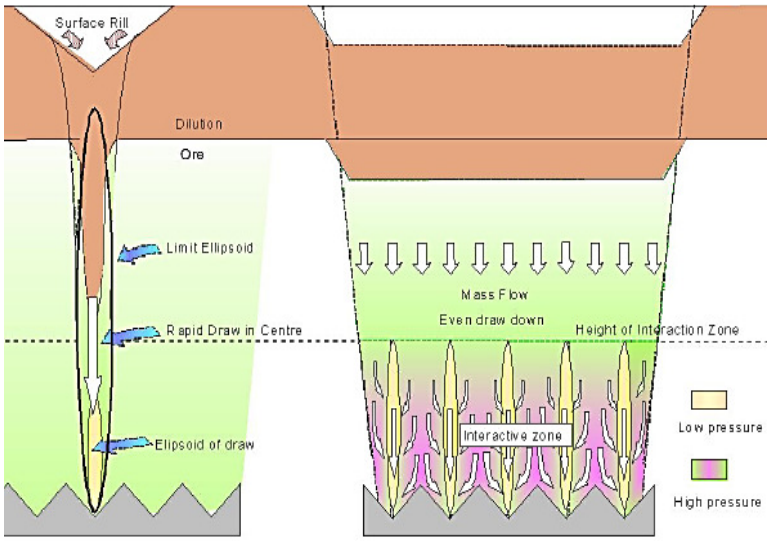

Figure 3.2. Laubcher's flow model (2000).

3.2.1.7. Susaeta (2004)

The gravity flow model proposed by Susaeta is the result of 4 years of research based on sand models experiments, conceptual analysis and back analysis from Codelco Mines. The author determined that gravity flow is a function of extraction, material properties (internal friction angle, moisture, density, fragmentation, rugosity, angularity of the fragments, etc) and the layout geometry. Susaeta identify and characterized 3 behaviors from the flow models:

- **Isolated Flow:** A draw point extracted in isolation generates a vertical chimney movement of a diameter- D_{ta}(Isolated Draw Diameter)-approximately constant in all over its height. D_{ta} dimensions depend on the internal friction angle and the material moisture.
- **Isolated –Interactive Flow:** When the drawpoints are located at a distance of 1.5 times the D_{ta} or less, occurs interaction during open flow.
- **Interactive Flow:** The difference with the isolated-interactive flow is that in the interactive flow model the material descends uniformly, according to the massive flow proposed by Laubscher. The distance to achieve an interactive flow must be less than 1.2 times the D_{ta}.

3.2.1.8. Power (2004)

Power conducted his research in a large scale 3D physical model (scale 1:30). From his experiments, he concluded that gravel is indeed the most accurate way to represent broken rock since particle size distribution has a significant impact on the geometry of the extraction and movement zones. The major contribution is regarded to the fact that the author exposed evidence that 2D physical models are not valid for the study of gravitational flow.

3.2.1.9. Castro (2006)

Recently, as a part of the International Cave Study II, it was constructed the 3D largest physical model at the date, using as a model media gravel instead of sand. Castro's research revealed that the isolated movement zones growth indefinitely when drawing from the drawpoint. The author proposes that the physical model used, will emulate in an optimum way the geometrical relation between particle size and the height of the ore column to be extracted. Sand models, by using a finer fragmentation would be overstating the spatial restrictions under which the flow is generated.

The author also stated that the main variables that will have an effect on the IMZ and IEZ geometries are the height of column and the cumulated extracted mass per drawpoints, neglecting the effect of the particle size distribution. In his research the author concluded that a more rigorous approach is needed to establish conditions under which small-scale models must operate in order to approximate the gravitational flow conditions at mine

scale. Consequently it is necessary to conduct a similitude analysis to help define a set of assumptions and limitations of the method within the framework of the investigation

3.2.1.10. Physical modeling summary

In Table 3.1 is presented a summary of physical modeling through history, as the main conclusions obtained from the experiments to date.

Table 3.1. Summary of physical modeling and its main conclusions.

Reasercher	Year	Place	Dimenssions	Model Media	2D-3D	Main Conclussions
Kvapil	1965 1992	Sweden	-	Sand	2D	Characterizes the ellipsoidal flow zones. Provides the mathematical relationships related to gravity flow for granular material in silos
McCormick	1969	-	Height 23 m Lenght:14 m Width: m	Sand	2D	Characterizes the geometry of extraction as a cylindrical zone. The width of the cylinder depends on the width of the drawpoint
Marano	1980	Zimbabwe	Height: 2.4 m Lenght: 0.76m Width: 0.76 m Scale 1:80	Sand	3D	Total similitude cannot be achieved by using sand as model media. The results derived from experiments with a single drawpoint are not valid when drawing from multiple drawpoints
Yengue	1980	Colorado, Usa	Height: 2.4 m Lenght: 0.76m Width: 0.76 m Scale 1:80	Sand	2D	The assumptions made to relate the failure of cohesionless materials to the yielding behavior of the rock column neglects the interlocking structures upon which the flow pattern is dependent. The flow geometry depends, therefore, upon the packing geometry and the boundary conditions imposed upon the draw.
Laubscher	1981 1994 2000		-	Sand	3D	Identifies the Isolated Draw Zone with Kvapils motion ellipse. Also states his interactive flow theory
Peters	1984		Height 23 m Lenght:14 m Width: m	Gravel	2D	There's no effect of the particle size on flow geometry. There's no interaction when the drawpoints are spaced at 2 times the extraction ellipse diameter
Susaeta	2004	Chile	Height 23 m Lenght:14 m Width: m	Sand	3D	At a 1.5 times the width of the IMZ there's isolated-interactive flow. Creates the uniformity index and also states that sand models are valid as a model media for prototypes with fine fragmentation
Power	2004		Height 23 m Lenght:14 m Width: m	Gravel	3D	The particle size does have an impact on the geometry of the extraction and movement zone. He states that 2D physical models are not valid for gravity flow phenomena studies
Castro	2006	Australia	Height 23 m Lenght:14 m Width: m	Gravel	3D	Drawpoints must be spaced at least the width of the IMZ, so that there is interaction between them. The height and width of both extraction and movement zone are function of the extracted mass and the ore column height

3.2.2. Full scale tests

The advantage of full scale trials over reduced physical models is that scalability issues can be avoided (Castro, 2006); however, to define general rules governing flow from other cases of study is extremely difficult. Therefore, besides physical modeling for the understanding of gravity flow, several attempts have been made to study flow mechanisms and the zone of influence of a drawpoint using different layouts at mine scale (Alvial, 1992; Hustrulid, 2000). From the full scale experiments performed in block caving mining, can be emphasized the research conducted by Alvial (1992), Laubscher (2000) and more recent work by Brunton *et al*. (2012).

Alvial attempted to conduct a mine-scale trial in a block caving geometry; this by placing markers (old tires) at the production level of an abandoned sector located above the sector Teniente 4 Sur at El Teniente mine. However, due to the low quantity of recovered markers (19 markers have been recovered in 10 years), the author was not able to determine the shape of the extraction zones in field. Alvial concluded that the trajectory of markers was influenced by rock mass characteristics, draw rate and the presence of major structures.

Brunton *et al*. designed and implemented at Ridgeway Deeps mine (from 2008 to 2010) experiments by placing metal and electronic markers using the *Smart Marker System* (Whiteman, 2010). The aim of these experiments was to quantify the development of the extraction zone in time and the flow behavior. The recovery of markers to date indicates a chaotic flow behavior that differs from the conventional theory based on numerical and physical models.

On the other hand, full scale tests regarding to gravity flow in Sub Level Caving mines has been largely developed. However, Castro (2006) stated that the extensions of the sublevel flow behavior to block caving knowledge not been justified in the literature and therefore, it is not possible to extrapolate these results.

All approaches to gravitational flow models in broken rock require good calibration and validation of data. The ideal would be obtaining these data from mine-scale tests (Just, *et al.,* 2004; Rustan, 2000). However, experience has shown that mine-scale experiments are expensive, time-consuming and often the results of these tests have not delivered results that can be used effectively for the development of valid models as it was concluded by Gustafson (1998), Just(1981) and Sandstrom (1972) [17].Difficulties associated to mine scale test have resulted in the extensive use of physical models to understand the governing mechanisms of gravity flow and dilution entry ;validating the use of physical modeling by considering adequately the scale effects and the limitations derived from these simplified models.

[17] Cited in Halim, 2004.

3.3. Similitude Analysis

Physical modeling is the use of representative reduced physical systems for the understanding of a defined phenomenon; it has been extensively used as a tool for design and research in a wide number of engineering disciplines. The success in the use of reduced models for studying diverse physical systems is based on the fact that physical quantities can be fully described by the fundamental laws of mechanics (Langhaar, 1951).The effectiveness of a reduced model depends on the degree of similitude that it has with respect to the prototype (Castro,2006).

Similitude involves the concept of correspondence or homology between two systems: a prototype and a model. There are three types of similitude:

- **Geometric Similitude:** two systems are geometrically similar when the distance between homologue points is given by a constant length scale factor λ_L
- **Kinematic Similitude:** two systems are similar in their kinematics when two homologue events occurs at a constant time scale factor λ_T
- **Dynamic Similitude:** two systems are dynamically similar at homologous points when the ratio between the inertia and any external force is constant between model and prototype

Depending of the nature of the phenomenon under study, the above constraints or model laws impose initial and boundary conditions which the scaled model must satisfy. Full dynamic similitude is achieved when all the model laws have been fulfilled. It is well known that in reduced physical models using granular materials it is not possible to achieve full dynamic similitude (Pöschel, *et al.*, 2001). This however does not limit the applicability of the technique to study flow mechanisms as long as the probable distortions or deviations from the prototype conditions are well established (Fuentes, 1996)[18].

It's important to notice that the dominant forces in the granular flow depend mainly on the material characteristics, the initial and the boundary conditions.

For the physical model to be implemented there are many complex phenomena that will not be considered such as the tendency of caved rock to become cohesive or changes in the mechanical properties of the rock due to time or water infiltration affecting its shear strength characteristics. Also the particle breakage as material flows will not be considered. It would be extremely difficult to capture all the gravity flow problems through physical modeling or to understand the effect of all variables on granular flow. Nevertheless, a good approach is to consider only the dominant forces (gravity and friction) of the phenomenon under study, assuming that these are properly represented in the model and that the other forces are not involved or that its effect is negligible.

[18] Cited in Castro,2001.

3.3.1. Dominant forces

The flow of coarse granular material, as the prototype to be simulated, is subject to basically two types of main forces: gravity and friction. Gravity force is a natural phenomenon by which physical bodies attract with a force proportional to their mass. Friction instead is the force exerted by the grains among them, either by punctual or by superficial contacts (Castro, 2001).

In the physical model, however, and due to the scaling of the size of the particles, the material is several times smaller and this may generate other type of forces affecting the granular flow. The forces affecting granular flow are mainly:

i- Van der Waals forces
ii- Capillary forces
iii- Boundary effects
iv- Cohesive forces
v- Electrostatic forces
vi- Magnetic forces

All the above mentioned forces will have a different level of preponderance effect on the gravity flow for the physical model generating possible distortions. Therefore they must be quantified in order to achieve a better understanding of the overall phenomena.

3.3.2. Gravity forces

From Newton's Second law:

$$F = \sum F_i = F_1 + F_2 + .. + F_g = m\,a \qquad \textbf{Equation 2}$$

Where:

m: mass

a: acceleration

F: Net force

$F_{G:}$ Gravity Force

If gravity force domains above the other forces, then $\frac{F_1}{F_G}, \frac{F_2}{F_G}, .. \ll 1$ and therefore $F \approx F_g$. Then, Equation 2can be rewritten as:

$$F_g = m\,a \qquad \textbf{Equation 3}$$

Since, gravity force is mainly the weight $F_g = m\,g$, then:

$$\frac{m\,a}{mg} = 1 \Rightarrow \frac{a}{g} = 1 \qquad \textbf{Equation 4}$$

In terms of scale factors Equation 4 can be expressed as:

$$\lambda_a = \lambda_G$$

The definition of acceleration is given by:

$$a = \frac{dv}{dt} = \frac{dv}{dx} \times \frac{dx}{dt} = \frac{v^2}{L} \qquad \textbf{Equation 5}$$

Then, combining Equation 4 and Equation 5 it is obtained:

$$\frac{v^2}{L \times g} = 1 \qquad \textbf{Equation 6}$$

Transforming Equation 6 in terms of scale factors:

$$\lambda_V^2 = \lambda_L \lambda_G \qquad \textbf{Equation 7}$$

Since the model and the prototype are subjected to the same gravitational field, in terms of scale factors $\lambda_G = \frac{[F_G]_M}{[F_G]_P} = 1$. Therefore, Equation 7 can be expressed as:

$$\lambda_V = \sqrt{\lambda_L} \qquad \textbf{Equation 8}$$

3.3.3. Friction forces

When particles are in motion, and are surrounded by others, they experience contact through surfaces or through contact points as can be seen in Figure 3.3, generating friction forces among the contacts.

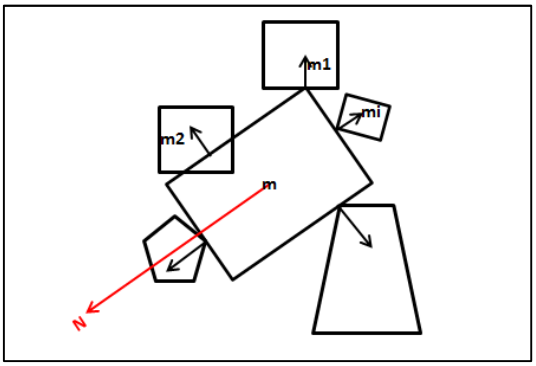

Figure 3.3. Resulting force of the friction forces for a particle within the extraction ellipsoid

Analogue to the analysis conducted for gravity, from Newton's Second law:

$$F = \sum F_i = F_1 + F_2 + .. + F_F = m\,a \qquad \textbf{Equation 9}$$

Where

m: mass

a: acceleration

F: Net force

$F_{F:}$ Friction force

If friction force domains above the other forces, then $\frac{F_1}{F_F}, \frac{F_2}{F_F}, .. \ll 1$ and therefore $F \approx F_F$. In addition $F_F = \tan(\phi)\, N$. Then, Equation 9 can be re-written as:

$$F_F = m\,a = \tan(\phi) N \qquad \textbf{Equation 10}$$

Since the normal force (N) can be approximated to the weight $F_F = \tan(\phi) m\, g$; then:

$$\frac{m\,a}{\tan(\phi) m g} = 1 \Rightarrow \frac{a}{g} = \tan(\phi) \qquad \textbf{Equation 11}$$

In terms of scale factors Equation 11 can be expressed as:

$$\frac{\lambda_a}{\lambda_G} = \lambda_{\tan(\phi)}$$

As stated in the previous section, if besides friction, gravity is a dominant force $\lambda_a = \lambda_G$.

Therefore, Equation 11 can be expressed in terms of scale factors as:

$$\lambda_{tan(\phi)} = 1 \qquad \textbf{Equation 12}$$

Equation 12 is one of the conditions that must be maintained in a gravity flow physical model. However, to accomplish conditions where the friction angle remains invariable between model and prototype is unachievable. Therefore it's an important factor to take into account when scaling the results from prototype to model (Castro, 2001).

3.3.4. Dominant forces and conditions required for similitude

In order to satisfy the conditions explained in the previous sections, it's summarized the conditions required for similitude when gravity and friction are the dominant forces.

Table 3.2.Summary of the conditions required for similitude

Variable	Factor	Scale Factor

Length	λ_L	λ_L
Area	λ_A	λ_L^2
Volume	λ_{Vol}	λ_L^3
Velocity	λ_V	$\lambda_L^{1/2}$
Time	λ_T	$\lambda_L^{1/2}$
Friction Angle	$\lambda_{\tan(\phi)}$	1

3.3.5. Other forces affecting gravity flow

As mentioned before, for smaller particles, other kinds of forces may develop, affecting granular flow. In order to comprehend the phenomena at a reduced scale, they will be studied to evaluate how these interparticle forces could affect gravity flow and the experimental results.

In fact many fundamental features of cohesive granular materials do not depend specifically on the nature of interparticle forces, but on the value of the cohesive granular Bond number (Castellanos, 2005), defined as the ratio between this attractive interparticle forces and the particle weight. Bond number therefore, is defined as:

$$Bo_G = \frac{F_A}{F_G} \qquad \textbf{Equation 13}$$

Where:

F_A: Attractive interparticle force

F_G: Gravity Force

When two particles are brought into contact they are subjected to capillary, Van der Waals forces, electrostatic and magnetic forces. In Appendix A, is detailed an extended review of the causes of these other forces affecting flow and it is explained and quantify their effect. Table 3.3 presents a summary of this review.

The quantification and remediation of these forces for the model media is detailed in Chapter 5.

Table 3.3. Summary of the interparticle forces affecting gravity flow.

Force	Cause	Parameters	Bond Number
Van der Waals	Attractive and repulsive forces due to permanent or induced dipoles.	δ_0 :Distance between molecules[m] h_W: Lifshitz- Van der Waals constant [eV] D:Stiffness of the material [Pa] R: Measure of the roughness of the material [m]	$F_{B\_VdW} = \frac{\frac{h_W R}{8\pi\delta_0^2}\left[1+\frac{h_W}{8\pi\delta_0^3 D}\right]}{F_G}$
Capillary Force	Condensed moisture on the particle surface.	γ: Surface tension [N/m] R: Particle radius [m]	$F_{B\_H} = \frac{2\pi\gamma R}{F_G}$
Electrostatic Force	Interaction of particles with an electrical charge.	R: Particle radius Q: Particle Charge H: Separation Distance ε_0: Permittivity of vacuum	$F_{B\_C} = \frac{\frac{Q^2\left[1-\frac{H}{(R^2+H^2)^{1/2}}\right]}{16\pi\varepsilon_0 H^2}}{F_G}$
Magnetic Forces	Motion of charged particles such as electrons. Also additional attraction may arise when the particles can be magnetized.	p: Degree of magnetization μ : Conductivity of the medium H :Separation distance between particles	$F_{B\_M} = \frac{\frac{p^2}{6\pi\mu H^2}}{F_G}$

3.4. Conclusions

The mains conclusions derived from a critical synthesis of the state of the art of physical modeling are described below:

i- Mining industry needs imperiously to improve the know how related to the governing mechanism due to gravity flow by the use of physical models, in order to maximize the profits. Physical models are presented then as an engineering tool avoiding full scale test without incurring in significant cost and time tests.

ii- Little theoretical information exists on the subject of drawing caved ore and granular materials. As stated by Yengue, this is a serious deficiency in the rock mechanics field and any information that is to be used for solving drawing issues, must be obtained from full scale tests or from physical models.

iii- The use of physical modeling with a single or multiple drawpoints has been useful in understanding the behavior of gravity flow of particulate materials. Gravity flow has been studied through several tools as physical modeling, numerical modeling and empirical tests. The physical modeling using gravel as a model media has been considered by some authors as the most suitable way for studying gravity flow of coarse granular materials. However other authors (Susaeta, 2004) have stated that sand models have been validated for gravity flow operations that present fine fragmentation, as the case of study.

iv- From the revision of the physical modeling through history, it can be concluded that this studies have been focused in the kinematic of the phenomena. However in most cases, these researches have been developed with the purpose to understand the overall phenomena and not as an engineering tool for a specific case.

v- Despite the research efforts, in the gravity flow field, the review of the experimental gravity flow studies to the date, show considerable differences among the used methodologies and parameters to be considered. Therefore a more rigorous method must be conducted in order to scale physical model results to mine scale.

vi- With the purpose to obtain the maximum knowledge from the physical model, the framework within the construction and experimental tests must satisfied the following limitations: geometrical, dynamic and kinematical similitude must be achieved ; however for the model media to be used (sand) it's only possible to accomplish geometrical and kinematical similitude. Dynamic similitude it's impossible to accomplish, since properties as resistance of the sand cannot be scaled.

vii- The flow of coarse granular material, as the prototype to be simulated, is subject to basically two types of main forces: gravity and friction, they are the dominant forces acting among particles. However, for smaller particles, other kinds of interaction may develop. The effect of this other forces must be in a first place identified and quantified, with the purpose to understand how it could affect gravity flow and the experimental results.

Within the extent and the framework of this research the following questions will be is answered:

i- What are the main parameters that affect the physical modeling in order to observe the governing mechanism due to extraction?
ii- What are the main forces affecting granular flow? How interparticle forces may affect gravity flow?
iii- Is it possible to scale the results from the physical model in order to estimate ore recovery and dilution entry?
iv- Are the mechanisms observed in a sand model applicable to mine scale?
v- What is the relation between mass flow, the gravity flow mechanisms and ore recovery?

CHAPTER 4

LIMITING EQUILIBRIUM ANALYSIS

This chapter describes the basis and formulation of a limit equilibrium analysis for the different sections of the Eastern Primary Stope. The purpose of this exercise is to determine a critical section for the construction of the physical mode, able to represent the problem to be solved and to answer the research questions stated in Chapter 2 and Chapter 3.

4.1. Introduction

In order to determine the critical section to be analyzed for the physical model, a limiting equilibrium analysis is conducted, to study as a first input the mobility of the ore located at the FW of the Eastern Primary Stope at Goldex Mine.

The chapter includes the basis and formulation of a limit equilibrium analysis for the different sections of the Eastern Primary Stope with the purpose to conduct the experiments in a critical section, able to represent the problem to be solved, generating a different approach to complement and support engineering design. The formulation includes the assumptions used to implement the model as the obtained equations to be used for the evaluation of the mobility of the wedge.

To contextualize the investigation, the main bases of analysis are centered in Coulomb's theory of Earth pressure. Coulomb's theory involves the consideration of stability, as a whole, between a soil wedge and a retaining wall. The force between the wedge and the wall surface is determined by considering the equilibrium of forces acting on the wedge when it's on the point of sliding either up or down the failure plane (Craig, 1974) as schemed in Figure 4.1.

This stability problem formulated above is very similar to the potential failure of the footwall for the Eastern Primary Stope. The vertical projection of the production level within the stope can be assimilated as the retaining wall and the wedge as the ore located in the footwall. The active case [19] is equivalent to extraction, since the stope is *moving* and the passive case[20] corresponds when there's no extraction. For the analysis, only the active case will be considered.

[19] Active pressure develops when the wall is free to move outward such as a typical retaining wall and the soil mass stretches sufficiently to mobilize its shear strength.
[20] Passive pressure develops if the wall moves into the soil, then the soil mass is compressed, which also mobilizes its shear strength.

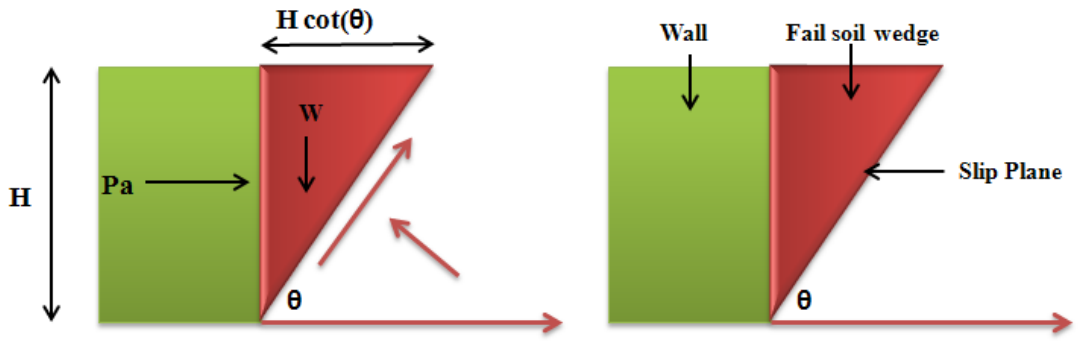

Figure 4.1.Conceptualization of a retaining wall according to Coulomb's Earth Pressure Theory (Craig, 2004).

4.2. Assumptions from the model

The conceptual limit equilibrium model is conducted to estimate the potential failure of the wedge located at the FW for the Eastern Primary Stope.

This section describes the assumptions of the model; it must be noticed that the analysis is based on a conceptual model, and therefore there are certain limitations within the framework of the study. These limitations can be understood by contextualizing the assumptions to be used as their implications.

The limiting equilibrium analysis is carried out using the following assumptions:

- The problem may be reduced to two dimensions and the calculations are carried out for unit thickness in the normal direction.
- The fragmented and bulked rocks mass properties have homogeneous and isotropic mechanical properties.
- The shear-strength of the material is defined using the Mohr-Coulomb failure criterion.
- The rock mass properties include its unit weight, and the parameters describing its shear strength. Since the Mohr-Coulomb failure criterion is used in the analysis, then the values of cohesion c, and friction angle, ϕ are required. The broken rock properties include its unit weight, γ, cohesion, c, and friction angle ϕ. Also the friction angle between the broken rock and the stope walls δ is required.
- Initially the whole ore column and the material in the wedge is broken.
- If there is a failure, it occurs on a shear plane having an inclination α. Failure occurs when the factor of safety, *FS*, defined as the ratio between the available shear force on the sliding plane and the shear force required to maintain equilibrium, becomes less than 1.0.
- The thrust from the broken rock is considered as suggested by Lupo (1996)[21] by means of an active earth pressure coefficient, K_A. It must be noted that the magnitude of the resultant active force is proportional to H_B^2, where H_B is the height

[21] Cited in Flores,2005.

of broken rock above the undercut, and it acts at an inclination δ with respect to the normal to the stope wall.

4.3. Limiting equilibrium analysis formulation

The model can be parameterized, in function of the geometrical parameters of the stope and the acting forces, as shown in Figure 4.2.

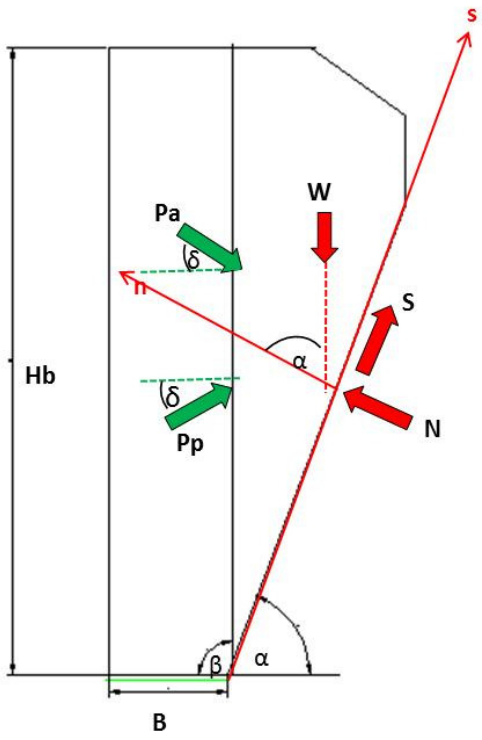

Figure 4.2.Conceptual scheme of the limiting equilibrium analysis

Where:

S: Shear stress in the failure plane.

N: Normal stress in failure plane.

Pp: thrust on the wedge due to broken rock filling the stope when the ore is not being drawn.

Pa: thrust on the wedge due to broken rock filling the stope when the ore is being drawn

W: weight of the wedge.

B: Length of the footprint.

δ: friction angle between the broken rock and the stope walls[22].

α: Inclination of the sliding plane

The acting forces on the sliding plane (normal and tangential) are summarized in the following equations:

$$N = Wcos(\alpha) + P_A[sen(\alpha)sin(\delta+\beta) - cos(\alpha)cos(\delta+\beta)] \quad \textbf{Equation 14}$$

$$S = Wsin(\alpha) - P_A[cos(\alpha)sin(\delta+\beta) + sin(\alpha)cos(\delta+\beta)] \quad \textbf{Equation 15}$$

The thrust for the active and passive are given by Equation 16 and Equation 17.

$$P_A = \frac{1}{2}\gamma_{flow}{H_B}^2\left\{\frac{\csc(\beta)\sin(\beta-\phi)}{\sqrt{|\sin(\beta+\delta)|}+\sqrt{\left|\frac{\sin(\phi+\delta)\sin(\phi)}{\sin(\beta)}\right|}}\right\}^2 \quad \textbf{Equation 16}$$

$$P_P = \frac{1}{2}\gamma_{caved}{H_B}^2\left\{\frac{\csc(\beta)\,\mathrm{si\,n}(\beta+\phi)}{\sqrt{|\sin(\beta-\delta)|}-\sqrt{\left|\frac{\sin(\phi+\delta)\,\mathrm{si\,n}(\phi)}{\mathrm{si\,n}(\beta)}\right|}}\right\}^2 \quad \textbf{Equation 17}$$

Where:

ϕ: Friction angle of the broken rock

β:Inclination of the retaining wall

δ:Friction angle between the wall and the wedge

The weight of the wedge (see Equation 18) can be calculated using geometrical parameters of the stope section as presented in Figure 4.3.

$$W = \gamma\left[\frac{kn}{m3}\right] \times \left[\frac{L3 \times L4}{2} + L4 \times L6 + \frac{L2 \times L1}{2} + L2 \times L3\right] \quad \textbf{Equation 18}$$

[22] The wall friction angle depends on the nature of the wall and the wedge. Its value ranges from ϕ /2 to 2/3 ϕ (Raj, 2007). For the case of study, it will be equal to the friction angle ϕ of the model media.

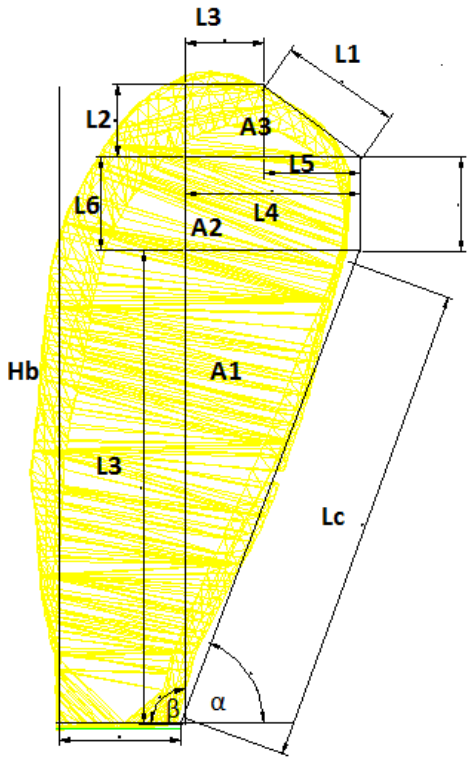

Figure 4.3. Parameterization of the geometry for the FW wedge.

Therefore, by parameterizing the geometry of the stope and the acting forces, the safety factor can be calculated as in Equation 19.

$$FS = \frac{Ntan(\phi)}{S} \qquad \textbf{Equation 19}$$

$$FS = \frac{(Wcos(\alpha) + P_A[sen(\alpha)sin(\delta+\beta) - cos(\alpha)cos(\delta+\beta)])}{Wsin(\alpha) - P_A[cos(\alpha)sin(\delta+\beta) + sin(\alpha)cos(\delta+\beta)]}tan(\phi)$$

4.4. Inputs for the analysis

In order to carry out the limiting equilibrium analysis, it will be needed some input parameters of the caved rock detailed below in Table 4.1.

As detailed in the previous section, by generating the limiting equilibrium equations, for each section of the stope, the weight of the wedge will be required. It will also be required the angle of the failure plane and the height of the stope for each section.

Table 4.1. Inputs of the caved rock for the analysis

δ	[°]	32
γflow	[kN/m3]	1.6
γcaved	[kN/m3]	1.9
ϕ	[°]	32
c	[kPa]	0

The analyzed sections for the Eastern Primary Stope are detailed in Figure 4.4 presenting a plan view of the stope. Figure 4.5 presents the section views with their correspondent geometrical parameters at a 1/200 scale.

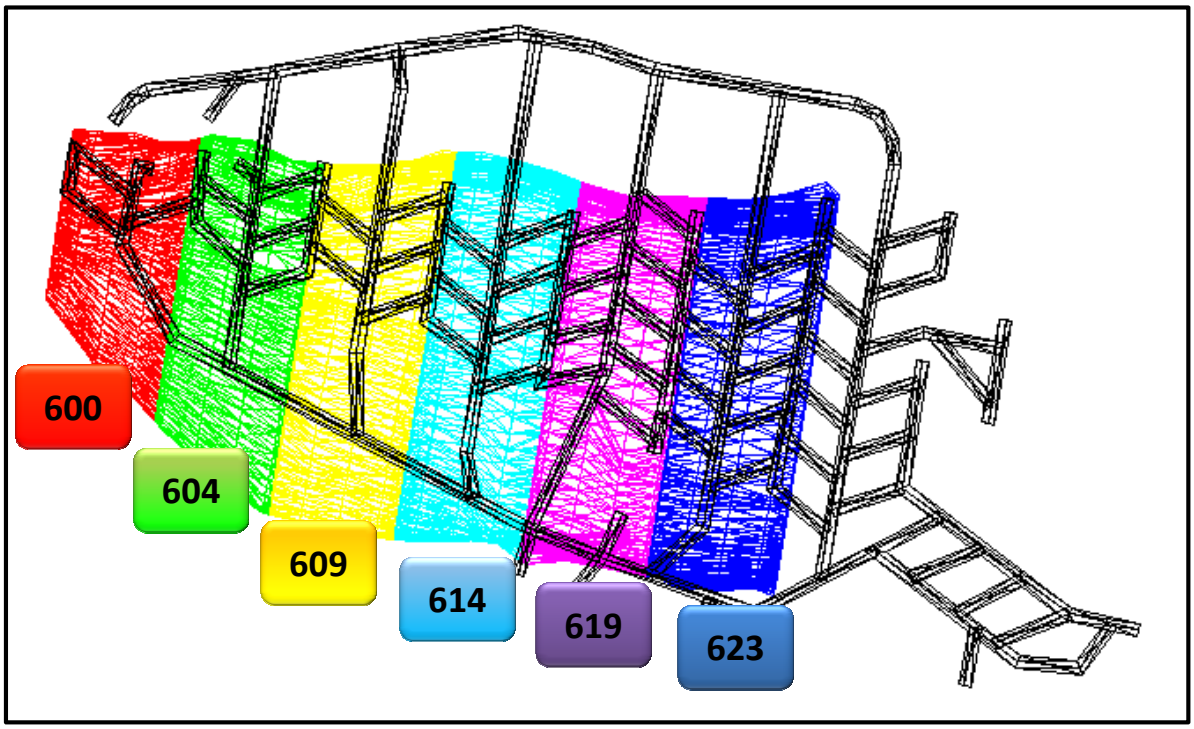

Figure 4.4. Plant view of the Eastern Primary Stope including the identifications of each section.

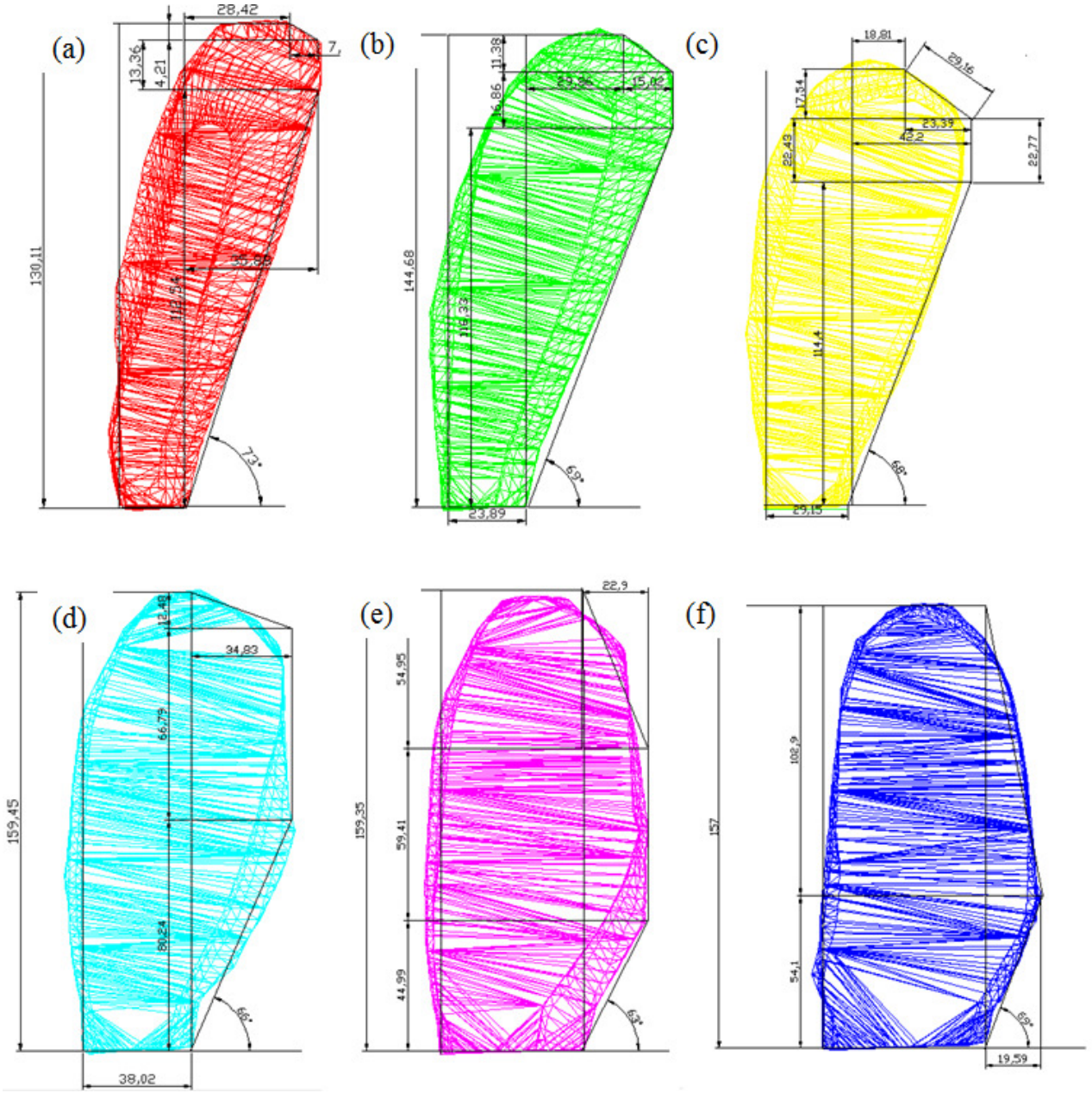

Figure 4.5.(a)Section 600.(b)Section 604.(c)Section 609.(d) Section 614.(e) Section 619. (f) Section 623

4.5. Main results and discussions

As discussed in Section 4.3, the safety factor can be calculated using the Normal and Shear stresses along the failure plain. Since the material is granular, there's no cohesion and therefore the Safety Factor can be calculated using Equation 19.

The factor of safety or the analyzed for the different sections is calculated and the results are summarized in Table 4.2 using the basic friction angle φ_b

Table 4.2. Factor of safety for the limiting equilibrium analysis using the basic friction angle.

Section [#]	FS Active	Tonnage Wedge [ton]	Ore Wedge/ Ore Section [%]	Failure
600	0.57	947,911	40.49	YES
604	0.60	1,365,261	36.57	YES
609	0.70	1,420,577	45.01	YES
614	0.73	1,418,765	16.25	YES
619	1.06	901,729	7.86	NO
623	1.10	553,613	16.30	NO

Founded on the limiting equilibrium analysis and according to the safety factor, for the sections 600, 604, 609 and 614 the wedge will be mobilized, although it can't be quantified the failure rate for the wedge. On the other hand, for sections 619 and 623 the wedge on the footwall won't move at all, since there's no shear enough.

However and since the percentage of ore located at the footwall for section 609 is about a 45% of ore reserves, this is the most critical section to be analyzed and therefore it will constitute the basis of the physical model, being a fundamental factor for the success of the implemented mining method.

Yet a natural discontinuity surface in hard rock is never as smooth as a sawn or ground surface of the type used for determining the basic friction angle. The undulations and asperities on a natural joint surface have a significant influence on its shear behaviour. Generally, this surface roughness increases the shear strength of the surface, and this strength increase is extremely important in terms of the stability of excavations in rock.

For the case of study, the failure plane can be assumed as a discontinuity and therefore, the shear strength of Patton's saw-tooth specimens can be represented by Equation 16.

$$\tau = \sigma_N \tan(\phi + i) \qquad \textbf{Equation 20}$$

Where :

$\phi_{b:}$ is the basic friction angle of the surface and

i : is the angle of the saw-tooth face or dilation angle.

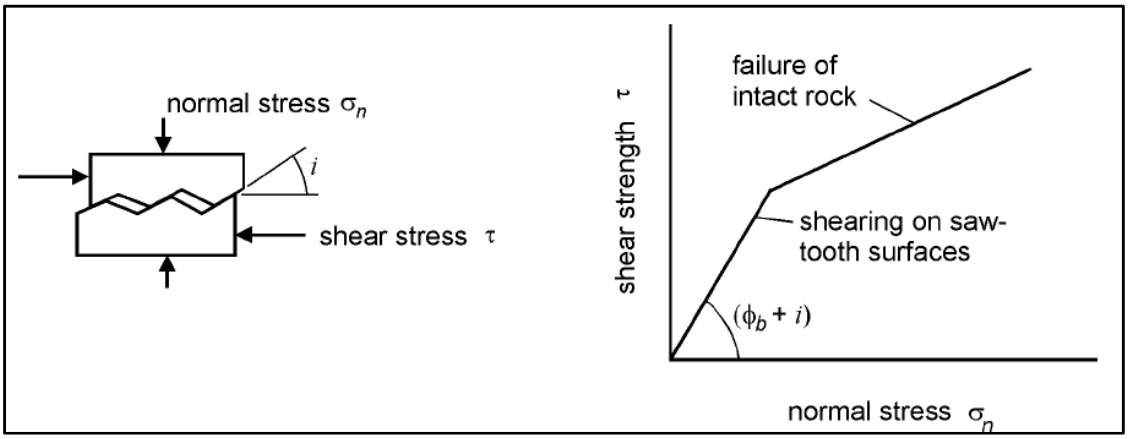

Figure 4.6. Patton's experiment on the shear strength of saw-tooth specimens.

Since there's no information regarding to the surface roughness, a sensitivity analysis for the safety factor is carried out for the dilation angle *i*.

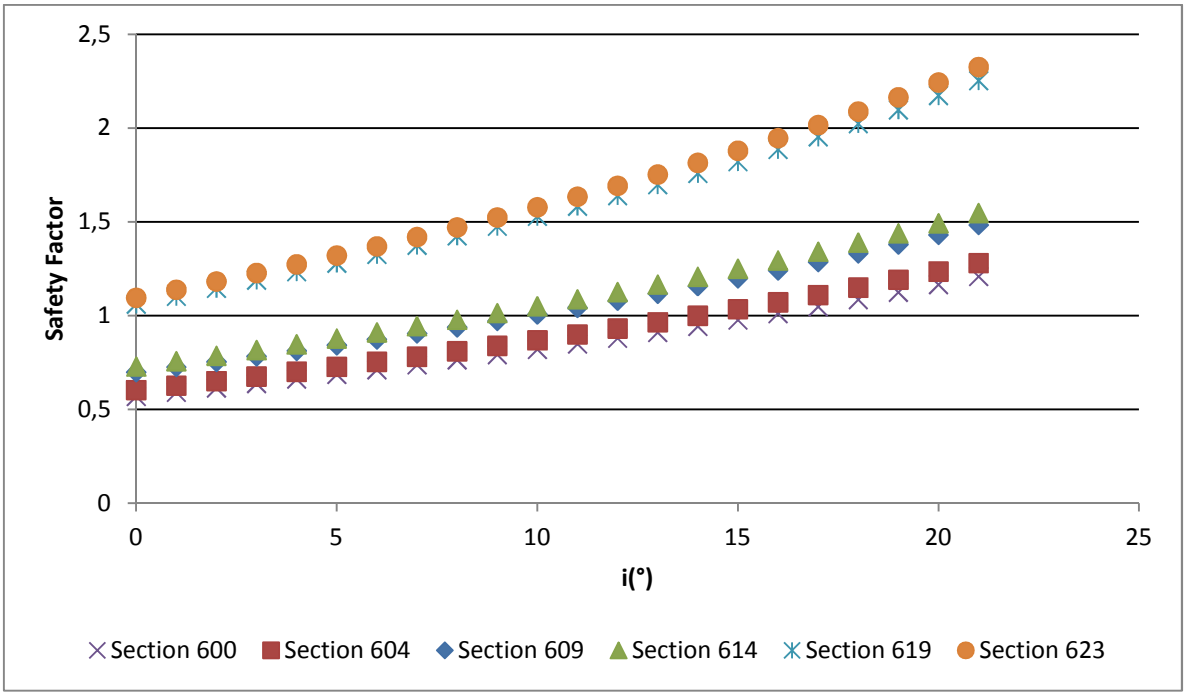

Figure 4.7. Sensitivity analysis for the safety factor varying dilation angle.

As presented in Figure 4.7, it can be comment that the base case presented in Table 4.2 is equivalent to a dilation angle equal to zero. However, if the dilation angle varies, there's the chance that the footwall wedge won't fail. For instance, if dilation angle is above 10°, the wedged will not fail for any section of the stope.

CHAPTER 5

RESEARCH METHODOLOGY

This chapter describes the research methodology for the physical modeling. It includes a similitude analysis based on the experimental frame defined in Chapter 3 in order to define a simplified model for gravity flow in the Eastern Primary Stope. The experimental frame justifies the methodology and determines the boundary and initial conditions of each experiment. The chapter also includes a description of the experimental set up, including all installations and equipment used to characterize the model media and measure the extraction and movement zones.

5.1. Introduction

As described in Chapter 3, the success in the use of reduced scale models for studying diverse physical systems is based on the fact that physical quantities can be fully described by the fundamental laws of mechanics. The effectiveness of a reduced model depends on the degree of similitude that it has with respect to the prototype.

This chapter therefore, delineates and justifies the research methodology used in this thesis. It describes the similitude analysis conducted in order to justify the materials, boundary conditions and experimental procedures adopted to study the gravity flow for the Eastern Primary Stope. The purpose is to define a set of assumptions and limitations of the method within the framework of this research.

The chapter also includes in detail the experimental set up based on the limiting equilibrium analysis developed in Chapter 4, as well as the main components of the laboratory where the experiments are conducted. In addition is incorporated a description of the instrumentation to determine the movement and extraction zones. The Chapter finishes with a description of experimental steps or testwork procedure.

5.2. Similitude analysis in granular flow for the Eastern Primary Stope

5.2.1. Conditions required for similitude

For the stipulated assumptions determined in Chapter 2 the analysis of similitude shows that the gravity flow patterns in model and prototype will be similar if:

1- There is geometrical similitude for the complete geometry. This includes the stope dimensions (height and area of draw), drawpoint dimensions and the particle size distribution

$$\lambda_L = 1{:}200$$

2- Gravity and bulk density in the model and the prototype are the same:

$$\lambda_G = \lambda_\rho = 1$$

3- The scale of times is related to the geometrical scale by:

$$\lambda_T = \lambda_L^{1/2}$$

4- The scale of stresses is related to the geometrical scale by:

$$\lambda_\sigma = \lambda_\tau = \lambda_L$$

5- The residual friction angles are the same: Dilatancy is a shear strength parameter that depends on the bulk density and stresses.

$$\lambda_{\phi_w} = 1$$

6- Wall friction angles are similar to the internal friction angle:

$$\phi_w = \phi$$

Table 5.1 presents a summary of the similitude analysis conducted at a 1:200 scale.

Table 5.1. Summary of similitude analysis for a 1:200 scale

Variable	**Scale Factor**	1:200
Length	λ_L	0.005
Area	λ_L^2	2.50E-05
Volume	λ_L^3	1.25E-07
Velocity	$\lambda_L^{1/2}$	0.07
Time	$\lambda_L^{1/2}$	0.071
Weight	λ_L^3	1.25E-07
Stresses	λ_L	0.005
Friction Angle	1	1

5.2.2. Effect of particle shape and friction angle on flow

Friction angle is a bulk material constant that depends on the properties of the individual particles, such as rock type, contact roughness, particle shape and the arrangement of grains. In this context, the shape of the particles (rounded or angular) strongly influences the friction angle (Castro, 2006). Moreover, sands that are the model media to be used are characterized for being materials that have experienced a high degree of erosion and in general have a spherical particle shape. Therefore, these effects on the friction angle must be considered when conducting the analysis of results.

Furthermore, by using sand as a model material, it must be taken into consideration that fine materials could change from being purely frictional to cohesive materials as the particle size is reduced and capillarity u electrostatic effects may be in the same order of magnitude of gravity forces. These effects are quantified and discussed below in this Chapter.

On the other hand, the angle of repose is the maximum angle that allows a heap of soil to remain stable without sliding failure. It may be said that the shape of sand deposition is normally cone and sand grains are oriented a certain angle of deposition repose is made. This angle is such that no stability occurs. Thus the angle of repose is somewhat correlated to the sand internal friction angle (Ghazavi, *et al.*, 2008).

Ghazavi *et al*.(2008), conducted tests on three types of sand in which the angle of repose and angle of internal friction were measured separately but at the same density in order to achieve a correlation between them. The authors found that the angle of repose, φ, and internal friction angle, ϕ, were related by the following empirical correlation given by Equation 21.

$$\phi = 0.36\varphi + 21.2 \qquad \textbf{Equation 21}$$

This correlation will be used in order to estimate the model media friction angle.

It must be noticed that it is generally reported that the angle of repose, as the friction angle, increases with increasing sliding and rolling friction coefficients and deviation from spheres, and decreases with increasing particle size (De la Hoz, 2007).

5.3. Defining model conditions for the physical model

5.3.1. Model media

5.3.1.1.Particle size

In the previous section it was shown that physical modeling in granular flow must satisfy a series of rules, determined by the similitude analysis based on the dominant forces governing the phenomenon and other forces affecting gravity flow. The model media, for the case of study needs to be characterized, since, geometrical properties of caved rock that have influence on its flow mechanics are the particles size distribution and the shape (Castro, 2006).

Table 5.2. Particle's size distribution used to scale the particles in the physical model (Agnico-Eagle,Goldex Mine 2011)

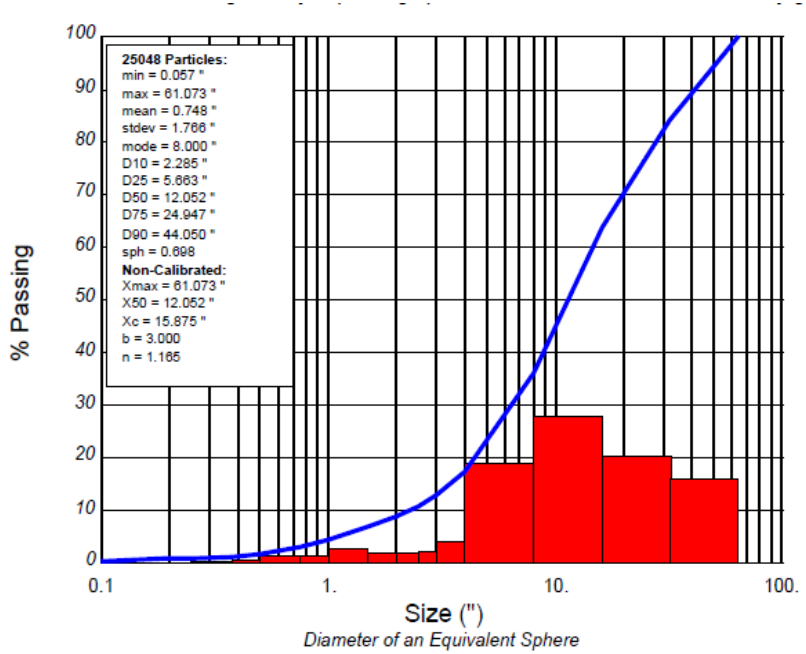

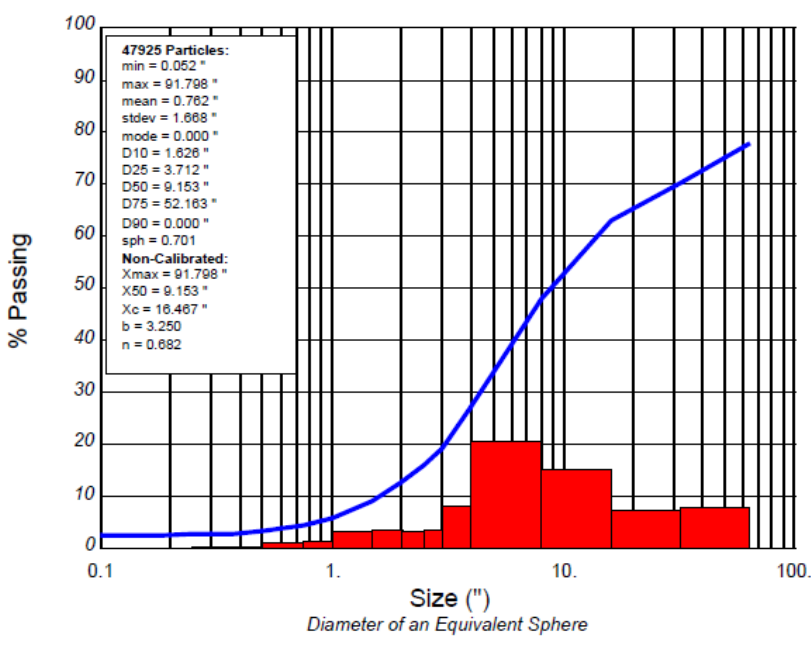

In order to achieve geometric similitude the media used in the physical model is scaled (1:200) according to the blasted rock of Goldex Mine. This is accomplished by using coarse sand with an identical fragmentation as blasted rock at the mine. Based on the information proportioned by Goldex Mine for caved rock, the particle size distribution is plotted as shown in Table 5.2.

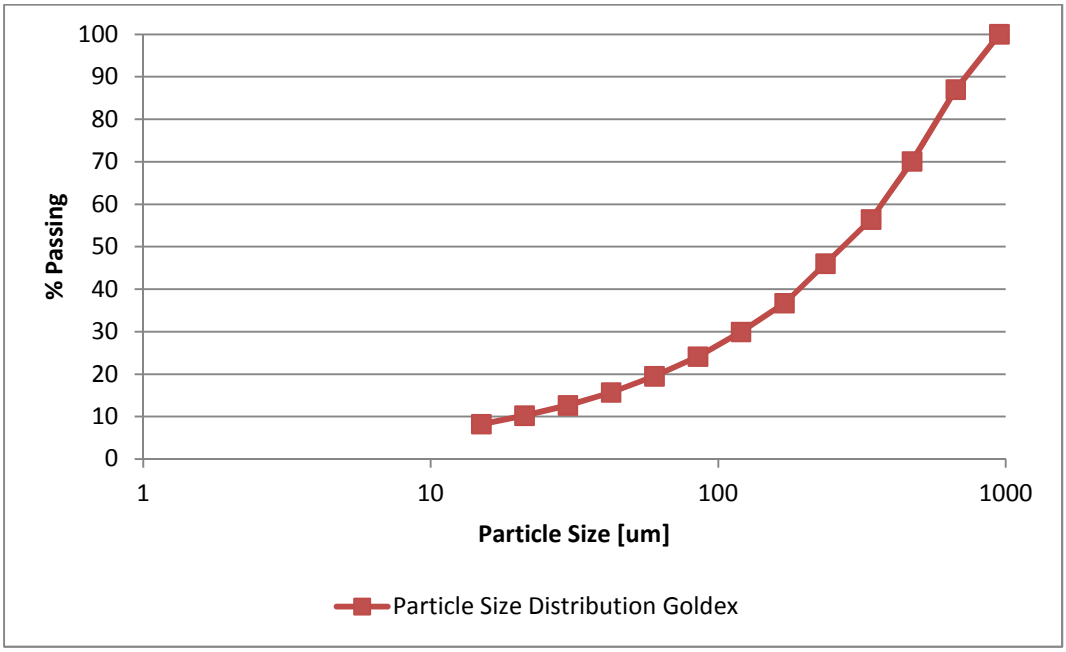

Figure 5.1. Particle size distribution at Goldex.

5.3.1.2.Shear strength parameters

The effective shear strength parameters c (cohesion) and ϕ (friction angle) are defining parameters into the gravity flow mechanisms. Since the material to be used as a model media is a granular material has no cohesive strength. Therefore, in the following it would be only characterized the model media friction angle.

The angle of repose is estimated according to the ASTM C 1444-00. The results are shown in the Appendix C. By using the measured results of the angle of repose, the friction angle can be calculated using Equation 21.

Table 5.3. Estimation of the friction angle for the model media

Test [#]	ϕ [°]
1	31.4
2	32.2
3	31.5
Average	32

It must be alto stated that the bulk density in the model should be close to 1.9 [t/m3] as in the prototype.

5.3.1.3.Forces affecting granular flow for the model media

As discussed on Chapter 3, beyond gravity and friction forces acting on smaller particles, other kinds of forces may develop, affecting granular flow. To determine the effect of these forces on the model media, they be evaluated with the purpose to diminish these effects, by imposing that gravity and friction are the dominant forces.

For these effects it will be considered that many fundamental features of cohesive granular materials do not depend specifically on the nature of interparticle forces, but on the value of the cohesive granular Bond number (Castellanos, 2005), defined as the ratio between the attractive interparticle forces and the particle weight. Based on the hypothesis that gravity is the dominant force it will be evaluated and discussed the effect of the other forces acting on gravity flow behavior. The model media particle size distribution and properties (humidity) will be adjusted to accomplish the similitude analysis.

i- Van der Waals forces:

The Bond Number associated to the Van der Waals Forces is defined by :

$$F_{B\_VdW} = \frac{F_{VdW}}{F_G} \qquad \textbf{Equation 22}$$

In Appendix A, it is stated the value of the Van der Wall force based on the Lifshitz theory for the model media as:

$$F_{VdW} = 8{,}76 \times 10^{-10}[N] \qquad \textbf{Equation 23}$$

Since gravity strongly depends on the mass of the particle the Bond Number is evaluated, for each particle size to be used as model media.

[23] For the detail of the parameters used for calculation, see Appendix A (Section A.1.1)

Table 5.4. Effect of the Van der Walls forces versus the gravity force as a function of the particle size

Sieve	Size	Van der Wall Force	Gravity	F_{B_VdW}	$1/F_{B\_VdW}$
[#]	[um]	[N]	[N]	adim	adim
#6	2800	8.76E-08	2.43E-03	3.60E-05	27774.64
#8	2360	8.76E-08	1.46E-03	6.01E-05	16630.69
#12	1700	8.76E-08	5.45E-04	1.61E-04	6216.14
#16	1180	8.76E-08	1.82E-04	4.81E-04	2078.84
#20	850	8.76E-08	6.81E-05	1.29E-03	777.02
#30	600	8.76E-08	2.39E-05	3.66E-03	273.29
#40	425	8.76E-08	8.51E-06	1.03E-02	97.13
#50	300	8.76E-08	2.99E-06	2.93E-02	34.16
#70	212	8.76E-08	1.06E-06	8.30E-02	12.06
#100	150	8.76E-08	3.74E-07	2.34E-01	4.27
#140	106	8.76E-08	1.32E-07	6.64E-01	1.51
#200	75	8.76E-08	4.68E-08	1.87E+00	0.53

As observed from the results obtained for the Bond Number associated to the Van der Waals Forces, the material smaller than #50 will present a behavior in which the gravity is at least 34 times the Van der Walls force between particles. In addition about 7% of the model media is beyond #50. In order to eliminate the effect of the Van der Waals forces between particles this fraction will be removed from the model media to be used in the physical model. The adjusted particle size distribution can be seen in Figure 5.2

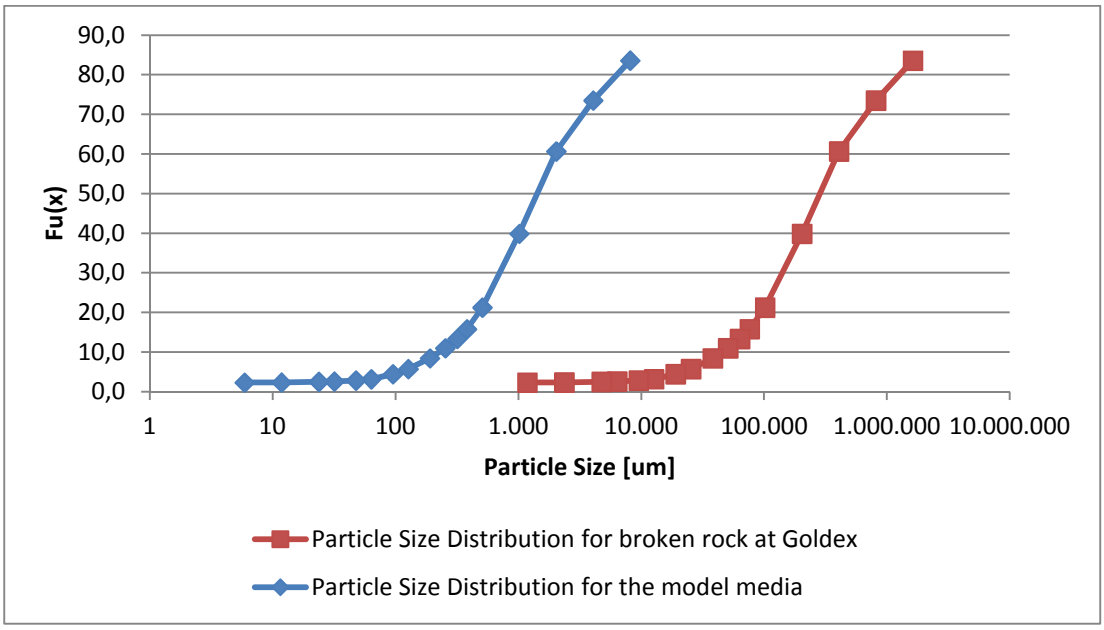

Figure 5.2. Particle size distribution at Goldex and for the model media.

ii- Capillary Forces:

Capillary forces are caused by condensed moisture on the surface of the particle. For two smooth, spherical particles of radius R and a fluid of surface tension γ, this contribution is:

$$F_H = 2\pi\gamma R \qquad \textbf{Equation 24}$$

As stated in Chapter 3, capillarity is dependent, among other factor on the particle radius. Therefore, for each particle size it can be determined its contribution as seen in Table 5.5.

Table 5.5. Effect of the Capillary forces versus the gravity force as a function of the particle size

Sieve	Size	Capillary Force	Gravity	F_{B_H}	$1/F_{B\_H}$
[#]	[um]	[N]	[N]	adim	adim
#6	2800	1.32E-03	2.43E-03	0.54	1.84
#8	2360	1.11E-03	1.46E-03	0.76	1.31
#12	1700	8.01E-04	5.45E-04	1.47	0.68
#16	1180	5.56E-04	1.82E-04	3.05	0.33
#20	850	4.01E-04	6.81E-05	5.88	0.17
#30	600	2.83E-04	2.39E-05	11.81	8.47E-02
#40	425	2.00E-04	8.51E-06	23.54	4.25E-02
#50	300	1.41E-04	2.99E-06	47.24	2.12E-02
#70	212	9.99E-05	1.06E-06	94.60	1.06E-02
#100	150	7.07E-05	3.74E-07	188.96	5.29E-03
#140	106	5.00E-05	1.32E-07	378.40	2.64E-03
#200	75	3.53E-05	4.68E-08	755.86	1.32E-03

The analysis shows that capillary forces can be very strong if the moisture of the model media is considerable. In order to avoid this effect, the model media is dry in ovens, diminishing the moisture almost completely. Therefore, the effect of capillarity can be neglected.

iii- Electrostatic Forces:

It has been found that for fine particles, electrostatic charging invariably arises due to the tribo-electric charging phenomena; this effect generates a prevalence of the Van der Waals forces. Therefore since the effect of Van Der Waals forces is diminished by removing a fraction of the particle size distribution, effect of electrostatic forces can be neglected.

iv- Magnetic Forces

A rather specific additional attraction may arise when the particles can be magnetized. Depending on the degree of magnetization, very high attraction forces can be achieved.Since the material is not magnetized this effect can be neglected.

5.3.2. Boundary Conditions

The boundary conditions in terms of gravity flow studies are given by the height of draw, which in this case is represented by the height of the stope. Additionally, boundary conditions to consider are the area of draw, the drawpoint dimensions and the boundary roughness.

The boundary conditions of the physical model for a given scale $\lambda_L = 1:200$ should satisfy the following:

- The height and all the dimensions of the stope are given by the geometrical scale factor $\lambda_L = 1:200$
- The dimensions of the drawpoints are also scaled by λ_L as well as their position.
- The area of draw incorporates 11 drawpoints for section 609.
- The walls in the model should represent a rough wall. This is accomplished by gluing the media on the footwall and the hanging wall of the stope. The end walls are smooth walls representing and infinite stope.

5.3.3. Extraction and method of draw

Currently the extraction of blasted rock at Goldex Mine is carried out using load-haul-dump (LHD) equipment. The extraction rate to be simulated corresponds to an average draw rate of 174 tons per drawpoint per day, similar to the simulations performed in FLAC3D.

The instantaneous draw rate in the scale model is given by:

$$\lambda_Q = \lambda_L^{5/2}$$

This means that in a scaled model the draw rate must be considerably smaller than in the mine according to the geometrical scale factor. The scaled draw rate will be equivalent to 0.21 [gr/min]; this draw rate it is very difficult to achieve because of the time it would take each experiment (about 200 days), therefore to replicate this draw rate would be unfeasible.

It was settled to use a draw rate of 21 [gr/min] for the extraction of each drawpoint for practical reasons. Although the extraction rate is not scaled, it will give an idea of the mechanisms governing failure of the footwall ore as well ore recovery.

5.4. Design for the physical model

In the following is described the design of the section to be modeled, in order to develop the construction and set up of the physical model.

5.4.1. Design for level 76 and section 609

The section 609 was chosen in function of the amount of reserves located in the footwall wedge and the limiting equilibrium analysis conducted for the different sections of the ore body (see the detail in the Chapter 4).

The conceptual design for the physical model is described in the following figures (Figure 5.3). The section 609 has 11 drawpoints, and all the geometries were scaled according to the similitude analysis replicating the stope geometry.

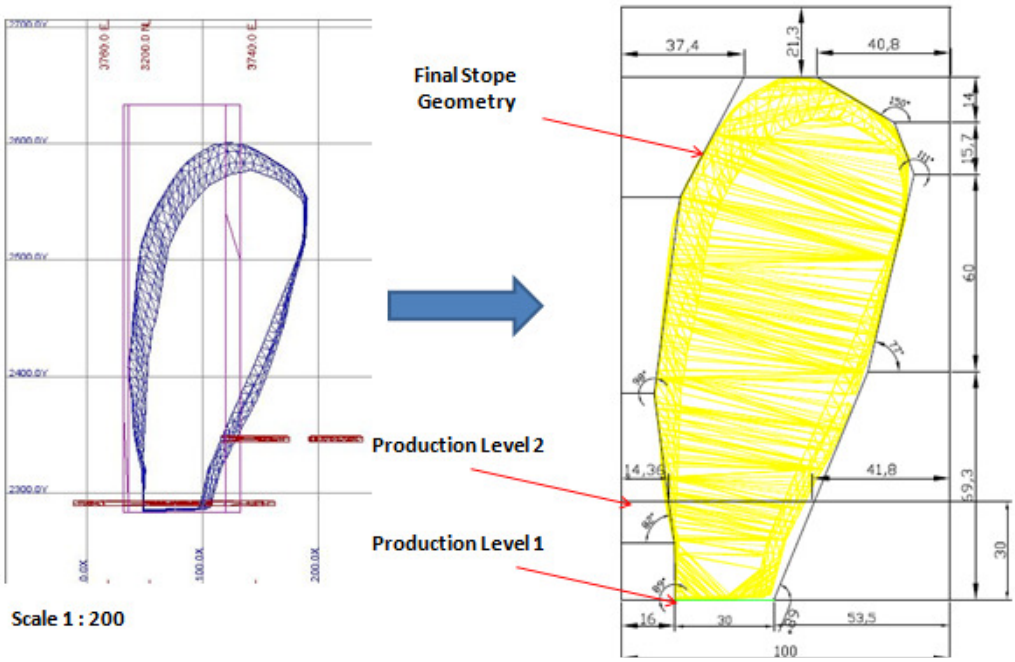

Figure 5.3. Conceptual design for section 609. Scale 1:200. Measures in cm

The main structure is supported by an iron frame, as shown in Figure 5.4.

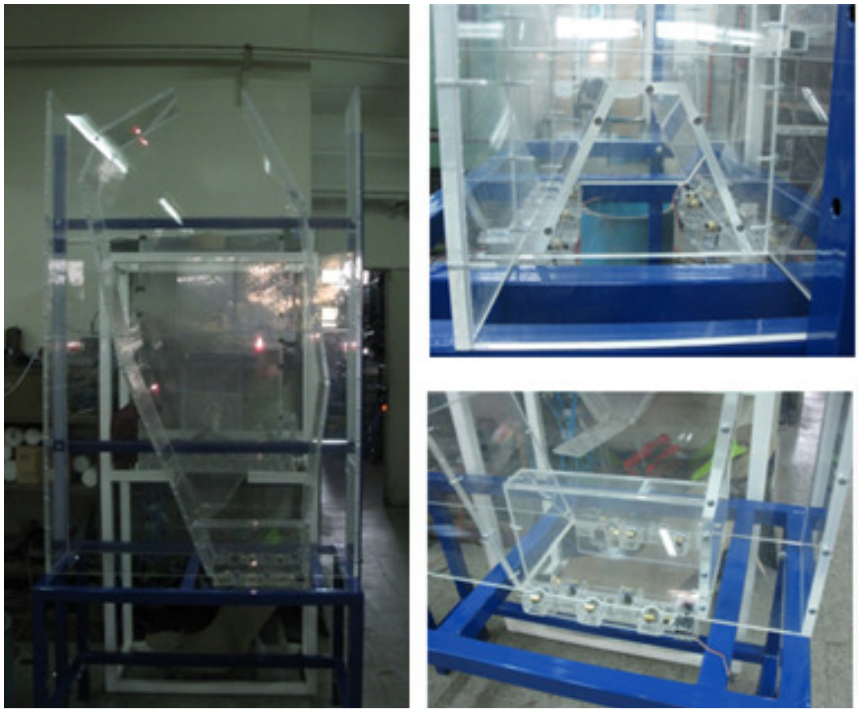

Figure 5.4. (Right) Physical Model. (Left) Drawpoints Level 76 and apex through section 609.

Based on the current layout at Goldex (Level 76), the extraction level for the physical model was designed as presented in Figure 5.5.

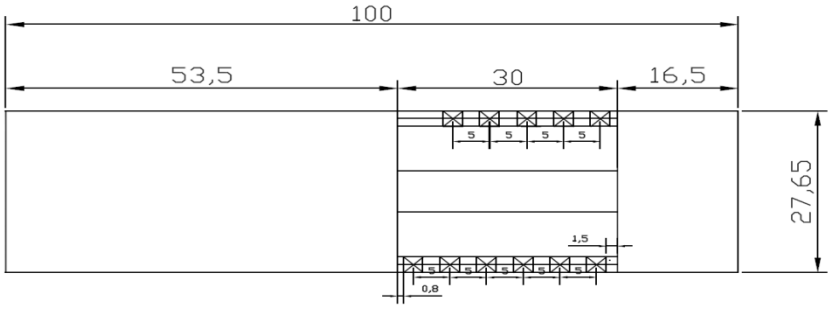

Figure 5.5.Plan view of the design for level 76.All measures in cm. Scale 1:200.

5.4.2. Experimental Set Up

The physical model obtained was built at the Block Caving Laboratory, University of Chile. The model consists on the following components:

1. **Main Assembly:** The assembly consists of four dismountable Plexiglas walls that delineate the final geometry of the stope for the section 609.The base of the assembly incorporates the extraction system (11 drawpoints and the drawbell geometry). The plexiglass assembly is supported by four vertical steel columns and

6 horizontal rows that give the structure the needed stability. The maximum dimensions of the model are 1.6 m height x 1 m length x 0.25 m width.

2. **Loading system:** The material is loaded manually. Coarse sand is stored in big jars and it's handled using ladles .During the filling of the material, the sand is loaded into the model and compacted reaching the bulk density of the material in the mine. At the same time material is being loaded the labeled markers are positioned in the model.
3. **Extraction material system:** It consists in 11 drawpoints, where each one has a shovel installed. These shovels are linked to a servomechanism that gives an electrical impulse and simulates the LHD extraction. The servomechanism is controlled by software that allows varying the extraction rate.

5.4.3. Instrumentation

5.4.3.1.Labeled Markers

The extraction zone is defined by the envelope that encloses the material that has been drawn from the drawpoints. With the aim to determine this zone labeled markers are used; these markers are obtained from the maximum size of the model media. Each labeled marker is painted with different colors using spray, being the color the characteristic representing the position in the vertical axis. At the same time, the markers are labeled with numbers identifying its initial position in the physical model in the horizontal plane, as shown in Figure 5.6.

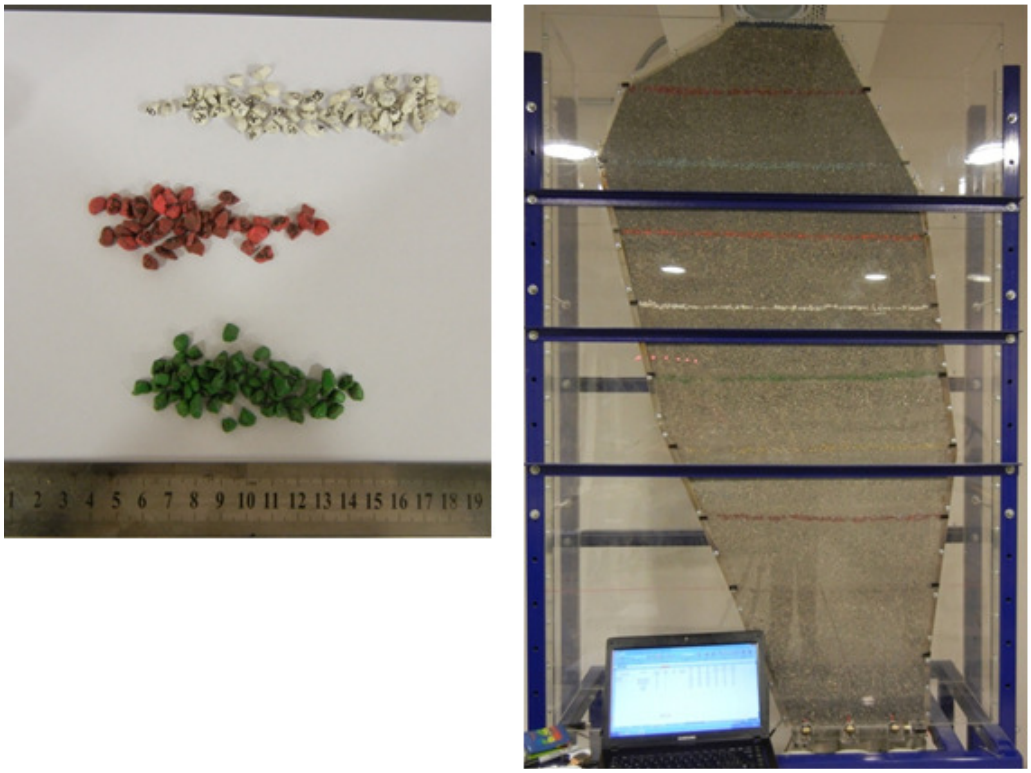

Figure 5.6.(Left) Labeled markers used during experiment 1. (Right) Markers placed in the physical model

Markers were recovered and its label recorded along with the mass drawn and exit time, by an observer located next to the drawpoints. Since the initial position of the recovered markers is known as the mass at which they appear at the drawpoints it was possible to draw the contours that define the extraction zone.

5.4.3.2.Extraction system

The extraction system for the drawpoints consists in a servomechanism device and software developed by the Block Caving Laboratory, so the extraction is controlled by a computer software (see Figure 5.8). Each drawpoint has a small shovel that draws the material out; these shovels are linked to the servomechanism device as shown in Figure 5.7. The servos used for the extraction system, are typical of aeromodelling and consist in a device similar to a DC motor that have the ability to be in any position within its operating range, and remain stable in that position; these servos have the capacity to be controlled both in speed and position.

As commented before, the system allows changing the rate of extraction for the drawpoints varying the velocity of the servomechanism.

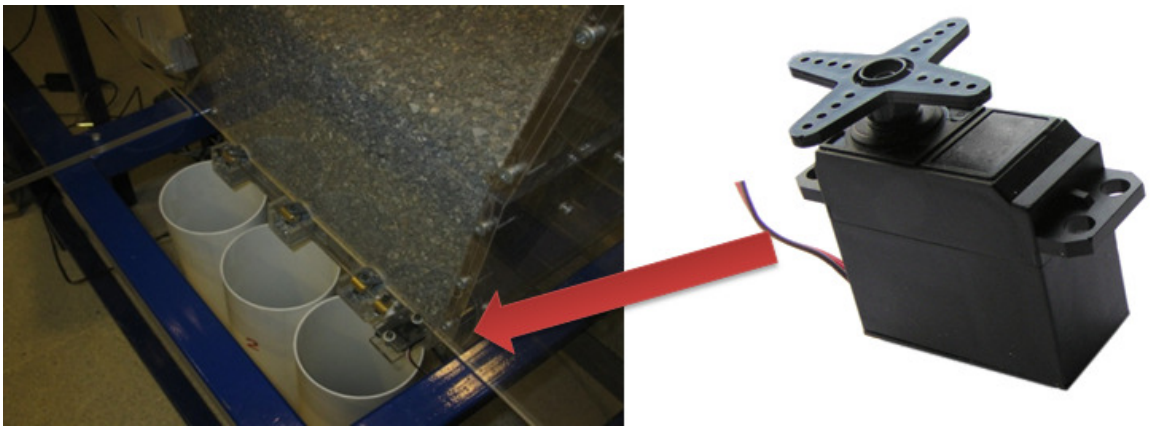

Figure 5.7. Drawpoints and extraction system activated by the servomechanism

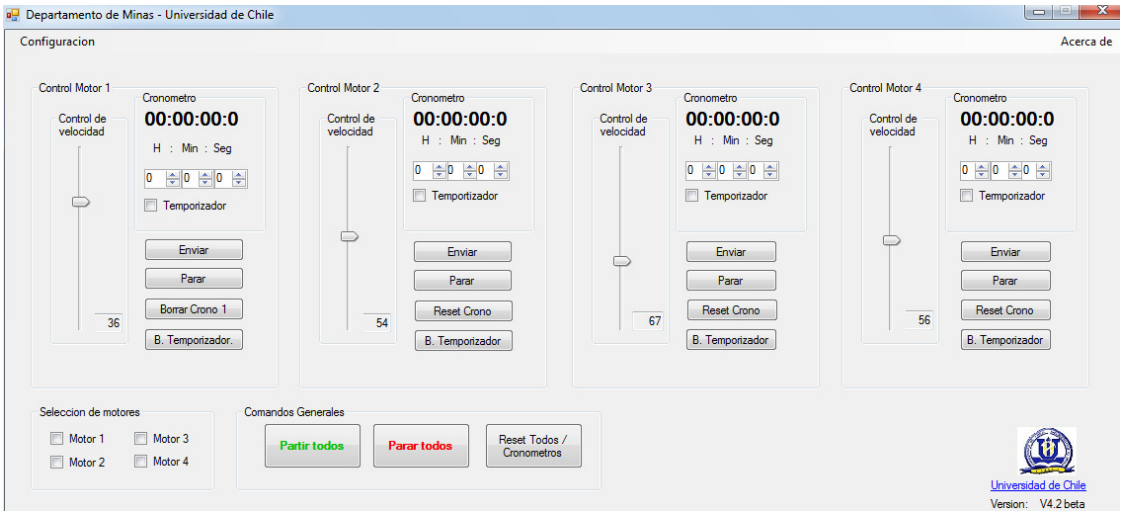

Figure 5.8. Software developed for the extraction system

5.5. Experimental frame

5.5.1. Methodology for the experimental study

In the present research the mobility of the ore located in the footwall of the Eastern Primary Stope for Goldex Mine will be studied. Based on the physical model results, a draw strategy or a new design that will maximize the ore recovery will be proposed, also it will be determined the dilution entry mechanism for a unstable case.

The physical modeling considers a series of stages outlined below:

1. **Similitude analysis.** It defines the scale factors for the variables of interest. These factors depend on the forces that dominate the phenomenon, as well as material characteristics of the prototype (mine) and the material to be used in the model. Based on the assumptions made at this stage the restrictions and limitations of the results of the model are defined. The similitude analysis is shown in detail in Chapter 3.

2. **Construction of the physical model and the extraction system.** In this stage the model will be constructed based on the similitude analysis.

3. **Diagnosis and calibration of the model.** At this stage in the laboratory the experiences will be started in order to verify the correct operation of the extraction system according to the experimental plan based on the proposed design and the background observed in the mine. The relevance of this stage is to identify the limitations of the system.

4. **Experiments:** Following the aforementioned stages and once the experimental equipment has been built; the experimental procedure is performed in order to understand the granular flow behavior as the material is extracted from the drawpoints, guided by the experimental plan.

5. **Proposals for further studies and design.** As a final outcome from the experiments the draw mechanism governing the gravity flow for the Easter Primary Stope is determines. These results will help to improve ore recovery and minimize dilution. In case it is needed, the construction of another extraction level to recover the immobilized ore of the footwall will be proposed.

5.5.2. Experimental Plan

This section considers a description of the experimental plan and the particular experimental objective to be developed. The experimental plan (detailed in Table 5.6 and Figure 5.9) is based on the objectives proposed in section 2.1 (Project Objectives) and is settled with the aim to define the failure mechanisms of the FW and potential draw recovery at production level at Goldex Mine.

The experimental results are presented in the next chapter.

Table 5.6. Experimental plan

Experiment	Draw strategy	Objective
1	**Isolated raw**	To determine isolated flow zone diameter geometry and to test the proper operation of the model.
2	**Uniform draw**	To determine the potential failure of the broken rock located at the FW of the main stope and to quantify primary ore recovery when drawing from level 76.
3	**Uniform draw**	To determine the potential failure of the broken rock located at the FW of the main stope and to quantify primary ore recovery when drawing from level 76 and from the proposed new level 73.
4	**Uniform draw**	This experiment is a duplicate from experiment 3, in order to quantify the experimental error and results accuracy.
5	**Uniform draw**	This experiment simulates continuous dilution entry at the top of the stope. The aim is to quantify potential dilution entry mechanism and ore recovery for a unstable case.

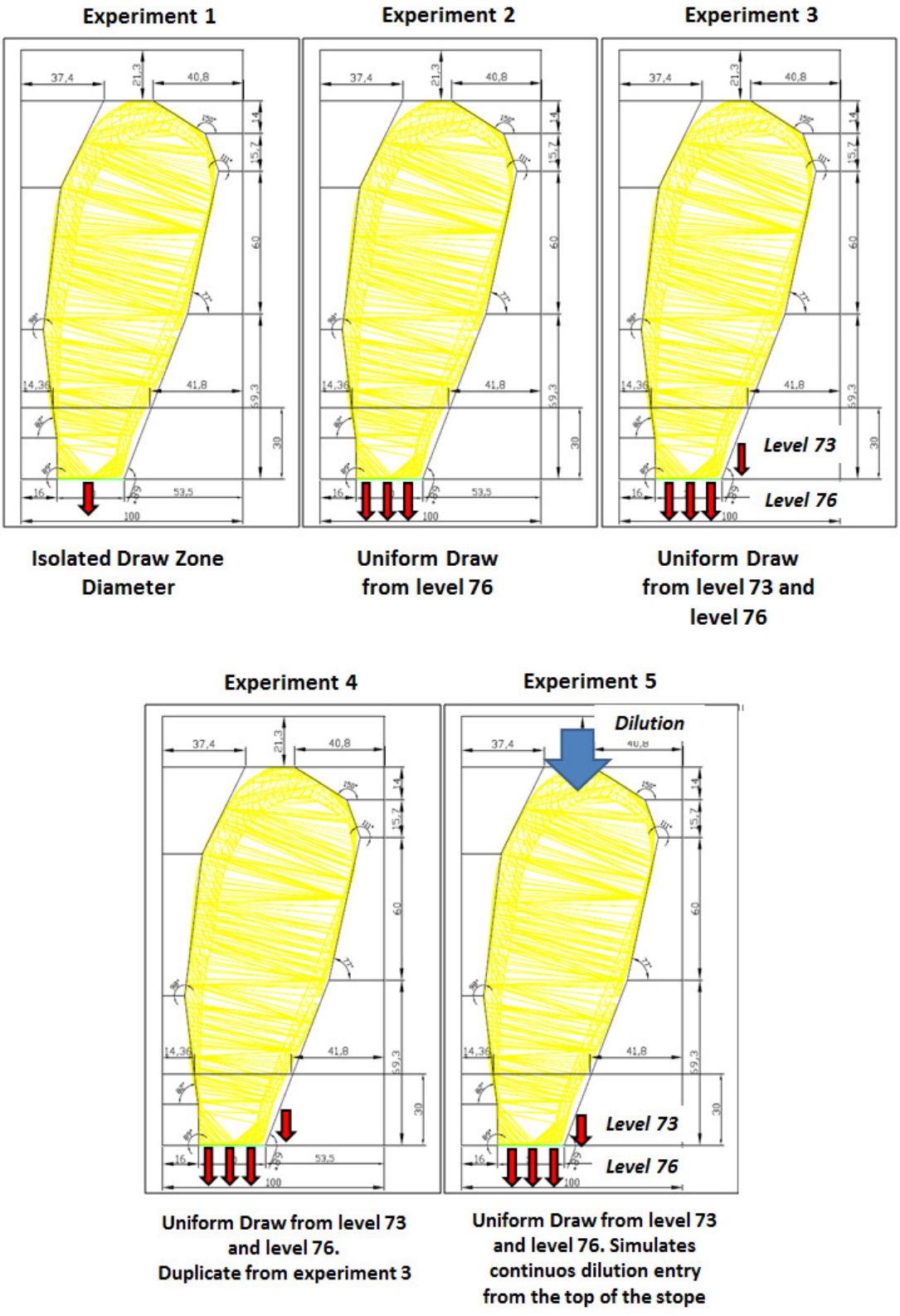

Figure 5.9. Scheme of the experimental plan

5.6. Testwork procedure

The following is the description of the testwork procedure conducted for each experiment. The routine considers the next steps:

1. **Material preparation:** Previously conducting the experiments coarse sand is adjusted by sieving to the Goldex Mine particle size distribution. The material is dried in an oven, in order to eliminate the humidity effect and capillarity between grains. As discussed before, the markers are painted and labeled in order to identify them during extraction. If refilling is needed, the model media is dyed using red dust for simulating dilution entry.

2. **Calibration of the extraction system**: Before filling and also during the experiments, the extraction system is calibrated by changing the servomechanism velocity; also the angle of the blades located at each drawpoint is varied. This calibration is conducted during the all experience in order to achieve uniform draw between drawpoints.

3. **Filling**. During this stage the material is loaded in the physical model using ladles. Each loaded layer of the physical model will emulate the bulk material density at Goldex Mine, and therefore the material is weight out before loading. After the amount of loaded material is enough to reach a level of markers, loading is stopped and labeled markers are placed by using a plank on the surface as the location of each markers recorded. For experiments considering dilution, when the IMZ reaches surface, the dyed model media is loaded at the top of the physical model emulating dilution entry.

4 **Extraction process.** In the extraction process material is removed from drawpoints by means of the servomechanism device. The conducted extraction is uniform and each cycle of extraction is of about 10 minutes. For each cycle of extraction, the material of each drawpoint is dumped into a PVC tube, and then markers are recovered. As the markers are recovered, their labels, the accumulated mass drawn and time are recorded.

5.7. Conclusions

In this chapter it was described the research methodology used for the implementation of a simplified physical model for the Eastern Primary Stope. The research methodology includes.

- Similitude analysis, concerning to the conditions required for similitude and the effect of the material characteristics on flow.
- Definition of the model conditions, concerning to the model media characterization, the shear strength parameters and the effect of forces affecting granular flow.
- Boundary conditions, concerning to the extraction and method of draw.
- Experimental Set Up, concerning to the design of the physical model and the experimental set up as the instrumentation to be used
- Experimental frame, concerning to the experimental plan and the test work procedure to be conducted for each experience.

In the next chapter are presented and analyzed the results of the experiments conducted, using the methodology stated previously.

CHAPTER 6

PHYSICAL MODELING EXPERIMENTAL RESULTS

This chapter presents the results and analysis of the experiments conducted in the physical model of a 50 m section of the Eastern Primary Stope at Goldex Mine. The experiments conducted aim to understand the gravity flow behavior of broken rock and the governing mechanism for the failure of the footwall of the stope by means of an axisymmetric physical model with multiple drawpoints.

The chapter includes the results of an Isolated Draw Zone test, and the results from the experiments carried out performing a multiple drawpoint extraction in the model for the different drawing and design strategies proposed. As a result from the first experiments a new extraction level is proposed and tested. The results are analyzed and the effects on ore recovery for the different flow mechanisms observed and the dilution entry mechanism (for an hypothetical unstable case) are discussed.

6.1. Introduction

This chapter presents the results of the experimental plan detailed in Section 5.5.2 for the physical model of the Eastern Primary Stope considering the current mine conditions. The experiments for different draw scenarios and design strategies at a defined scale (1:200) were conducted in the Block Caving Laboratory of the University of Chile. The purpose of these experiments was to quantify the ore recovery for the footwall of the Eastern Primary Stope and determine the draw mechanism governing flow for a stable case (without dilution) and a unstable case (with dilution) in order to propose a design to increase ore recovery.

In a first stage an Isolated Draw Zone experiment was performed to estimate the IMZ diameter .This result was used to eventually propose the design of a new extraction level constructed at the footwall of the stope. The test was also used to calibrate the correct operation of the extraction system for the physical model.

The second experiment conducted was a multiple drawpoint extraction under concurrent draw, this is the base case, and it's performed to determine the potential failure of the broken rock located at the footwall of the main stope using the current mine conditions. The next experiments use the results from the IMZ test. The initial design is modified by adding a new extraction level –located 30 meters above level 76- with the purpose to observe the gravity flow mechanism due to extraction from both levels. The experiment considers drawing until the equivalent of the planned extraction from level 76 is finished. Once this extraction was completed, a simultaneously and uniform extraction from both levels was performed. This experiment is duplicated to obtain an experimental error and to enhance the precision of the results.

Finally an experiment simulating dilution entry at the top of the stope was performed. The objective was to quantify potential dilution entry mechanism and ore recovery, as well as the governing mechanism for dilution entry for an unstable case. For each experiment ore recovery and the mobilized zone are obtained using the information from the extracted markers. The markers were labeled and their initial position is known ; by means of these positions it was possible to determine the immobilized ore from the stope due to extraction as the ore recovery. The interpolation and the plotting are conducted using a MATLAB subroutine included in Appendix D.

6.2. Experimental Results

The experimental results are performed based on the experimental plan described in Section 5.5.2. Below are displayed the obtained results and its main discussions.

6.2.1. Experiment 1

6.2.1.1.Description and main results

The isolated movement zone was analyzed using colored markers as explained in the previous section. For this experience the extraction was conducted only in one drawpoint. Once the IMZ reached the surface of the stope the extraction is completed (see Figure 6.2) and the isolated movement zone diameter was measured for different heights.

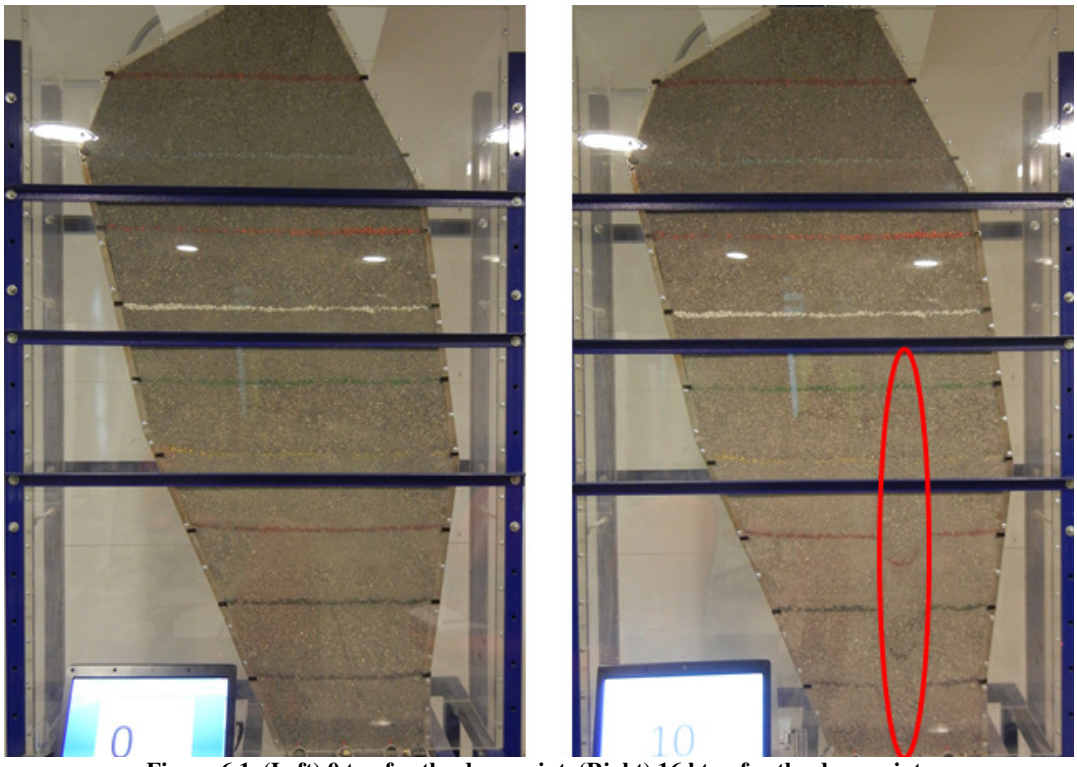

Figure 6.1. (Left) 0 ton for the drawpoint. (Right) 16 kton for the drawpoint.

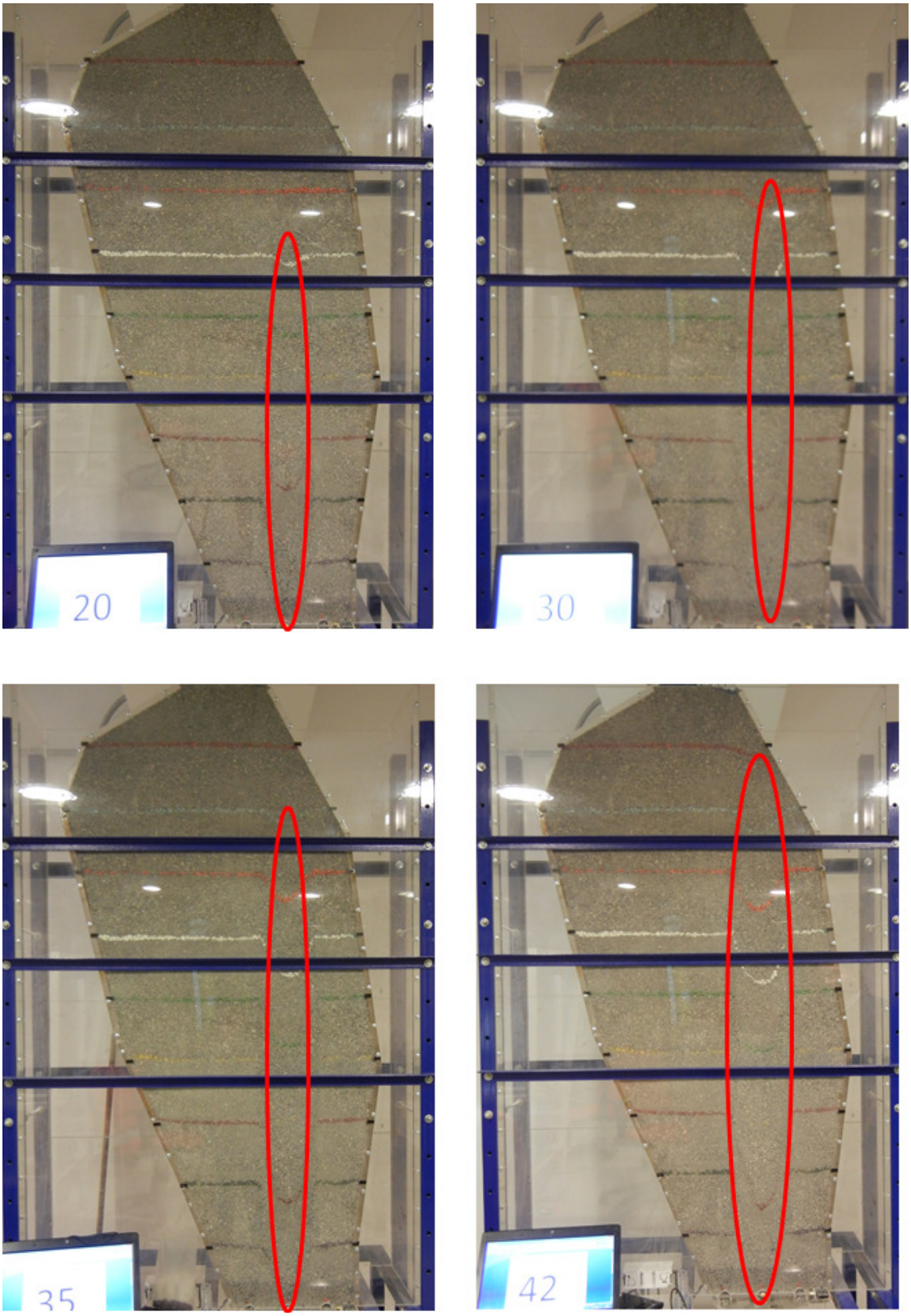

Figure 6.2. (Left Up) 33 kton for the drawpoint. (Right Up) 49 kton for the drawpoint. (Left Down)58 kton for the drawpoint. (Right Down) 68 kton for the drawpoint-IMZ reached the surface.

The results from the measurements of the final isolated movement zone are presented in Figure 6.3.

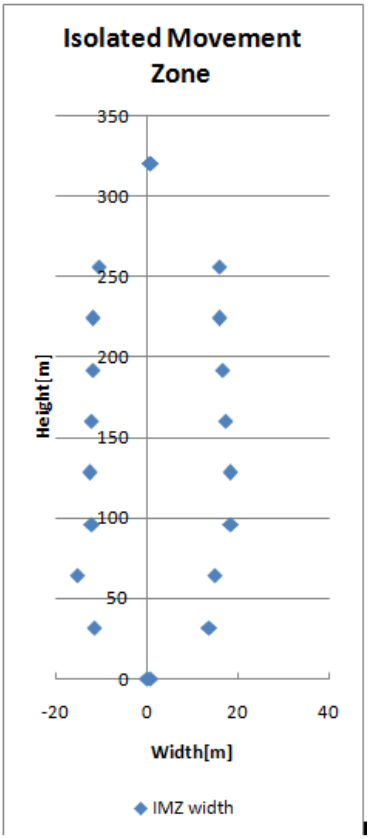

Figure 6.3. Isolated Movement Zone

The maximum width of the IMZ will determine the connection with the low porosity zone due to the extraction from level 76. This width results in 15.4 cm in the model, that scaled is equivalent to 30.8 m in the prototype (mine scale).

6.2.2. Experiment 2

6.2.2.1.Description and main results

As an antecedent of the mobility of the FW wedge it was known the research developed by ITASCA, using FLAC3D described in Section 2.4. In this study it was established the mobility for the FW wedge using the current production level. It was also investigated the mobility of the wedge using an extra production level located 30 meters above level 76. Therefore, in a first instance the objective of this experiment is to determine the mobility of the wedge under uniform draw using the current layout. The extraction from the 11 drawpoints was uniform and it was conducted until the equivalent of the 27% of the ore was extracted.

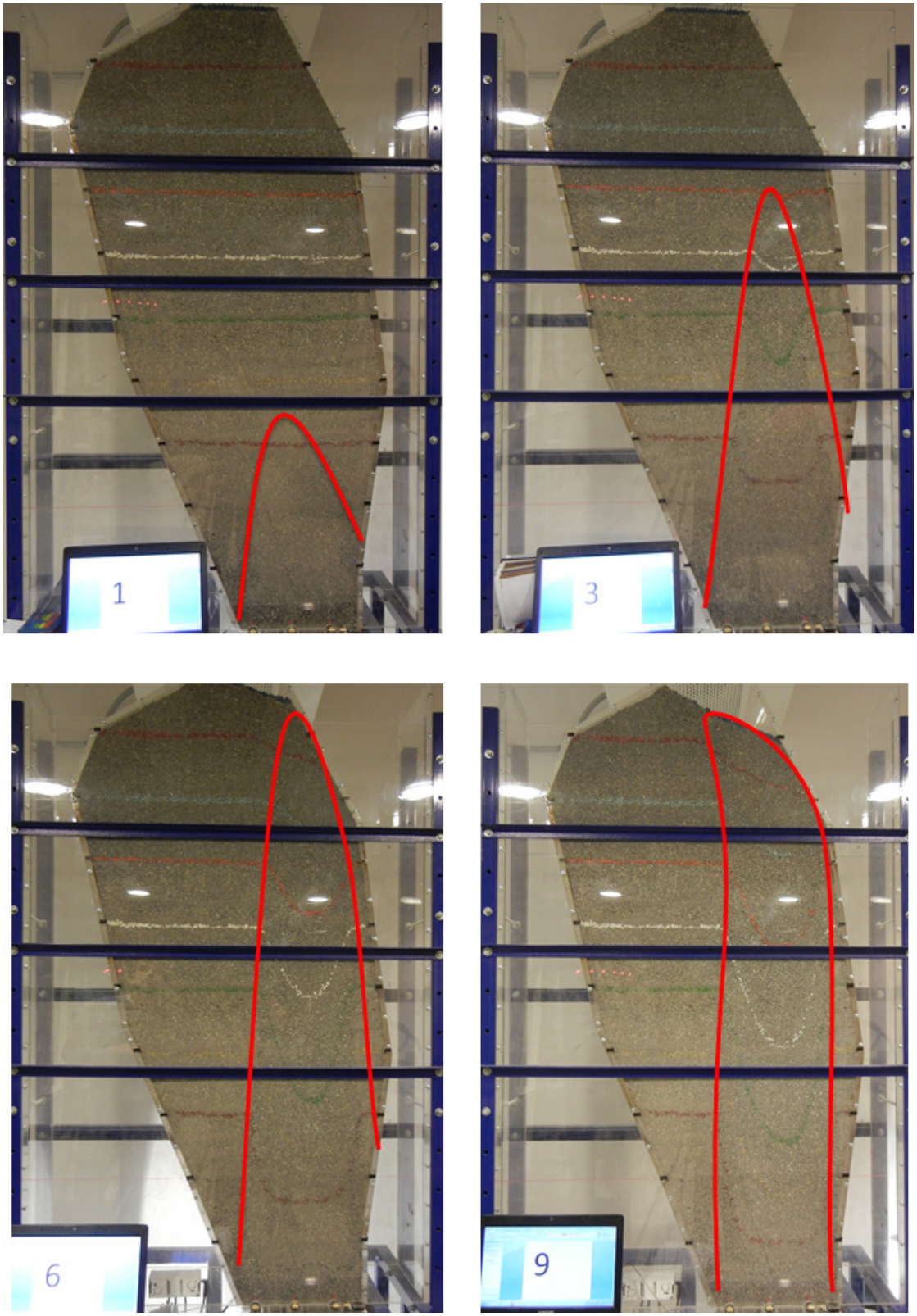

Figure 6.4. (Left Up) 1 kton from each drawpoint. (Right Up) 4 kton from each drawpoint. (Left Down) 10 kton from each drawpoint. (Right Up) 15 kton from each drawpoint.

During the experiments it was observed that the flow developed upwards towards the hanging wall as this represents a lower strength path for the movement to develop. The movement zone is slimmer at the bottom that at the top of the stope, as presented in Figure 6.4 and Figure 6.5. From the visual inspection trough the plexiglass it was observed also that the wedge is not mobilised at all.

It can also be seen from the experiment, that when the movement zone reaches the top of stope, the ore moves downwards by rilling (Figure 6.5)

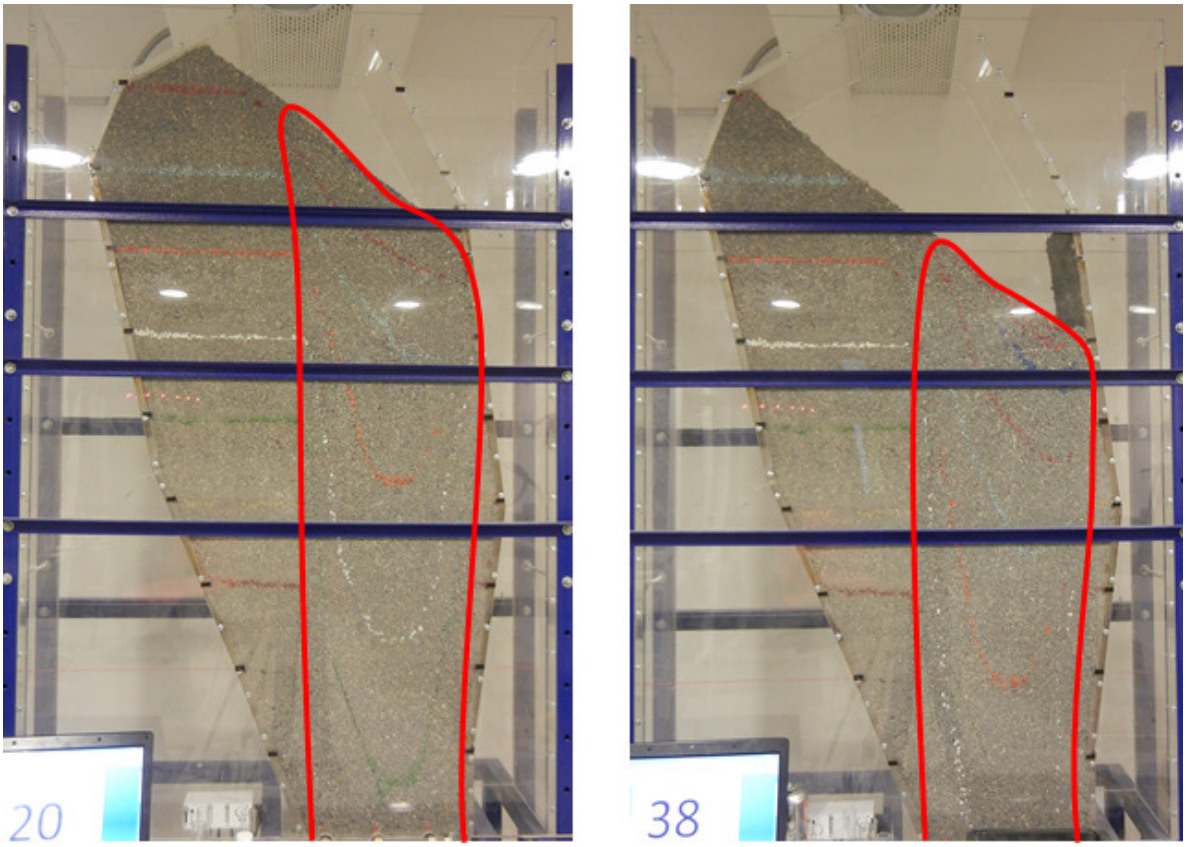

Figure 6.5.(Left) 33 kton for each drawpoint. (Right) 63 kton for each drawpoint.

In last part of the experiment, there's still no movement of the footwall. Only the rilling mechanism generates material movement from the top of the stope downwards as shown in Figure 6.5

The recovered markers are plotted as shown in Figure 6.6 and Figure 6.7.

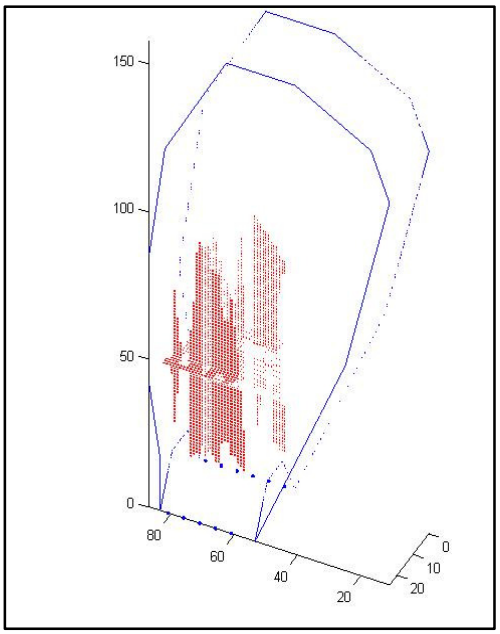

Figure 6.6.Recovered markers 3D view of section 609.

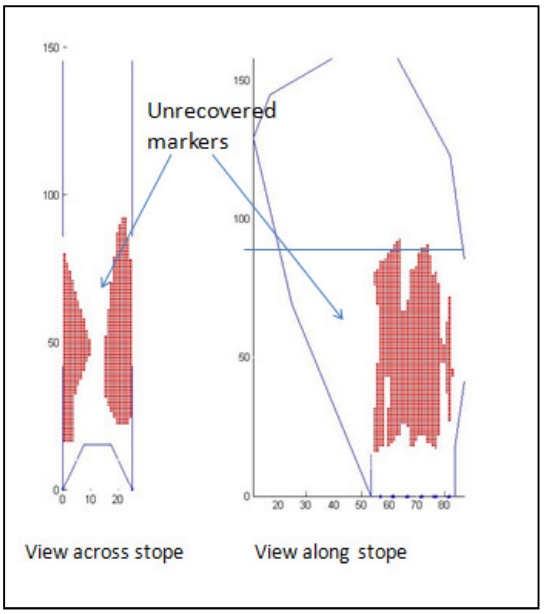

Figure 6.7.Recovered and unrecovered markers. View across and along the stope. Axis en cm

The plotting of the extracted markers provides evidence of to the poor interaction across the mayor apex. An important lesson from this experiment was the fact that that the markers don't supply much information of the zone located at the drawbell. Therefore, for the subsequent experiences the amount of markers in this area is increased.

6.2.2.2.Proposal of design of Goldex for another extraction level

The proposed design is based on the results from the IMZ test. Since in Experiment 2 it was established that the material located outside the projection of the production level is not

mobilized, the design of the new level will maximize ore recovery if the movement zone develops vertically avoiding an early interaction with the flow zone of level 76. If the flow zone due to extraction from level 73 deviates horizontally towards the higher porosity zone created by the extraction of the current level, the material will not be recovered.

The proposal for design projected for Goldex locates the connection of the new drawpoints at 30 m above the current level and 16 m away from the ore body as shown in Figure 6.8.

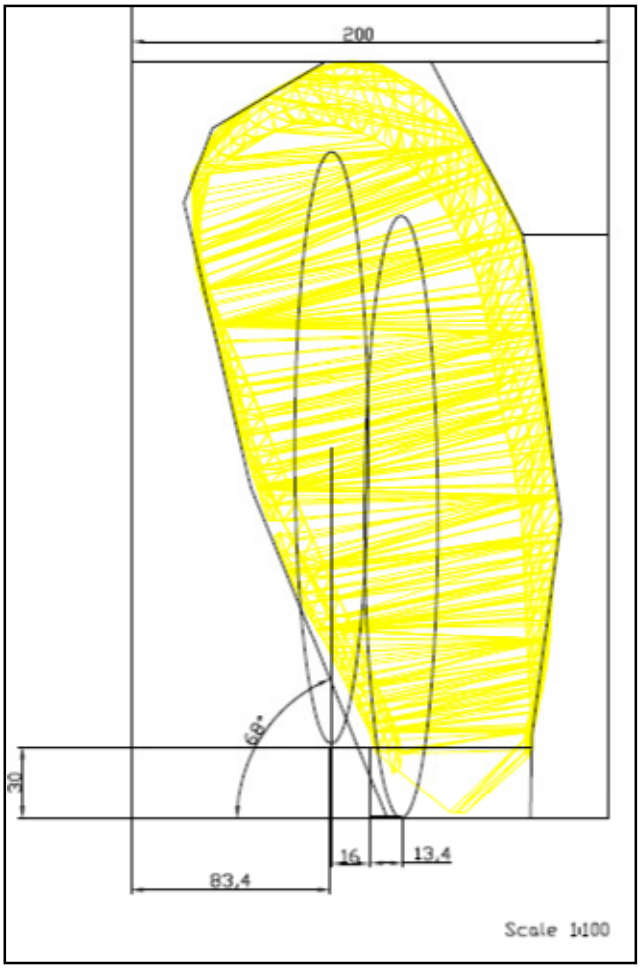

Figure 6.8.Proposal for new extraction level. All measures in meters.

Figure 6.9 shows a cross section of the design of the new extraction level, considering 3 drawpoints spaced at 22.35 m each. The dimensions of the drawpoints are equivalent to the drawpoints from level 76.

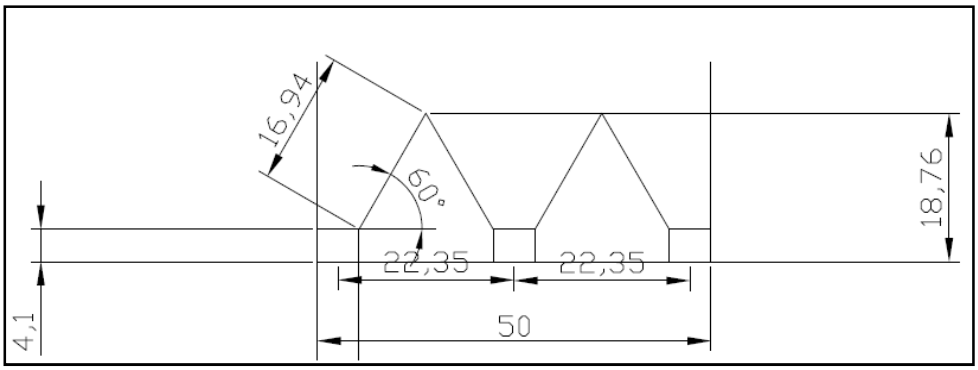

Figure 6.9. Cross section of the design for level 73. All measures in meters

The design specifications implemented at the physical model are detailed in Table 6.1.

Table 6.1. Detail for the design of level 73.

Drawbell angle	°	60
Drawpoint Spacing	[m]	22.35
Drawpoint Height	[m]	4.1
Drawpoint Width	[m]	5.3

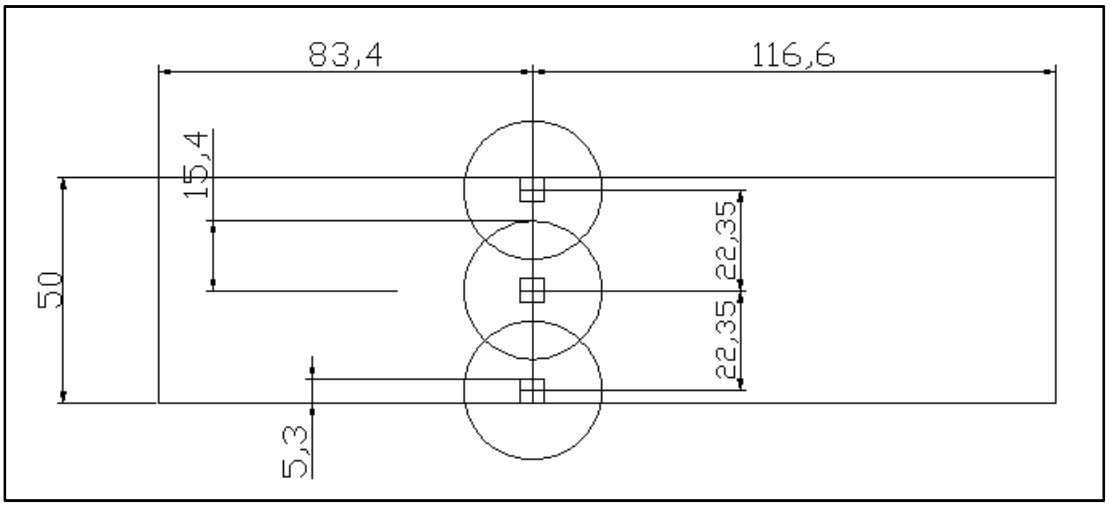

Figure 6.10.Plan view of the design for level 73.All measures in meters

6.2.3. Experiment 3

6.2.3.1.Description

The main objectives of this experiment were in the first place to duplicate the results from experiment 2, increasing the labeled markers to enhance the information from the lower zone of the stope and to accurate the results from ore recovery through the mayor apex. The extraction is performed from level 76 until December 2011, as programmed at Goldex.

The second objective from this experiment was to test the design of the new level proposed to Goldex, in order to quantify the improve in ore recovery due to the new extraction level as well as to observe the gravity flow pattern developed due to extraction from level 73.

In this experiment the labeled markers were placed in 13 layers, in each layer the markers were positioned 3 cm each in the horizontal; the markers in the vertical had different colors to observe the flow and the mobilized zone.

6.2.3.2.Results and main discussions performing extraction only from level 76

During the development of the experiment it was observed that when drawing from level 76 the flow develops upwards towards the hanging wall as this represents the lower strength path for the movement to develop as detected in experiment 2.

As observed in experiment 2, it was also detected on the experiment, that when the IMZ reaches the top of stope, the ore moves downwards by rilling (see Figure 6.4). In addition, as observed in experiment 1, there is still no movement of the footwall.

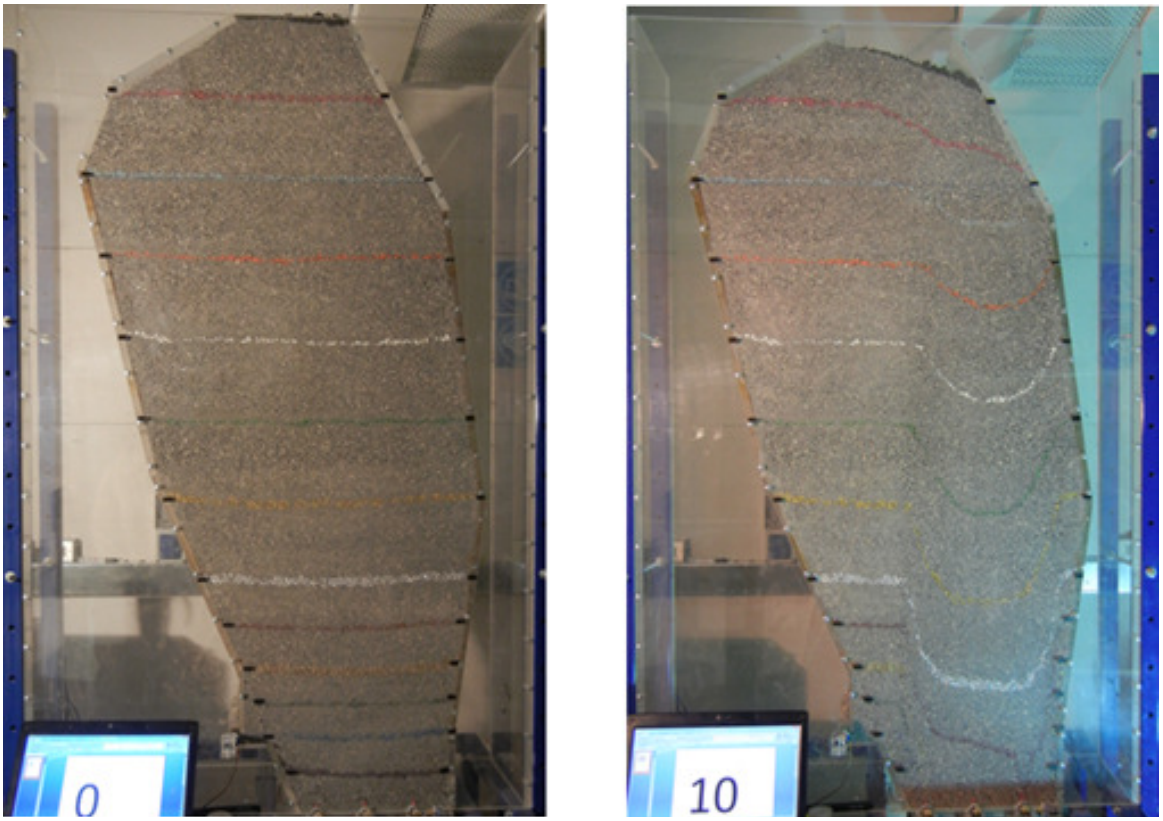

Figure 6.11. (Left Up) 0 kton from the drawpoints. (Right Up) 18 kton from the drawpoints.

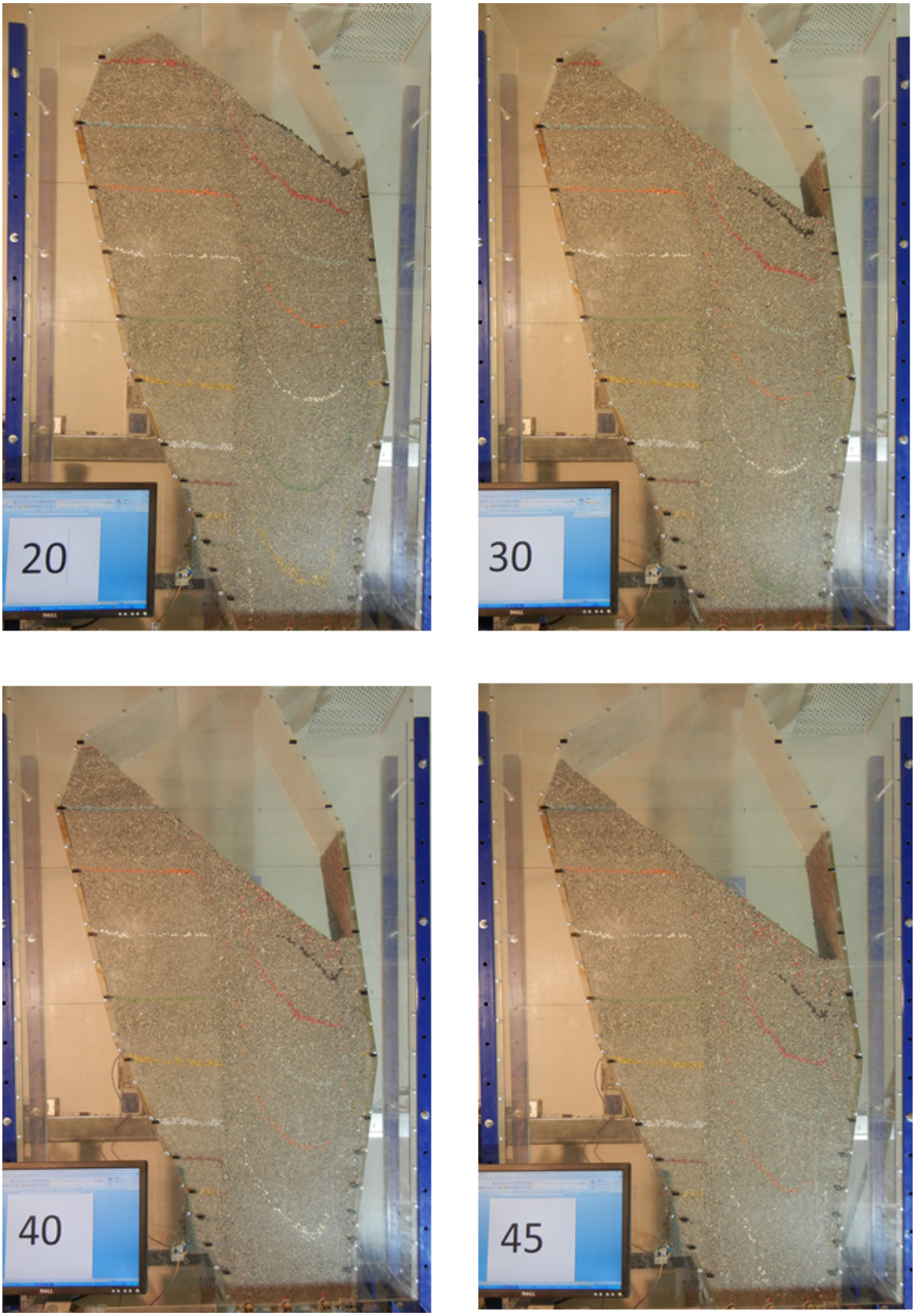

Figure 6.12.(Left-Up)38 kton from each drawpoint. (Right-Up)58 kton from each drawpoint. (Left-Down) 78 kton from each drawpoint.(Right-Down) 88 kton from each drawpoint.

In Figure 6.13 are presented the extracted zones through the mayor apex. Figure 6.14 shows the resulting extracted zone from drawing at Level 76.

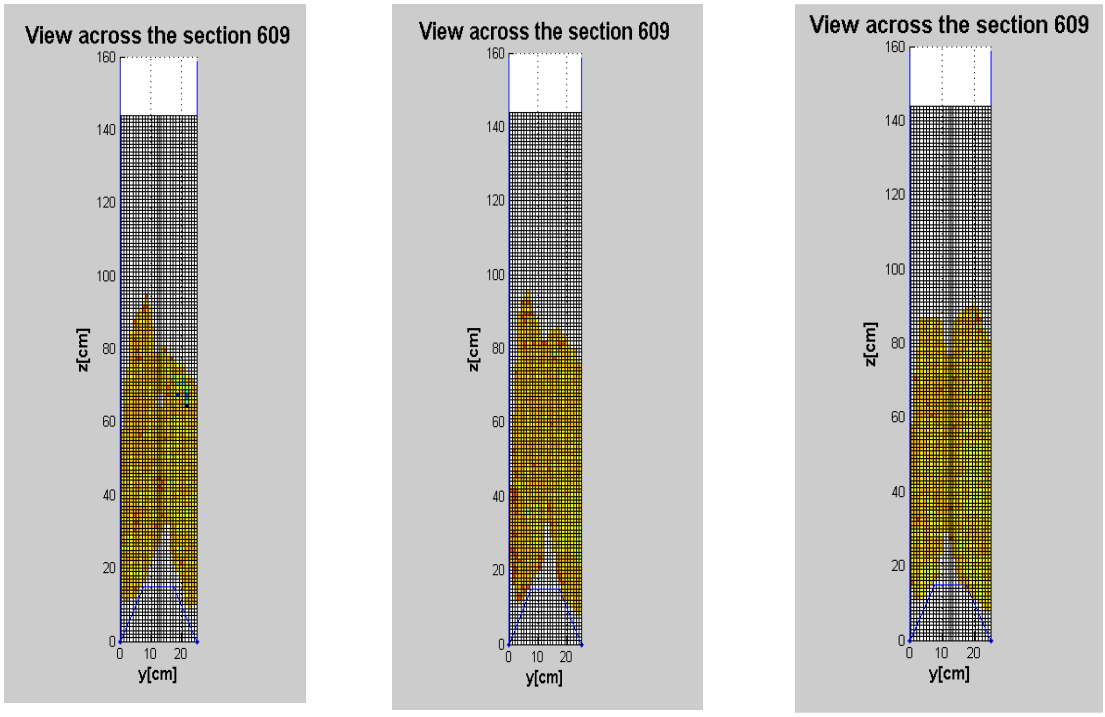

Figure 6.13. Views across the mayor apex due to extraction from level 76 for different sections (x=60,x=70,x=80) at model scale

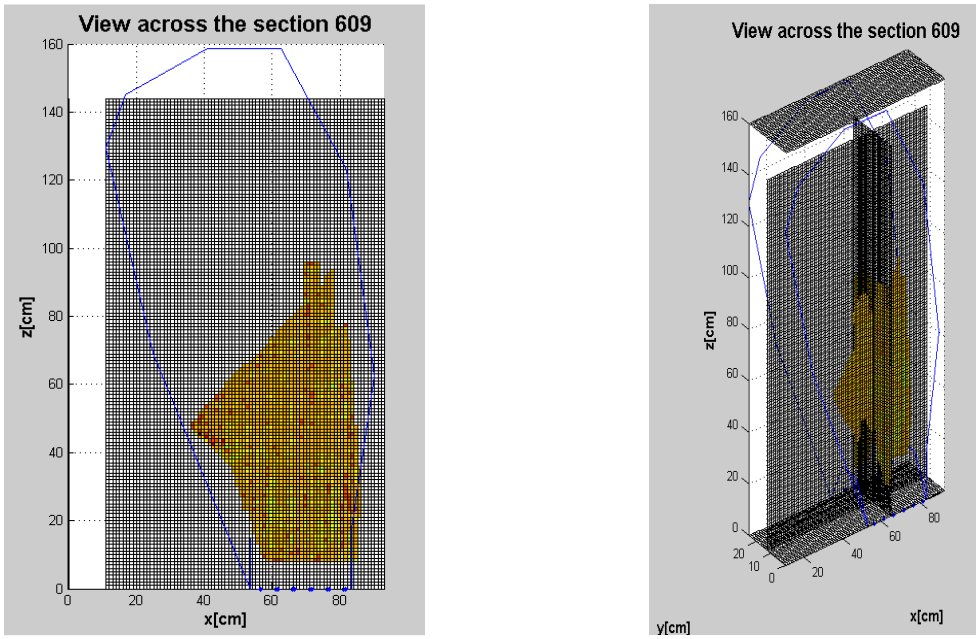

Figure 6.14. (Left) Side view of the extracted zone by drawing from level 76. (Righ) 3D view at x=60 cm.

The plotted zone shows a very low recovery of the material located at the footwall wedge. From the plotting it also can be determined the location of the IEZ interaction height about 60 [m] above the main production level.

6.2.3.3.Results and main discussions performing extraction from level 73 and 76

Once the extraction from level 76 is completed (performing the extraction only from level 76 until December 2011) the extraction is continued but also carrying out simultaneously uniform draw from level 73 and level 76.

In the next figures is shown the flow behavior due to the extraction from level 73.

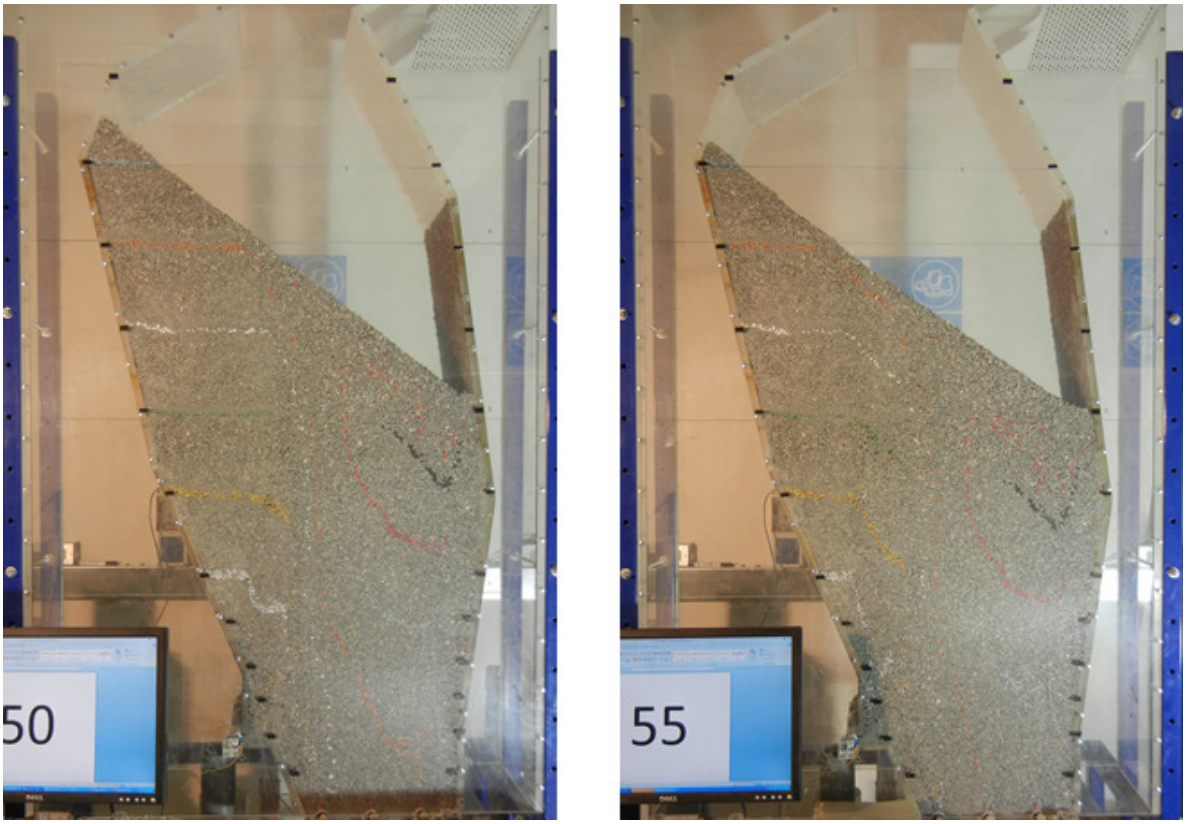

Figure 6.15. (Left)98 kton from drawpoints Level 76 and 6 kton from drawpoints Level 73. (Right)108 kton from drawpoints Level 76 and 13 kton from drawpoints Level 73.

As observed in Figure 6.15 the movement zone of the new level does not develops upwards, but towards the low porosity zone created by the draw at level 76.

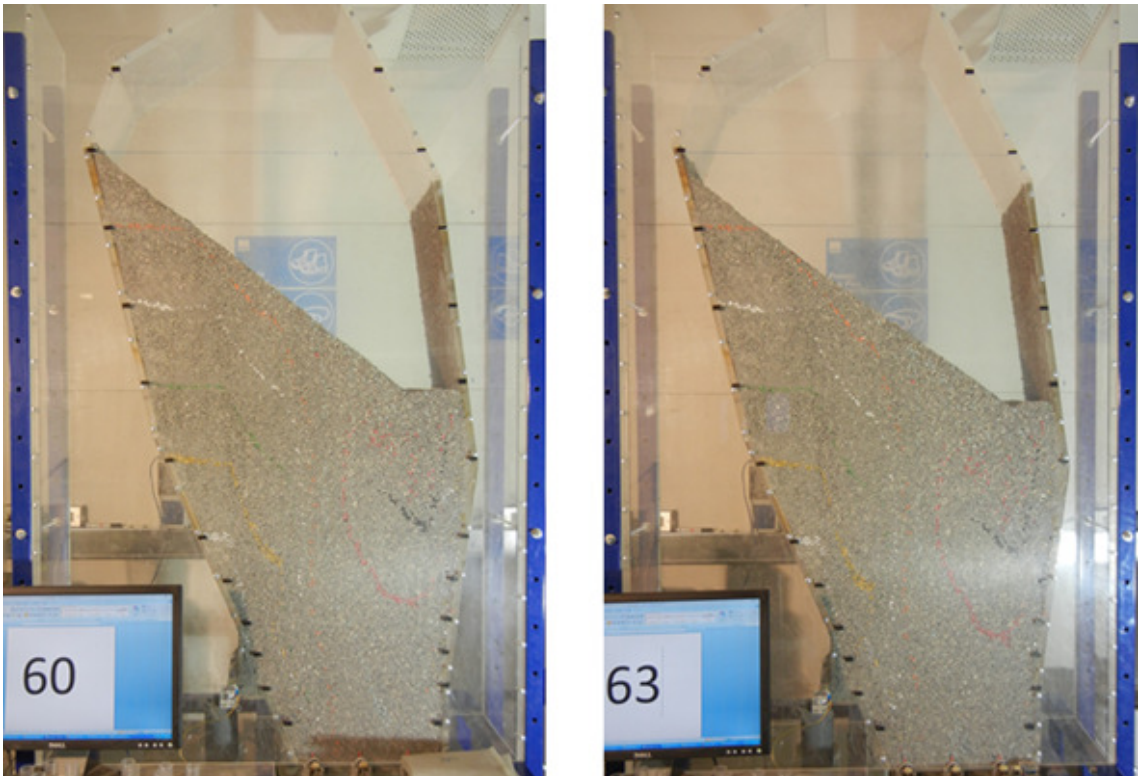

Figure 6.16.(Left) 118 kton from drawpoints Level 76 and 25 kton from drawpoints Level 73. (Right) 124 kton from drawpoints Level 76 and 32 kton from drawpoints Level 73

Figure 6.17 presents the plotting of the extracted zones through the mayor apex; Figure 6.18 shows the resulting extracted zone from drawing from level 76 and level 73.

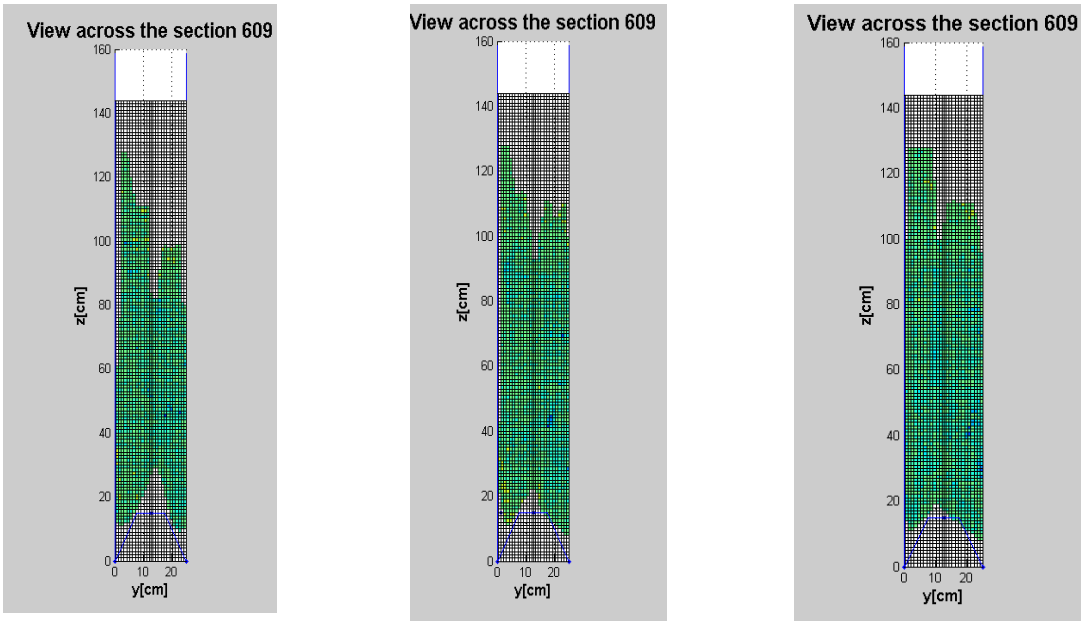

Figure 6.17.Views across the mayor apex due to extraction from level 76 and 73 for different sections (x=60,x=70,x=80) at model scale

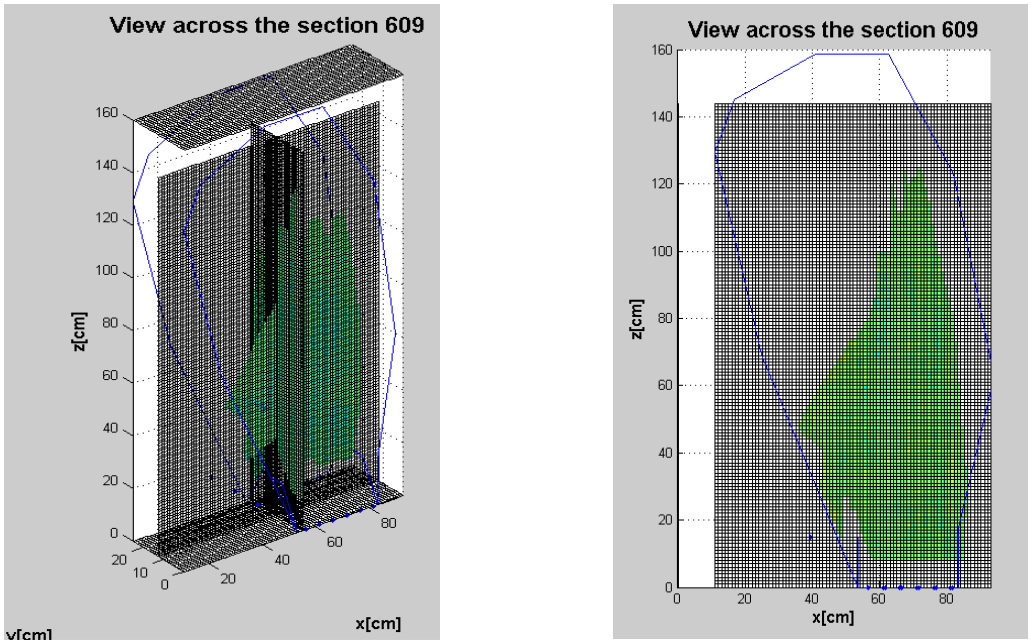

Figure 6.18.(Left) 3D view at x=50 cm drawing from 76 and 73. (Left) Side view of the extracted zone by drawing from level 76 and 73.

The plotted zone presented in Figure 6.18 shows evidence of a very low recovery of the material located at the footwall wedge, even though the implementation of a new extraction level. From the plotting it also can be determined the location of the IEZ interaction height across the mayor apex about 60[m] above the main production level.

From the results of the interpolation of the labeled markers shown in Figure 6.18 it can be seen graphically that the addition of the new level (level 73) increases the mobility of the material located at the footwall in a 6.5%.

6.2.4. Experiment 4

The main objective of this experiment was to duplicate the results from experiment 3, in order to improve the accuracy from the obtained results. Experiment 4 consists of identically replicate experiment 3; this because of the importance of determining rigorously, both recovery and the movement zone due to the extraction from the new level, with the purpose to quantify the increase in ore recovery by implementing extraction owing to level 73 as well as the mixing profile given through to the different displacements profiles by drawing from both levels.

Using the information from the labeled markers the extraction zone was plotted; by means of the markers positions it was determined the immobilized ore from the stope due to extraction from level 76 and also from level 73. In the following the plotted sections will be compared with the obtained from experiment 3.

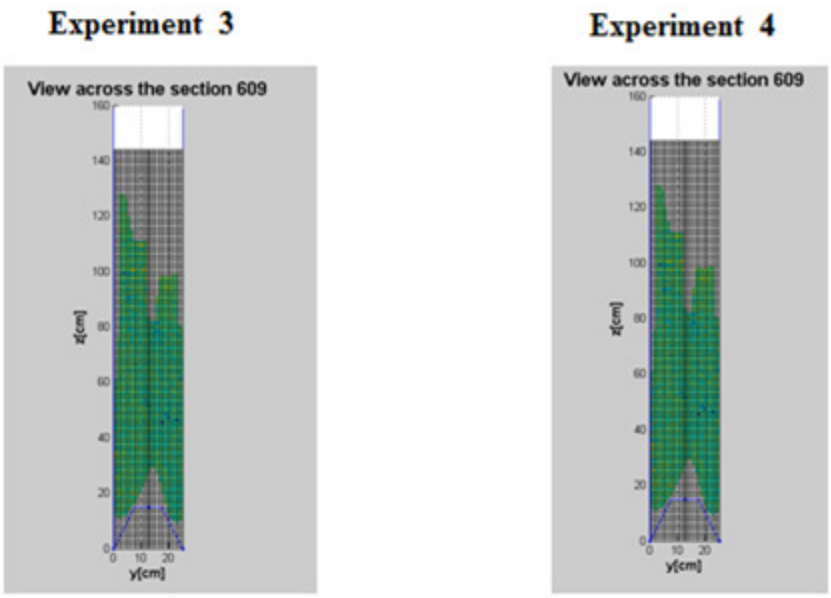

Figure 6.19.Comparisson of the view across the mayor apex due to extraction from level 76 and 73 for x=55 cm at the model.

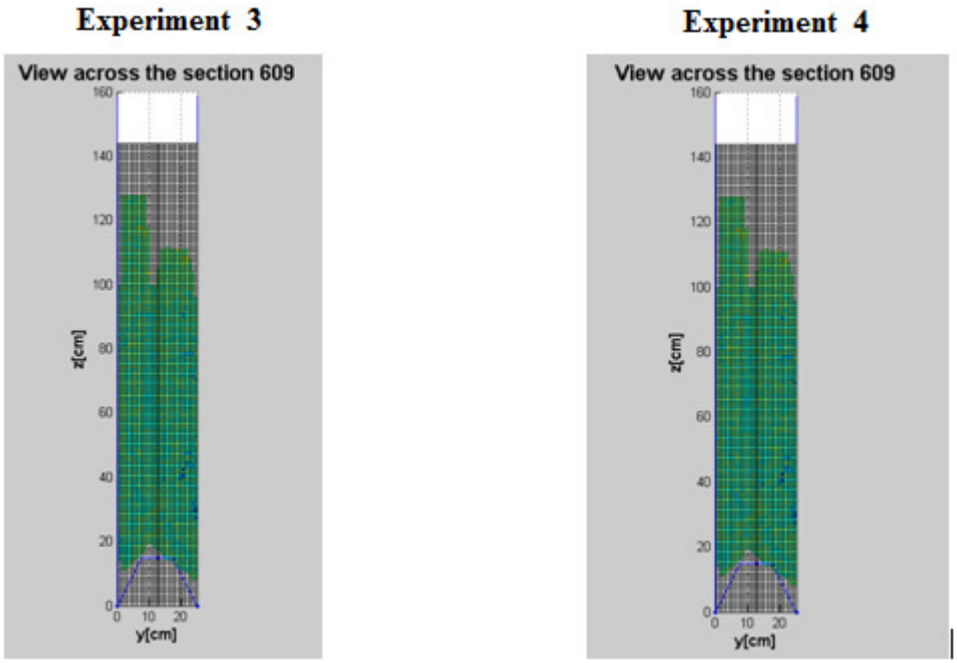

Figure 6.20. Comparisson of the view across the mayor apex due to extraction from level 76 and 73 for x=75 cm at the model.

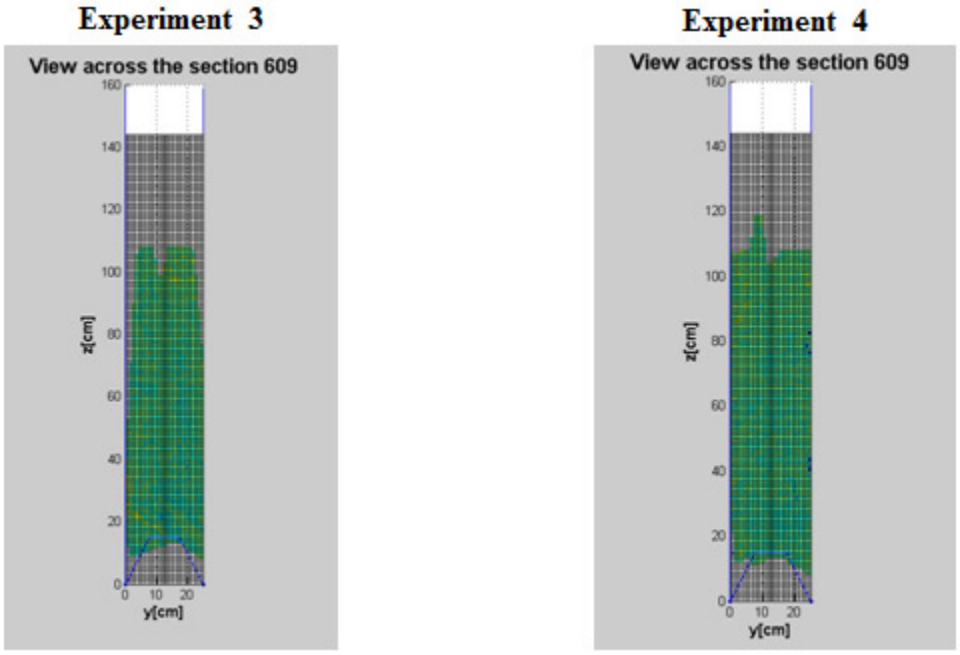

Figure 6.21.Comparisson of the view across the mayor apex due to extraction from level 76 and 73 for x=75 cm at the model.

From the information of the plotted sections and from the analysis of the recovered markers in both experiments, no major differences are observed. In fact, the extracted markers coincide in about a 95%. Experiment 4, validates the extraction by drawing from level 76 and from level 76 and 73 by increasing the reliability of the obtained results.

6.2.5. Experiment 5

6.2.5.1.Description and main results

The main objective of this experiment is to simulate in the physical model the unstable case for the Eastern Stope. To achieve this objective, the experiment is performed identically as experiment 4, but including dilution (depicted in red dust). The extraction for each drawpoint is continued until the dilution is reported at drawpoints. The dilution is reported in two stages, first the dilution entry at the drawpoint and when the drawpoint shows dilution at a 100%.

As a result of this experiment, the maximum ore recovery for the unstable case is obtained, by performing the extraction based on the dilution entry.

The results are shown in the next figures.

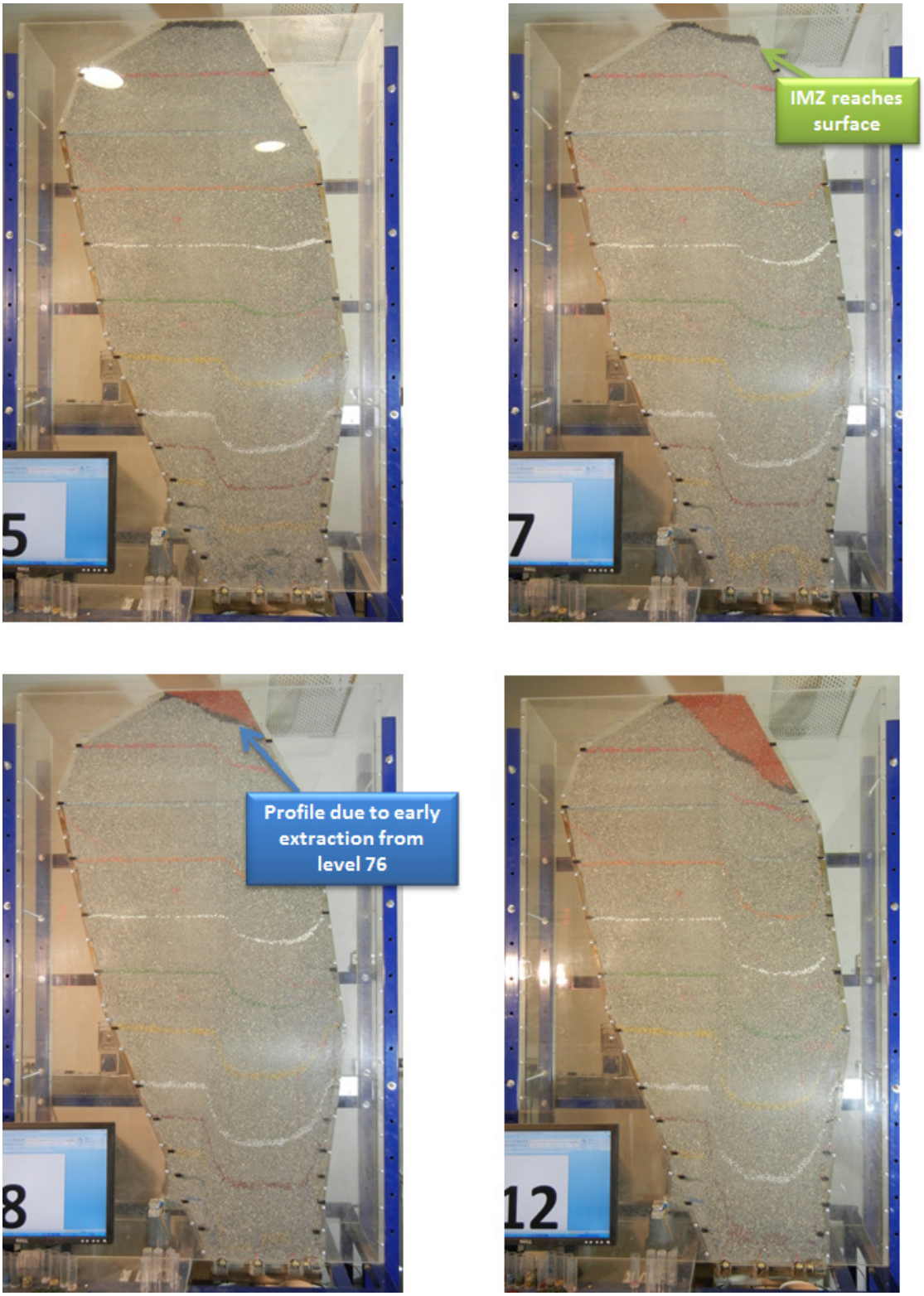

Figure 6.22.(Left Up) 8 kton for the drawpoint. (Right Up) 12 kton for the drawpoint. (Left Down) 14 kton for the drawpoint. (Right Down) 22 kton for the drawpoint.

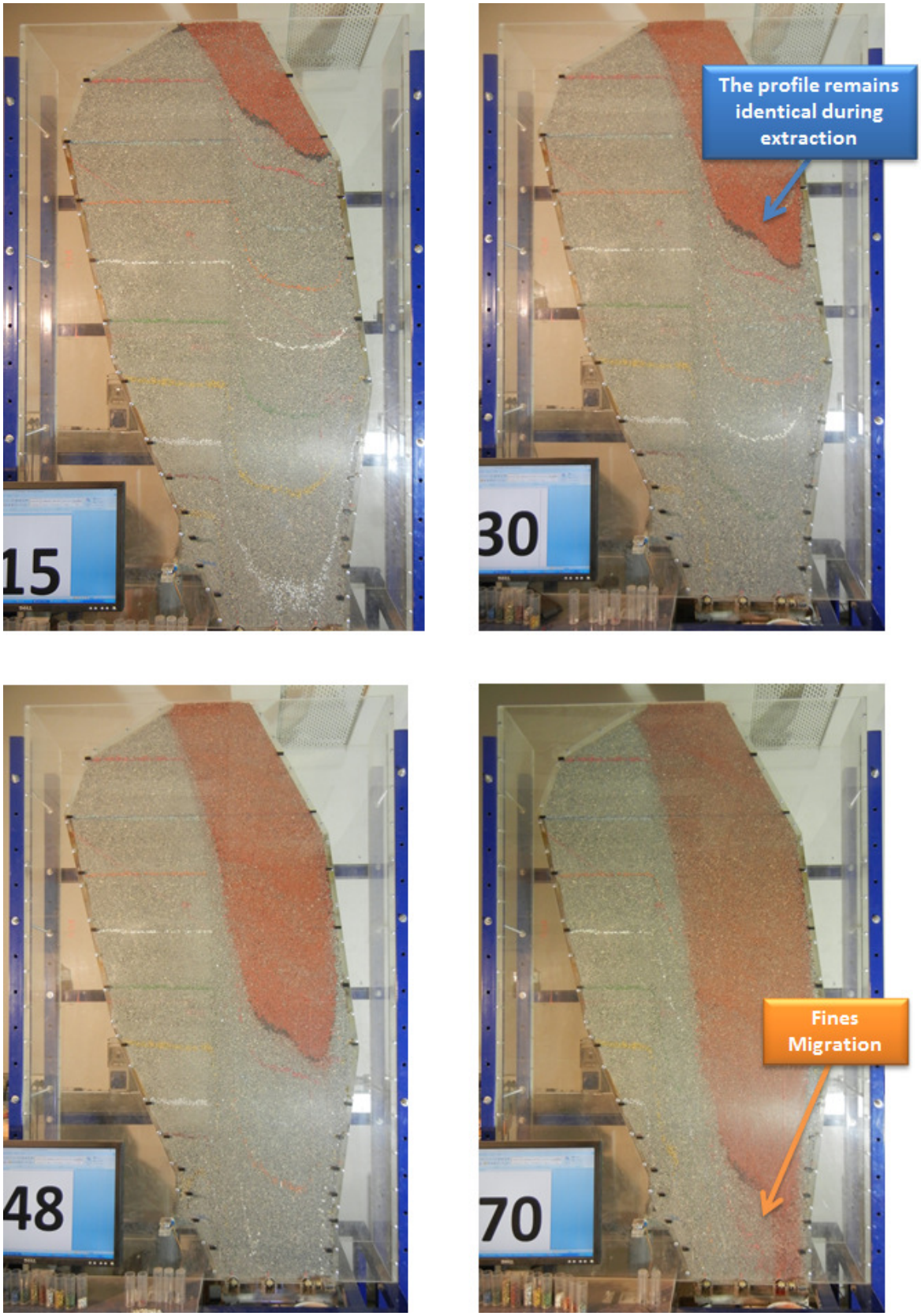

Figure 6.23.(Left Up) 28 kton for the drawpoint. (Right Up) 58 kton forthe drawpoint. (Left Down) 94 kton ton for the drawpoint. (Right Up) 138 kton for the drawpoint.

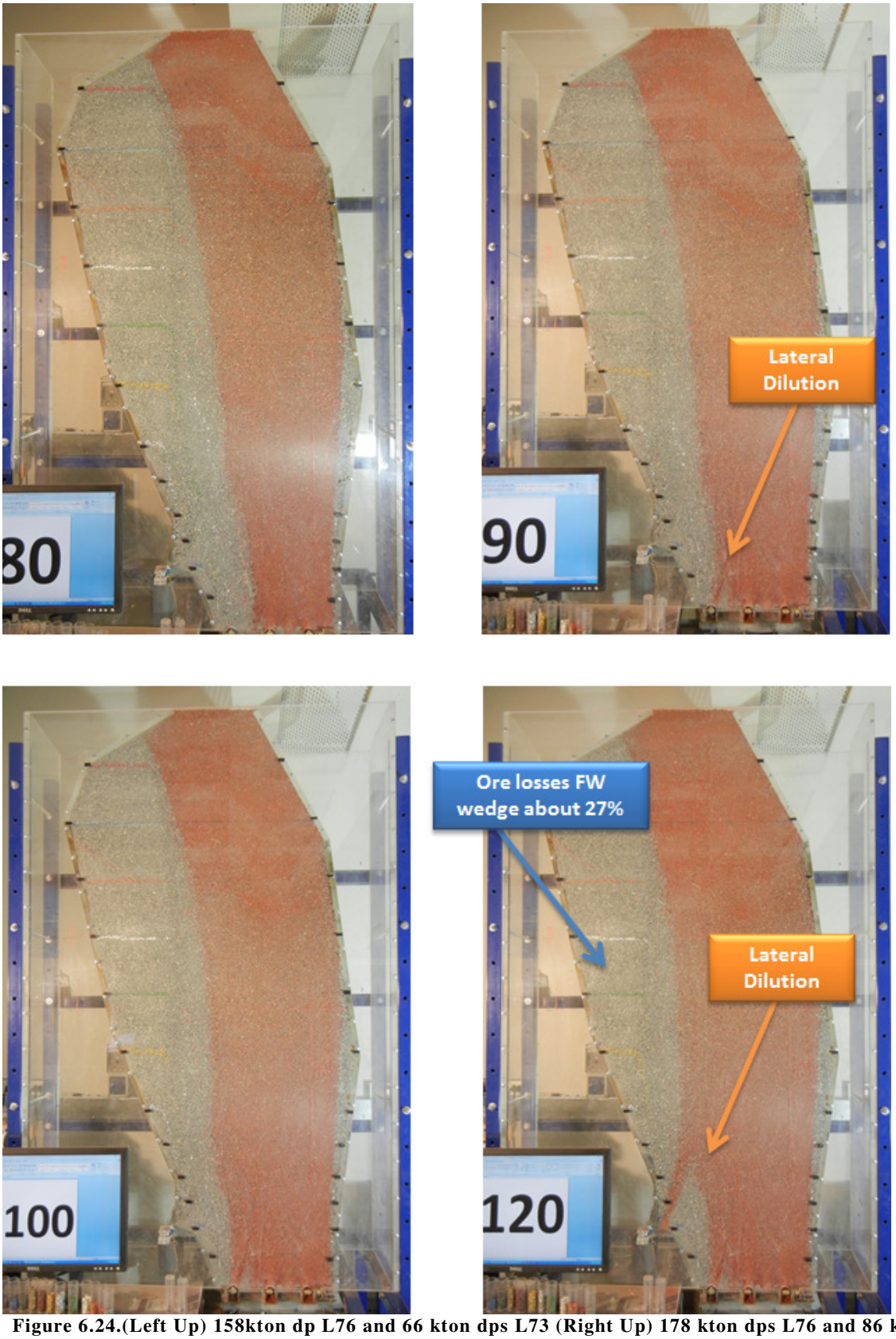

Figure 6.24.(Left Up) 158kton dp L76 and 66 kton dps L73 (Right Up) 178 kton dps L76 and 86 kton dps L73.(Left Down) 198 kton dps L76 and 106 kton dps L73 (Right Up) 238 kton dps L76 and 146 kton dps L73

From the analysis of the recovered markers, there's evidence that with the actual design proposed by Goldex for level 73, an important component of the mobilized zone due to extraction from level 73 is recovered before dilution entry at these drawpoints. As can be seen in Figure 6.25, the mobilized zone due to level 73 corresponds to the IMZ estimated in Experiment 2.

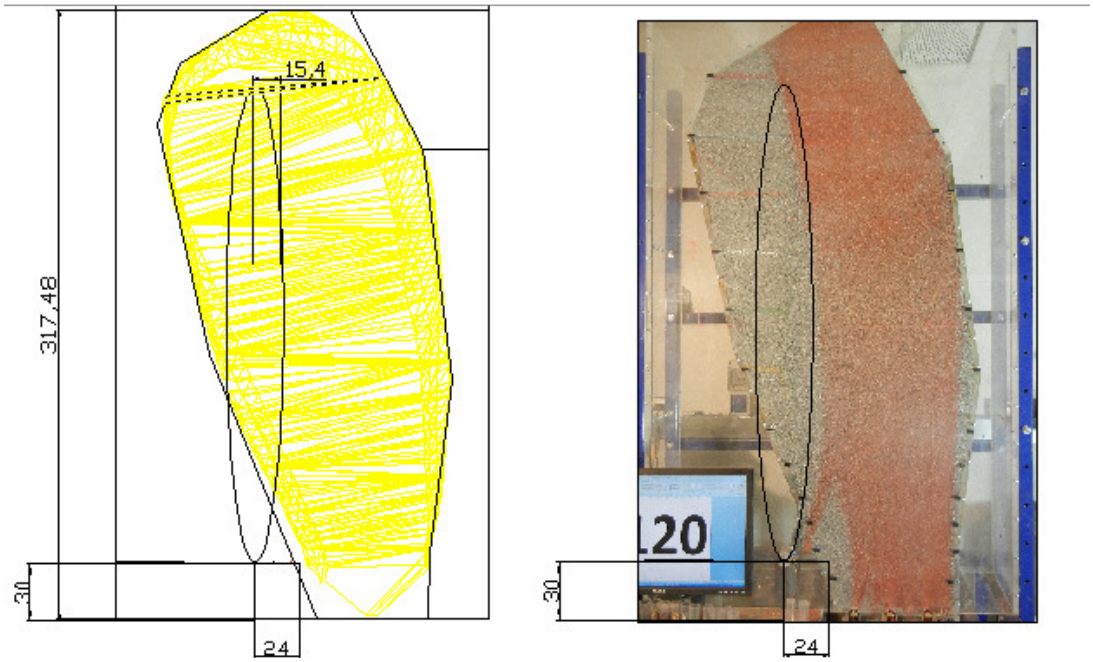

Figure 6.25. (Right) Ore reserves to be mobilized due to level 73 according to the design of the level. (Left) Mobilized zone due to the actual extraction from level 76 and 73

Using the information from the extracted markers the extraction zone was plotted. The extraction of material was continued until a drawpoint showed 100% of dilution, then extraction was stopped for the drawpoint but continued for the rest of them.

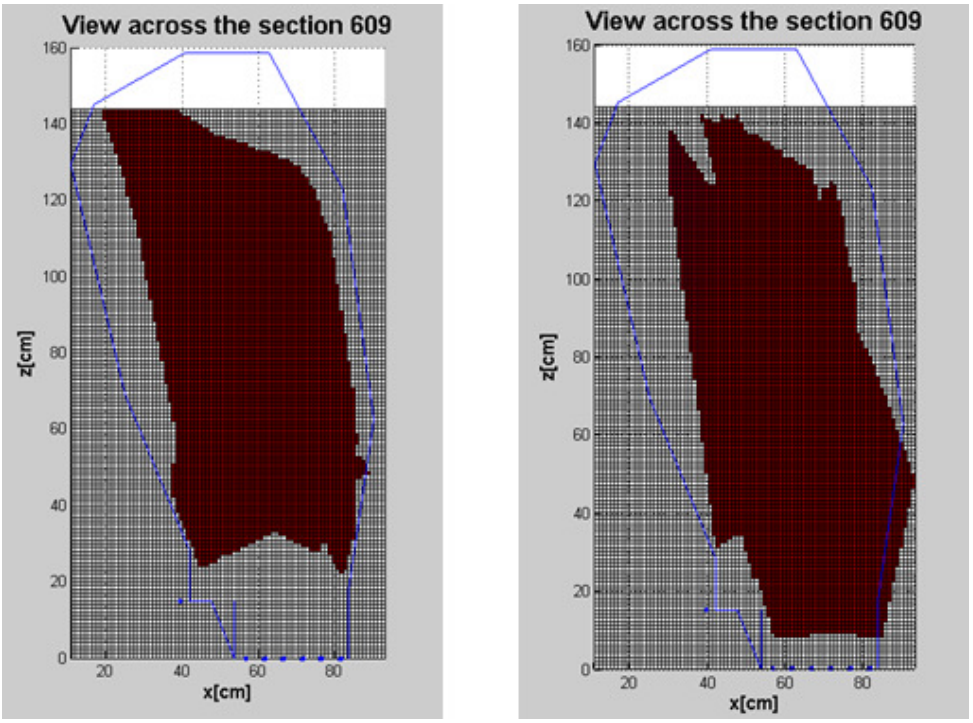

Figure 6.26. (Right) Recovered labeled markers. View across the minor apex. (Left) Recovered labeled markers. View at the border of the physical model.

Using the information from labeled markers, it was estimated the interaction height of the extraction zones across the mayor apex. The interaction height through the mayor apex is about 60[m] above the current production level, as can be seen in Figure 6.27.

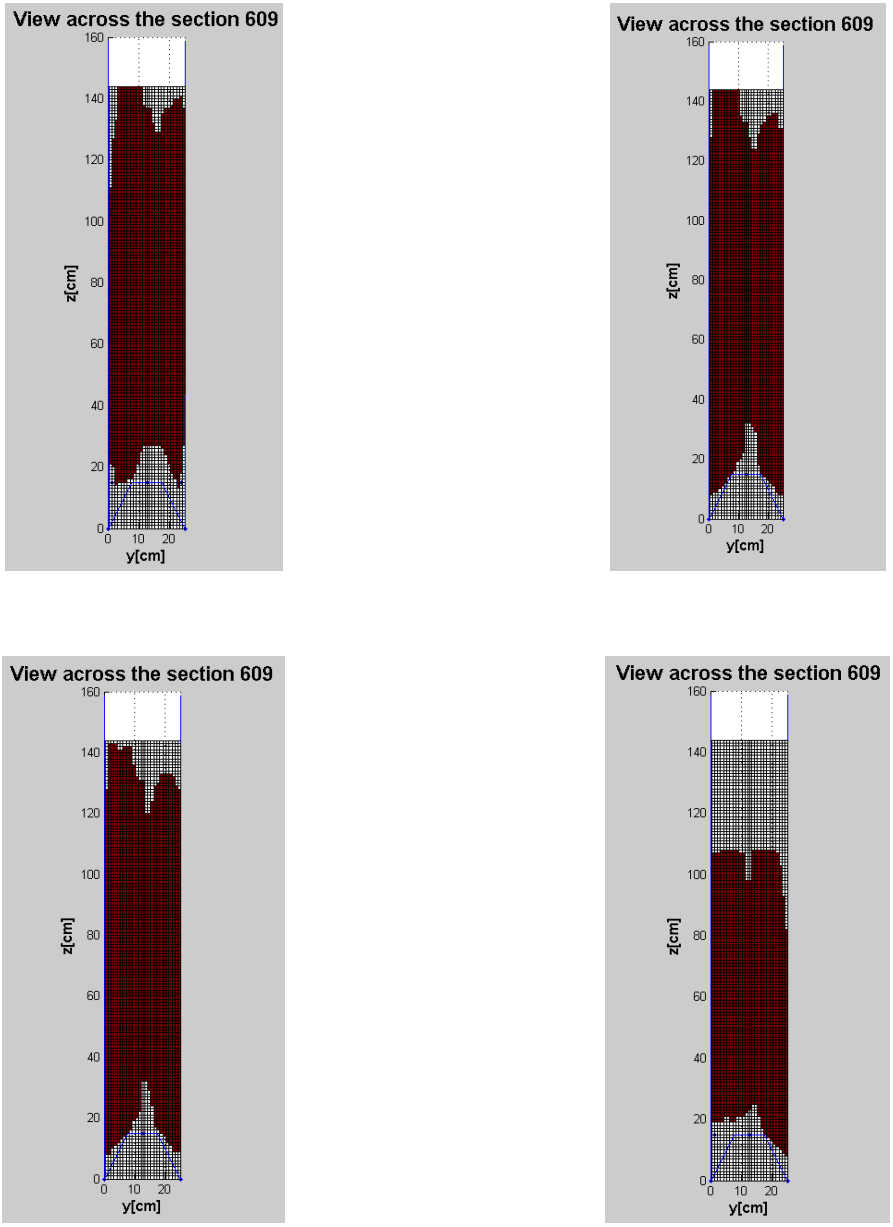

Figure 6.27.Recovered labeled markers. (Left-Up) View across section 609 x=50. (Right-Up) View across mayor apex section 609 x=60. (Left-Down) View across section 609 x=70. (Right-Down) View across mayor apex section 609 x=80.

6.2.5.2.Ore recovery and dilution entry analysis

In order to quantify ore recovery for the unstable case and the ore recovery from each drawpoint it will be defined ore reserves, dilution entry and dilution of a 100% percent at the drawpoints.

The next definitions assume that all drawpoints have the same height of column; although this may not be the case for the drawpoints located at the footwall it's a simplified approximation.

1. Ore reserves for drawpoints can be calculated as:

   $$Re[ton] = \frac{Vol_{Stope} \times \rho_{Broken\ Rock}}{\#Drawpoints} = 230\ 514\ [ton]$$

   Where:

   Vol_{Stope}: $Volume\ of\ the\ stope[cm3]$

   $\rho_{Broken\ Rock}$: $Density\ of\ broken\ rock\ \left[\frac{gr}{cm3}\right]$

   $\#Drawpoints$: $Number\ of\ drawpoints\ for\ the\ section(14)$

2. Dilution Entry for each drawpoint can be calculated as:

   $$dil_e = \frac{CumMass\_e}{Re} \times 100[\%]$$

   Where:

   $CumMass\_e$: Accumulated tonnage extracted until dilution is reported.

3. Dilution at a 100% for each drawpoint can be calculated as:

   $$dil_{100} = \frac{CumMass\_100}{Re} \times 100[\%]$$

   Where:

   $CumMass\_100$: Accumulated tonnage extracted until dilution is a 100%.

Table 6.2. Dilution entry and dilution at a 100% for each drawpoint

DPName [#]	dil_e [ton]	dil_{100} [ton]	dil_e [%]	$dil_{100\%}$ [%]
12	114,137	146,175	50	63
13	118,141	150,180	51	64
14	120,144	152,182	52	65
1	168,383	198,419	73	86
9	154,366	162,376	67	70
4	154,366	162,376	67	70
7	152,364	162,376	66	70
2	148,359	162,376	64	70
10	146,357	168,383	63	73
5	144,354	168,383	63	73
8	134,343	148,359	58	64
3	136,345	148,359	59	64
11	134,343	148,359	58	64
6	134,343	148,359	58	64

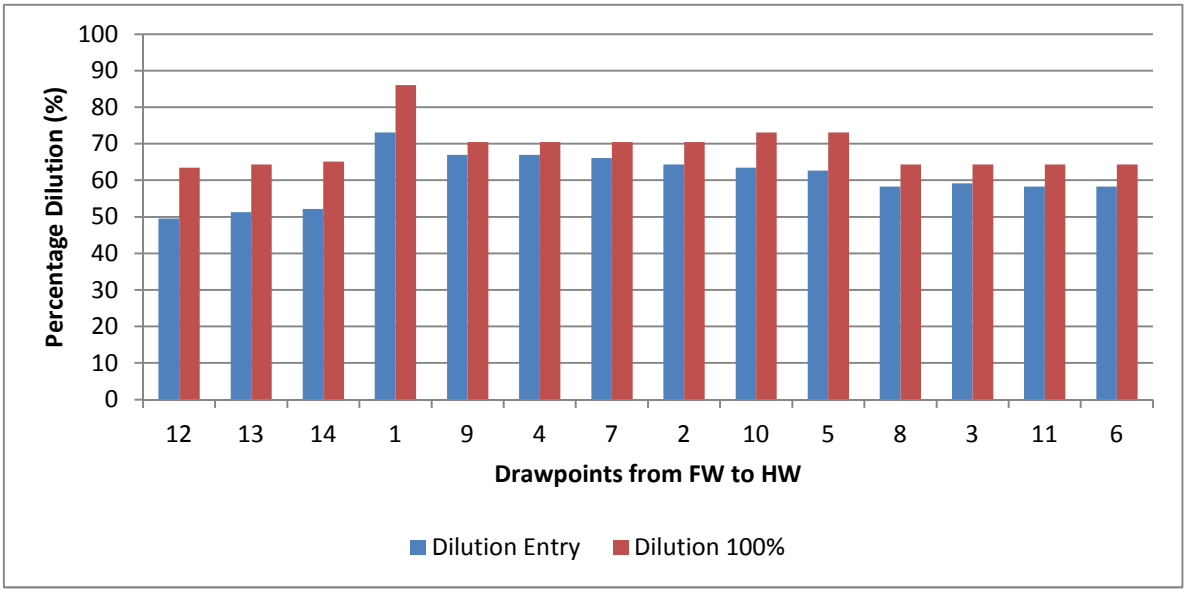

Figure 6.28. Dilution entry and dilution at a 100% for each drawpoint

The drawpoint location can be seen in Figure 6.29.

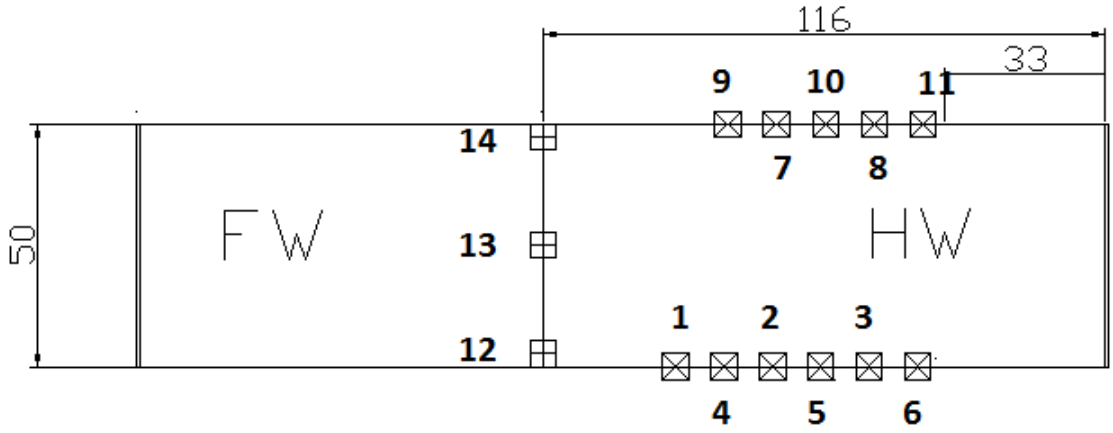

Figure 6.29.Drawpoints location and their ID

Based on this experimental result, ore recovery for each drawpoint and the basic statistics of dilution entry and dilution at a 100% can be resumed in Table 6.3.

Table 6.3. Statics of recovery, dil_{100} and $dill_e$

Mean Dilution entry(dil_e)	(%)	61% (+/. 6%)
Mean extracted ore (dil_{100})	[%]	69% (6.7%)
Max	[%]	86
Min	[%]	50

6.3. Conceptual results obtained from the experiments

The experimental plan and the obtained results can be schemed as 4 main cases, due to the observed governing mechanism of the caved rock flow; they are presented in Figure 6.30 and Figure 6.31 .

A summary of the experimental results is presented in Table 6.4; ore recovery estimation was conducted by using the information of the labeled markers as explained in a previous section.

Table 6.4. Summary of results for the experiments

Case	Experiment	Extraction	Dilution	Estimated Ore Recovery
1	Experiment 1 - Experiment 3 (first part)	Level 76	No	100%
2	Experiment 3- Experiment 4	Level 76 and 73	No	100%
3	Experiment 4	Level 76	Yes	54% (100% dil)
4	Experiment 4	Level 76 and 73	Yes	68% (100% dil)
5	Hipothetical	Level 76-73-65	Yes	90% (100% dil)

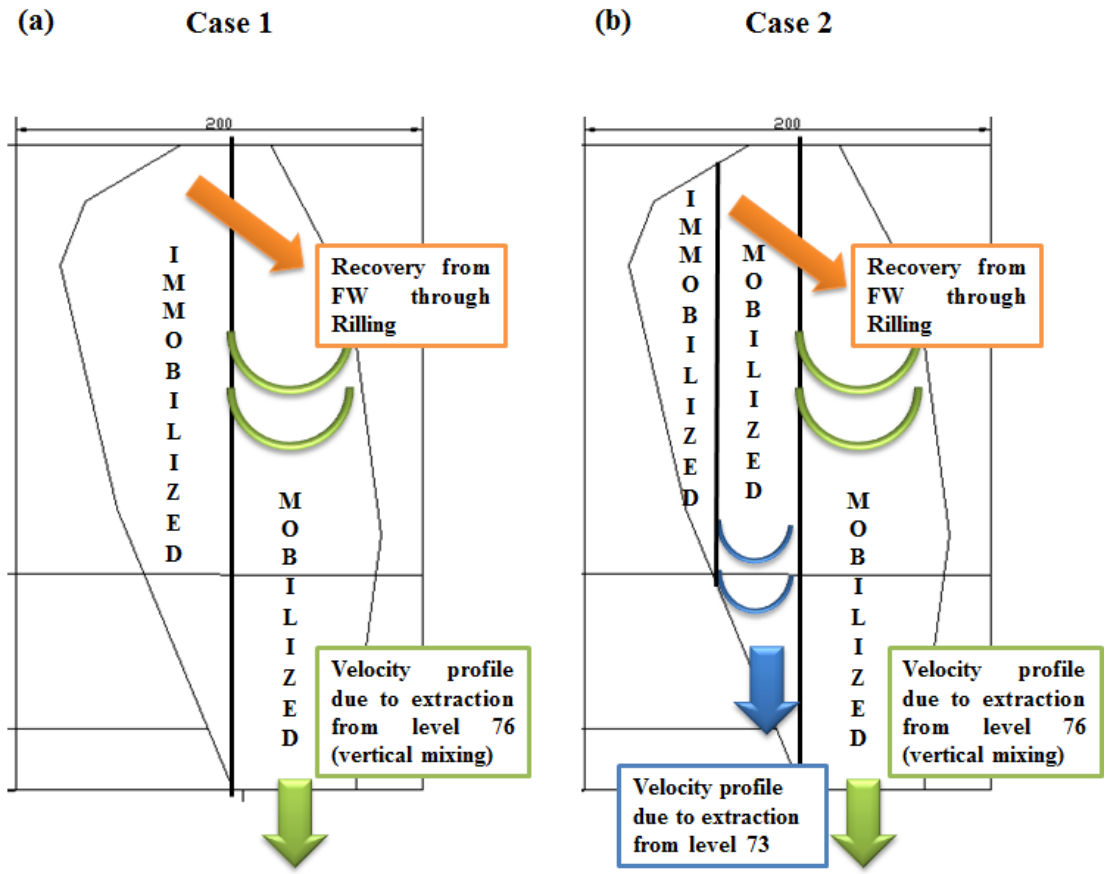

Figure 6.30. Conceptual scheme of the experimental result for Case 1 and Case 2 (Stable cases; without dilution)

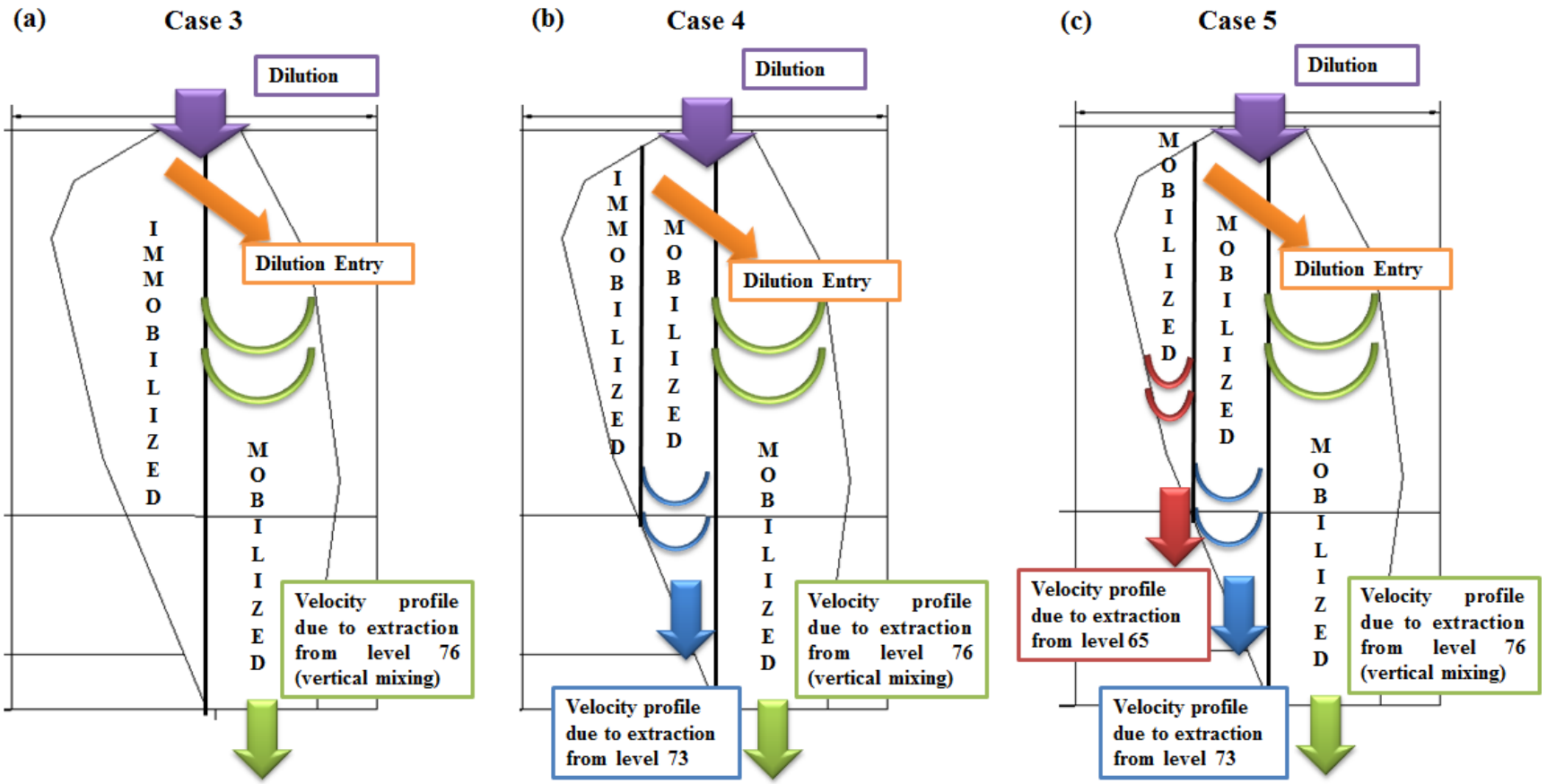

Figure 6.31. Conceptual scheme of the experimental result for Case 3, Case 4 and Case 5 (Unstable cases including dilution)

6.4. Proposal for design

Based on the results presented above in the previous sections, and in order to improve ore recovery for the main stope at Goldex, the proposed design must assure avoiding an a early interaction with the flow zone due to extraction from level 73 and 76.

In experiment 2, it was determined that the isolated movement zone diameter was about 30.8[m]. Using this result it was tested the design proposed to Goldex Mine for a new extraction level (level 73) located 30 meters above the main extraction level (level 76).

The results of these simulations at the physical model are detailed in previous sections (Section 6.2.). Substantiated in these results, and with the aim to increase recovery to maximize profits, is suggested the development of a new level located about 106 meters above the actual extraction level. From now on, this level will be identified as level 65. The design with multiple extraction levels will avoid in the first place an early interaction with the flow zone due to extraction from level 76 as well as the interaction between flow zones due to level 73 and level 65. The interaction between flow zones between level 73 and level 65 is accomplished by locating drawpoints at a distance at least equal to the IMZ diameter in plan view.

The detail of the proposed design is listed below in Figure 6.32 and Figure 6.33.

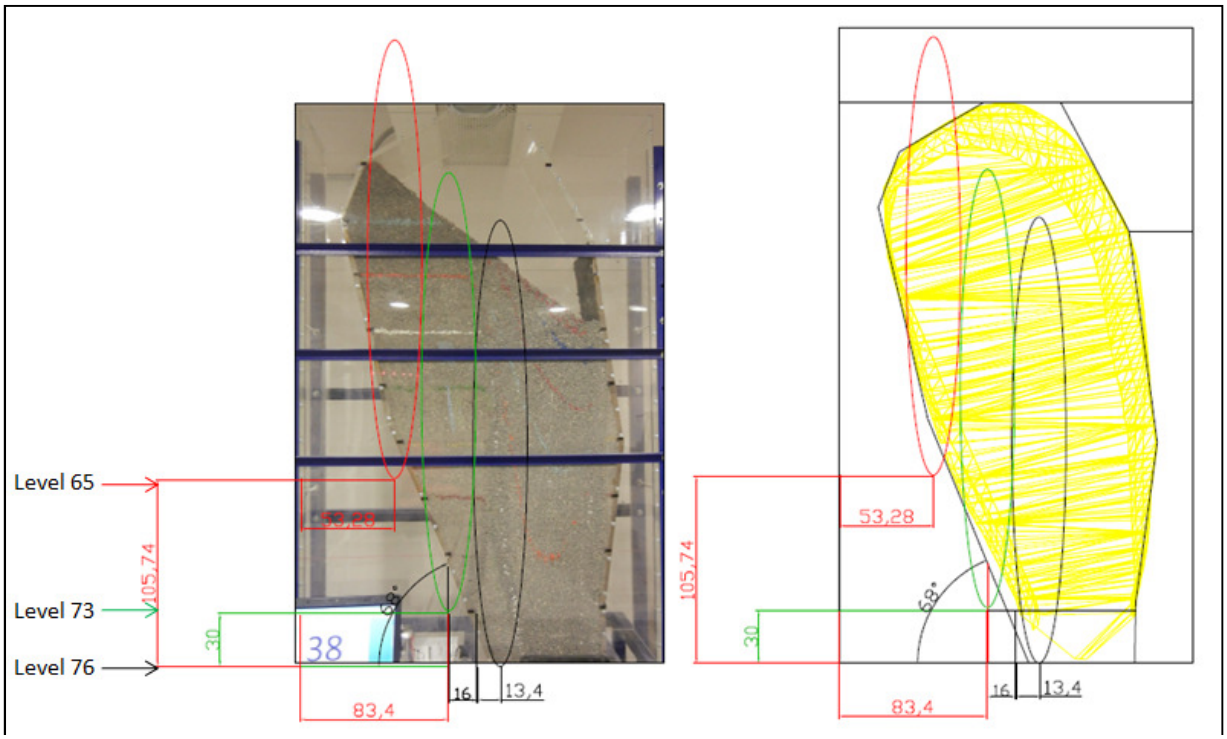

Figure 6.32. Design for multiple levels. Section 609 side view. All measures in meters

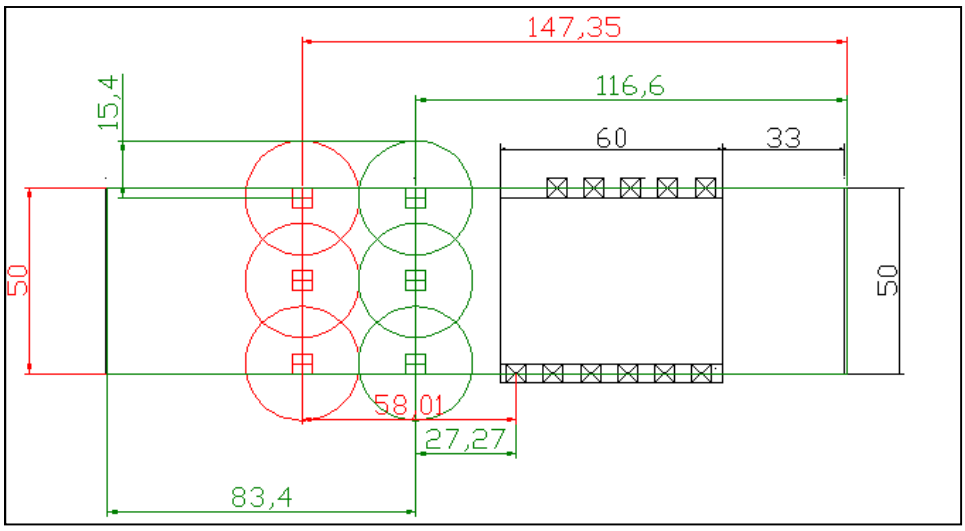

Figure 6.33. Design for multiple levels. Plan view. All measures in meters.

6.5. Conclusions from the experimental results

6.5.1. Case 1 (Stable case; drawing from the main level)

- When the uniform extraction from level 76 begins, the flow stream quickly propagates vertically up to the stope surface. Since the drawpoints are sufficiently close together, there is an evident interaction between them and it results on a vertical massive flow as wide as the footprint width of the extraction level. The flow is initially slimmer at the top than at the base, afterwards the movement zone widens until reaches the footprint width. This vertical flow develops preferentially towards the HW, since this represents the lowest strength path to develop (smaller height of column).
- The vertical massive flow doesn't mobilize the footwall on these conditions. Nevertheless, the ore located at the footwall surface is able to flow by the rilling mechanism. This flow consists of material sliding from the top downwards FW to the HW direction.
- In this case, the gravity flow mechanisms observed and mentioned above, the ore recovery should reach an approximate of a 100% for the stable case.
- From the experiment it can also be conclude that the extraction zones interact across the mayor apex 60 [m] above level 76.

6.5.2. Case 2(Stable case; drawing from level 76 and 73)

- When drawing both from level 76 and level 73, a fraction of the material located at the FW is mobilized. Still there is a passive zone located at the FW that is not mobilized by drawing from level 76 and that will be able to flow by rilling.
- Given the gravity flow mechanisms observed and mentioned above due to the uniform extraction from both levels, the ore recovery should reach an approximate of a 100% for the stable case.

6.5.3. Case 3 (Unstable case; drawing from the main level)

- When the uniform extraction from level 76 begins the flow stream quickly propagates vertically up to the stope surface as observed in the previous experiments. As soon as the flow breakthrough the surface the dilution is mobilized.
- As seen on the experiments without dilution, the extraction from level 76 results on a vertical massive flow as wide as the footprint of the extraction level. This vertical flow shows preferential movement towards the HW. The vertical massive flow doesn't mobilize the footwall on these conditions.
- Dilution entry for the drawpoints it is mainly influenced by the stope profile during the first part of the extraction. This profile is maintained throughout the extraction and determines tonnage at which dilution is reported at drawpoints of level 76, impacting on ore recovery. This indicated that vertical dilution depends on the cave profile and fines migration it's not so dependent on the draw strategy. Since this profile develops faster towards the HW, dilution entry for the drawpoints located near the HW is reported earlier.
- In this case the ore recovery would reach 54%.

6.5.4. Case 4 (Unstable case; drawing from level 76 and 73)

- The flow mechanism due to extraction from level 73 generates lateral movement of the broken rock. The mobilized zone due to the extraction from level 73 generates an early connection with the low density zone due to extraction from level 76, promoting dilution entry.
- This cause lateral dilution entry at level 73 starting from the HW towards the FW.
- Given the gravity flow mechanisms observed and mentioned above, the ore recovery would reach an approximate of a 68%.

In this chapter were presented the main results from the physical modeling, in order to complement this knowledge, the next chapter presents the numerical simulation of experiments conducted with the aim to link both methodologies.

CHAPTER 7
REBOP COMPARISON TO THE EXPERIMENTAL RESULTS.

This chapter describes the numerical modeling conducted in REBOP V 3.10.3 for the case of study, with the purpose to establish a comparison with the experimental results presented in this thesis.

From the analysis it will be established if the software is able to replicate the different draw mechanism observed during the physical modeling stage and generate a match between numerical and experimental results for each experiment.

7.1. Introduction

As commented in previous sections, much research has been conducted concerning to the gravity flow field; numerical, mathematical and empirical models have been developed for predicting flow behavior during draw of materials from silos and bin as flow prediction for block/panel caving mines. These studies in many cases have been validated with observations of flow in controlled laboratory-scale physical experiments and full scale tests. However, still remains a lack of understanding of the complex mechanism governing gravity flow due to the rock mechanics characteristics.

Nevertheless, since mine-scale laboratory tests are very expensive and time consuming, the industry trend is to develop numerical models capable of simulating numerically the phenomena under study.

REBOP - Rapid Emulator Based on PFC3D- (Pierce, 2010) is a relatively simple mathematical model for the upward propagation and widening of IMZs, and the corresponding internal movements of material; the model was first developed by Cundall *et al*.(2000) based on observations of flow in PFC3D simulations of draw. REBOP provides a rapid analysis of the movement and extraction of fragmented rock under draw in mine operations that use mining methods founded on gravity flow mechanisms. The software was recently developed and updated under the International Caving Study and the MMT, based on the mechanisms observed in PFC3, FLAC and physical models by Pierce in 2002. Its formulation is based on solving balance equations to determine the isolated movement zone due to extraction. Three main mechanisms were postulated to govern upward and outward growth of an isolated movement zone: porosity jump (or dilation), collapse and erosion. Incremental rules were developed to describe how each of these mechanisms controls the growth of discrete layers within the movement zone. The numerical formulation is explained briefly in Appendix B.

The code, as originally developed by Cundall *et al*. (2000), is controlled by a number of parameters that are not related to the physical properties of the caved material. As a result, the success of the simulations relies on calibration to observations made in PFC3D or physical models that attempt to mimic the mine in question (Pierce, 2010). Pierce actualization of the code, includes property based controls on flow as well as the potential impacts of cave advance, global free-surface rilling, fines migration or secondary fragmentation on material movements.

The purpose of the exercise is to determine the capability of REBOP, to replicate the physical results obtained, incorporating an estimation error and use the flow simulator as an engineering tool supporting design.

The main questions to be solved in this stage are the following:

- What are the estimation errors associated to REBOP?
- What is the potential ore recovery for the current situation at Goldex Mine by using numerical simulation?
- What are the main differences between experimental and numerical results in terms of the observed mechanisms? Are they comparable?

7.2. Scope of the simulation

The simulations in REBOP V3.10.1 will consider the replicate of the experiments detailed in Chapter 6 and summarized in Table 7.1.

The block model to be used is equivalent to the physical model to ensure the correct interpretation of the flow due to extraction. The model imported into the gravity flow simulator is an in-situ block model, i.e., it has not been diluted. Each block has a dimension of 2x2x2 m and it has an associated density, rock type, friction angle, fragmentation, and porosity.

Table 7.1. Summary of simulations for REBOP.

Case	Extraction
Case 0	Isolated Movement Zone (extraction from only one drawpoint)
Case 1	Extraction from Level 73 without dilution
Case 2	Extraction from level 76 and 73 without dilution
Case 4	Extraction from level 76 and 73 with dilution

The simulations described above will emulate the extraction for each experiment for a set of parameters representing the model media; as a result it will be obtained the data derived from the extracted markers, which will represent the gravity flow behavior for a given scenario.

7.3. Hypothesis of work

To quantify the results of the validation in REBOP, it is proposed the following hypothesis:

1- The real data considered to calculate ore recovery and estimation errors are the tonnage and the markers obtained from the physical model.
2- To estimate the accuracy of the simulations for the case including dilution, it will be calculated the mean square error, RMSE, (Pielke, 1984)[24]; an index that measure the average differences between predicted and observed values. It will also be considered the Relative Error, determined by the difference between the simulated and the observed value obtained at the physical model.
3- It will also be calculated the reliability of the simulation, quantifying the correspondence of both extracted and non-extracted markers, for physical and numerical modeling.
   Reliability is calculated by determining how many of the recovered/unrecovered markers in the numerical model are also recovered/unrecovered in the physical model. Reliability is calculated using Equation 25.

$$Reliability\,[\%] = 0.5 \times \left(\frac{Y^{REBOP}}{Y^{Physical\ Model}} + \frac{N^{REBOP}}{N^{Physical\ Model}} \right) [\%] \qquad \textbf{Equation 25}$$

Where:

Y^{REBOP} : Recovered markers both in the numerical and the physical model.
$Y^{Physical\ Model}$: Recovered markers in the physical model.
N^{REBOP} : Unrecovered markers both in the numerical and the physical model.
$N^{Physical\ Model}$: Unrecovered markers in the physical model.

[24] Cited in Vargas, 2010.

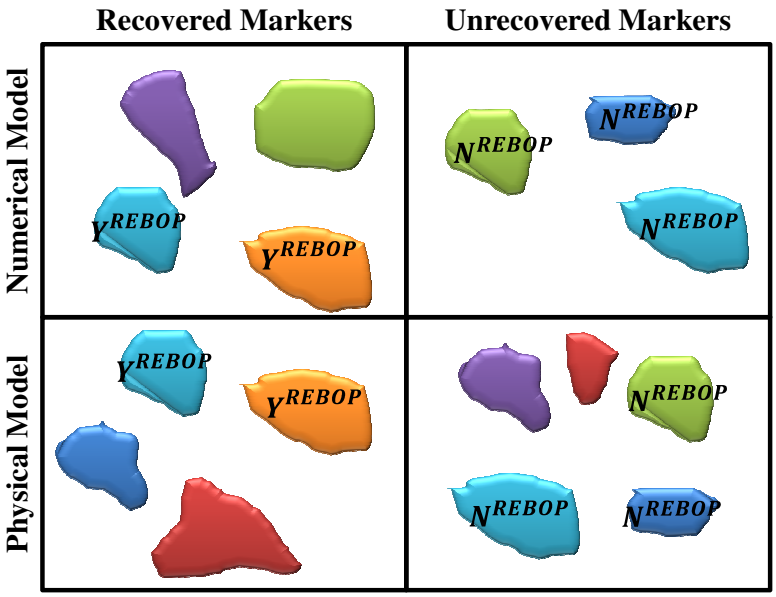

Figure 7.1. Scheme of the quantification of the reliability.25

This hypothesis defines how to measure the simulated ore recovery, and the relative and absolute error for the prediction conducted in the flow simulator.

7.4. REBOP Input Parameters

The software requires certain input parameters. Some of these data are directly related to the disposition of the extraction layout and the drawbell geometry; other parameters needed are related to specific gravity flow mechanism, such as friction angle, porosity, particle size distribution and density of the blasted material.

In this section the numerical model construction, the main inputs as their principal results and discussions are described.

7.4.1. Block model

The initial block model used for the calibration was build using the geometry of Section 609 of the main zone of production (GEZ).

The dimensions of each block are 2x2x2 with a density for the blasted rock of 1.9 [ton/m^3] and an in situ density of 2.7[ton/m^3].

The properties of the blasted rock associated to the given block model are listed in Table 7.2. The values are based in in-situ observations related to the properties of the blasted rock at the mine, a fragmentation study conducted by Goldex, and the determination of the friction angle for the model media used in the physical model.

[25] In this example, Realibility = 0.5x (2/4+3/5) = 55 %

Table 7.2.Rock mass properties for the block model

Properties	Unit	Value
Porosity In Situ	[%]	0
Maximum porosity	[%]	40
Friction angle	[°]	32
Mean diameter	[m]	0.19
Standard deviation of diameter	[m]	0
UCS	[MPa]	10^8

7.4.1.1. Cave period

The Cave Period is the period in the draw schedule at which the block is able to flow. In this particular case, the Cave Period was associated to the stability of the stope.

For the stable cases –Case 1 and Case 2- only the ore within the stope will be able to flow. This is achieved by adjusting the Cave Period property from the block model; in this case the material located outside the boundaries of the section won't be able to flow during the extraction.

For the unstable case- Case 4 - the ore as the dilution are able to flow and in order to emulate in the most accurate way the extraction from the physical model; dilution will come from the top of the stope. The block model differences can be seen in Figure 7.2, where the blue blocks can flow, and the purple ones remain stagnant due to the cave period property.

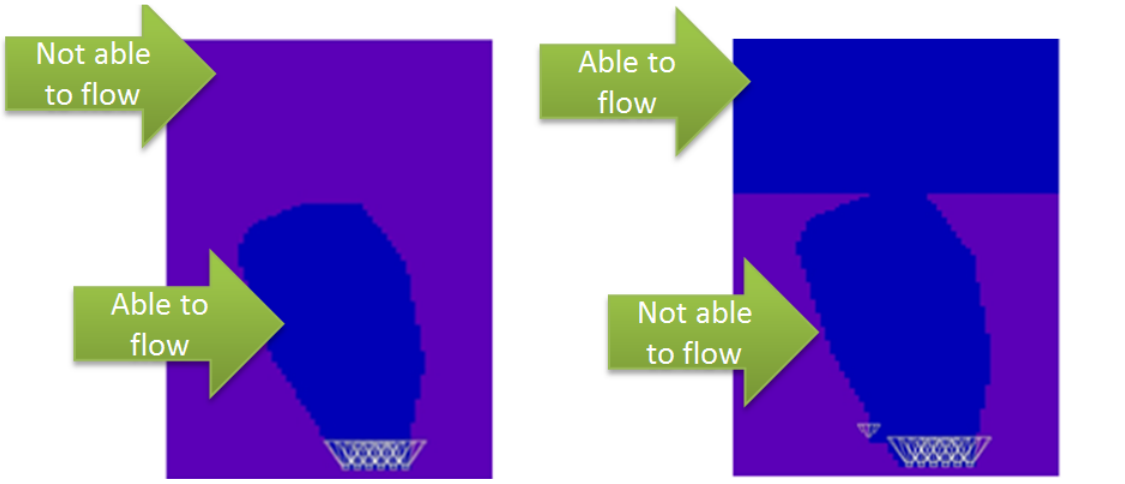

Figure 7.2.(Left) Block Model without dilution for the stable case.(Right) Block Model with dilution from the top of the stope for the unstable case.

7.4.2. Draw schedule

The draw schedule is programmed according to the extraction performed in the experiments. The extraction is uniform and in every period is extracted the equivalent to 174 tonnes/per draw point, as ITASCA's simulations conducted in FLAC3D.

The draw schedule for the stable case is conducted as in Experiment 3. The extraction considers uniform draw equivalent to the planned extraction of the mine at December of 2011 from level 76. Once this extraction is finished, the extraction from both levels is started.

On the other hand, the draw schedule for the unstable case is conducted as Experiment 5. In this case the extraction considers uniform draw and it's continued until the dilution is reported at the drawpoints.

7.4.3. Drawpoints and drawbell geometry

Both drawpoints distribution and the drawbell geometry are inputs given by the geometry of the model itself .Due to the level production design, each drawpoint could be represented as single cones having the following geometrical characteristics:

Table 7.3. Drawbell properties.

Variable	Unit	Value
Draw drift width	[m]	5.3
Draw drift height	[m]	4.1
Drawbell height	[m]	30
Wall angle	[°]	63

The drawbell geometry used at Goldex is presented in Figure 7.3.

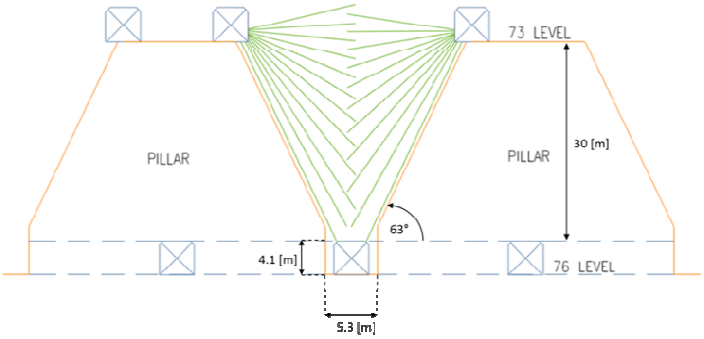

Figure 7.3.Drawbell geometry for the current extraction level.

The production level within the chosen section has 11 drawpoints for level 76. The new level (Level 73) includes 3 drawpoints located 30 [m] above the current production level. The location of the drawpoints for both levels can be seen in Figure 7.4 and Figure 7.5.

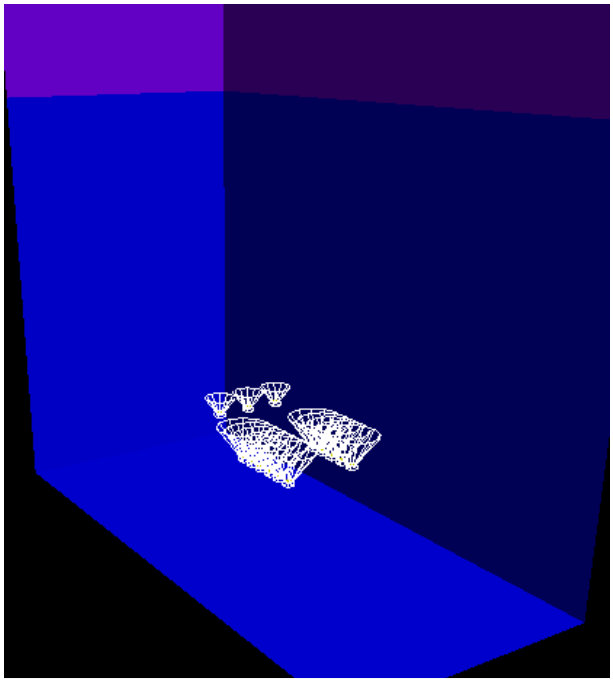

Figure 7.4.3D view of the drawpoint location

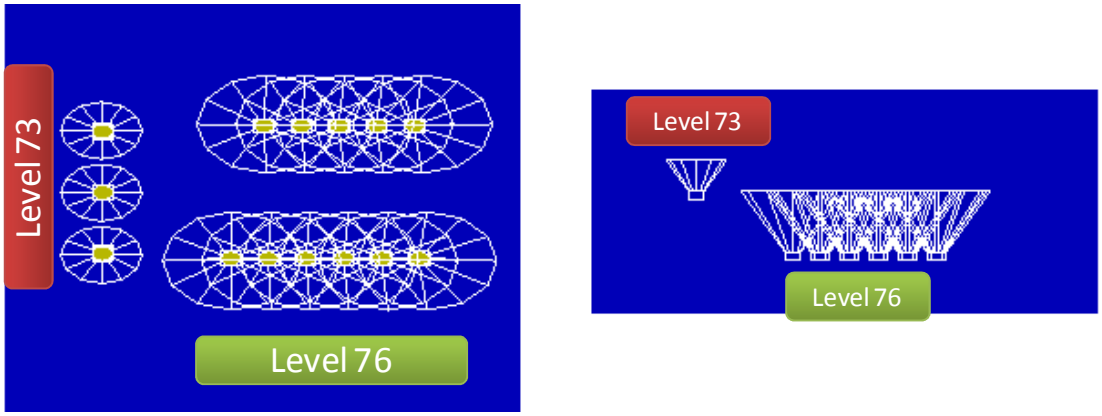

Figure 7.5.(Left). Plant view of the drawpoint location. (Right). Side view of the drawpoint location.

7.4.4. Trace markers

In order to improve the knowledge regarding to the ore flow, about 1200 markers were installed in the 609 GEZ section. The location of the markers seeks to answer whether the material would be extracted as in the physical model and if the numerical model is able to reproduce the gravity flow mechanism governing extraction. The markers initial position can be seen in Figure 7.6 and correspond to the same markers location as in the physical model. With the purpose to enhance the understanding regarding to the gravity flow mechanisms , colored layers are placed in the REBOP model (using grades), this layers will allow to plot the movement of the markers and compare them visually with the physical model results.

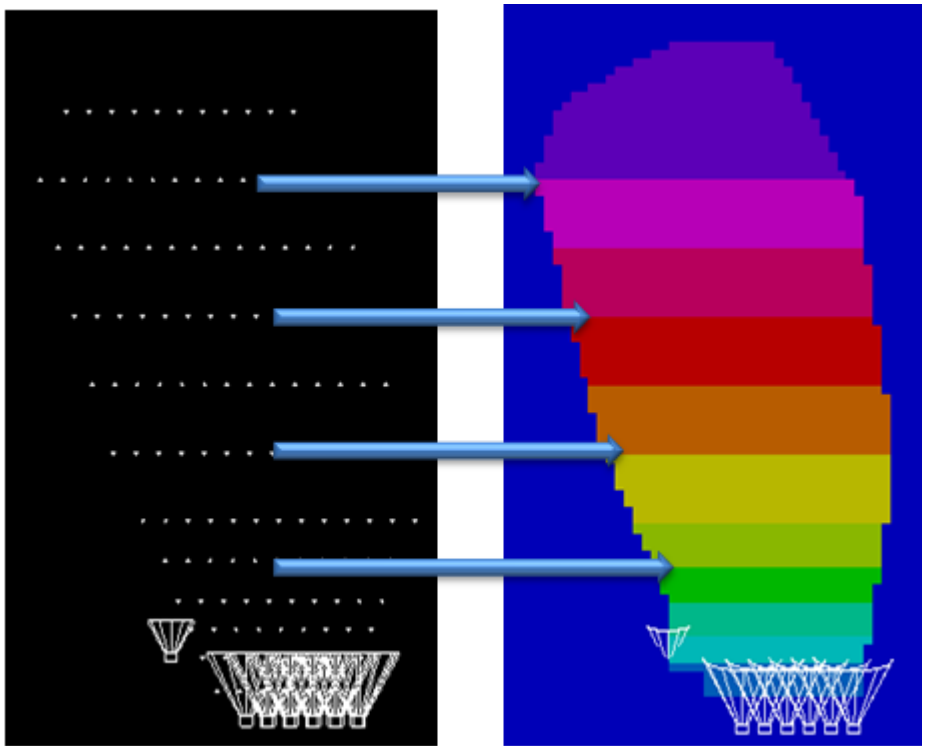

Figure 7.6 (Left) Markers location at the model. (Right) Coloured layers corresponding to the markers location at the model.

7.5. REBOP Simulation Results

The results from the REBOP simulations and comparisons with the physical model results are discussed in the following section. The analysis is separated in 4 main cases:

1- The base case, extracting from only one drawpoint (IMZ).
2- Extracting from the current production level (Level 76).
3- Extracting from the current production level (Level 73) and the proposed new level (Level 76).
4- Extracting from both levels including dilution from the top of the stope.

The results are analyzed in two stages, first a comparison between the extracted markers and in a second stage a visual inspection of the flow behavior mechanisms due to extraction for the stable and unstable case. For the simulations including dilution is conducted an analysis based on the dilution entry mechanism. If the flow simulator is able to represent the main mechanisms, it will be generated a predictive model of gravity flow properly calibrated, able to provide information about the dilution entry point for the case of study and also be useful as a tool for further investigation using different draw scenarios.

7.5.1. Case 0 (Stable case; Isolated Movement Zone)

Case 0 consist in the extraction from only one drawpoint, in order to estimate the IMZ diameter by extracting under conditions of isolated flow. In this condition an ellipsoidal

shaped volume of material above the drawpoint moves downward and dilates; the material surrounding the movement zone remains immobilized.

This simulation is performed with the purpose to calibrate the software, using the proper inputs estimating the mobilized zone in isolated draw. When performing this experiment at the physical model, the purpose was to establish a proper design, that in the case needing of the implementation a new extraction level, the movement zones wouldn't interact improving ore recovery from the footwall. The interaction would be accomplished by avoiding the overlap between flow zones from level 73 and level 76; this is achieved by locating the drawpoints at a distance at least equal to the IMZ diameter in plain view.

In the following the results between the measured IMZ radius at different heights for the physical model with the results obtained from the simulation are compared. This simulation is key in order to quantify how comparable are the movement zones.

The results shows evidence that REBOP presents a good match with the IMZ diameters measured at the physical model. The geometry of the IMZ characterized by its height and diameter is identical for the HIZ range from 0 [m] to 110 [m]. In addition, the maximum IMZ width obtained in the simulation is 30.4[m] versus the 30.8 [m] obtained from the physical model at prototype scale as presented in Figure 7.7.

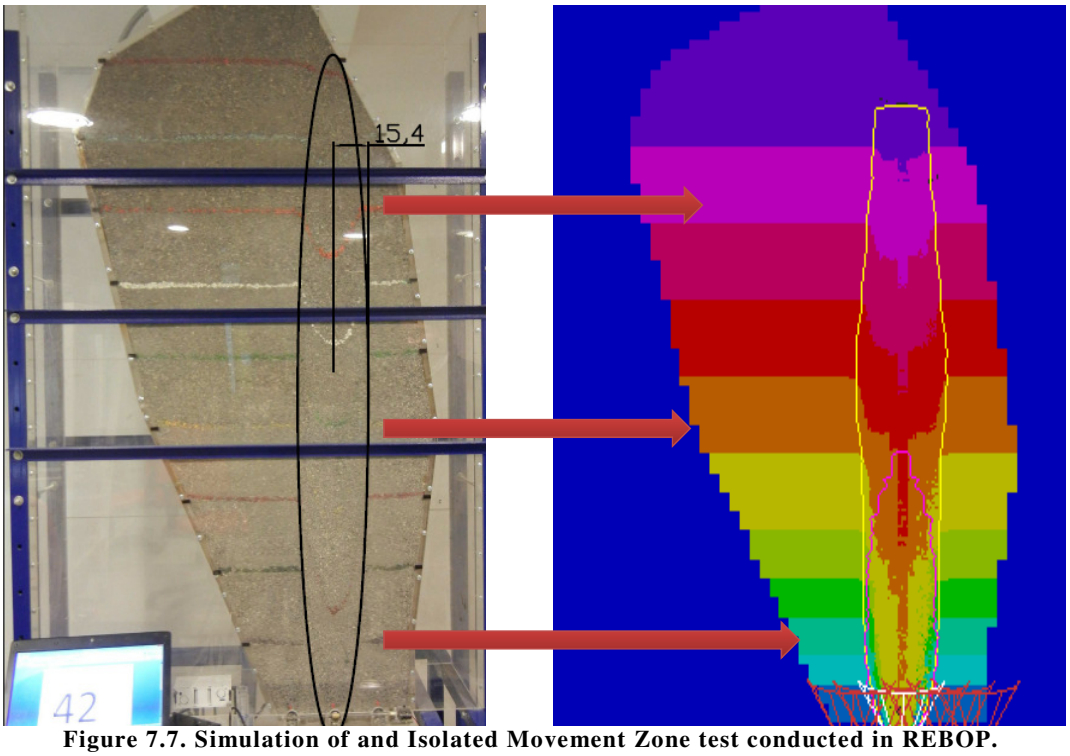

Figure 7.7. Simulation of and Isolated Movement Zone test conducted in REBOP.

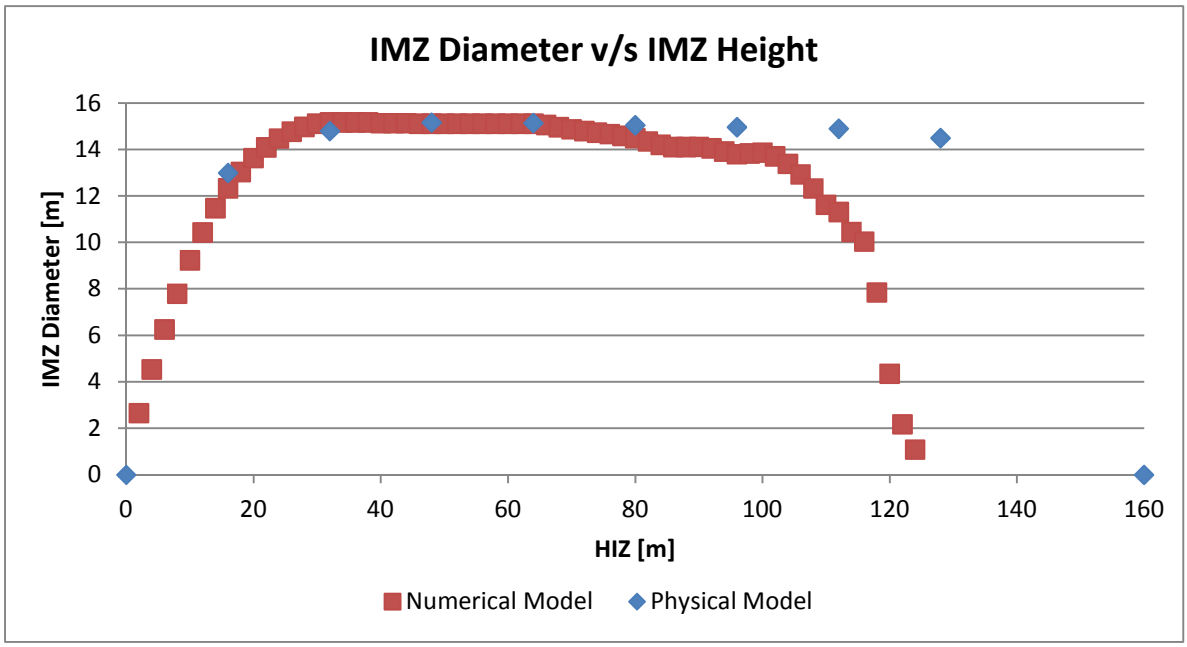

Figure 7.8.Comparison between the IMZ test and the IMZ REBOP simulation at model scale.

As commented previously, friction angle (ϕ) appears to have a direct impact on the shape of the IMZ at its base. Tuzun and Nedderman (1982) suggest that the limiting angle at the base of the IMZ (φ) - can be approximated by Equation 26 which corresponds to the angle of failure in a cohesionless Mohr-Coulomb material.

$$\varphi = 45° + \frac{\phi}{2} \qquad \textbf{Equation 26}$$

For both, numerical and physical modeling, the angle of repose can be calculated from the results shown in Figure 7.8 by manipulating Equation 27.

$$tan(\varphi) = \frac{IMZ\ D[m]/2}{IMZ\ H[m]}$$

$$\varphi[°] = arctan\left[\frac{IMZ\ D[m]/2}{IMZ\ H[m]}\right] \qquad \textbf{Equation 27}$$

Where:

$IMZ\ D[m]$: Isolated Movement Zone Diameter.

IMZ H[m]: Isolated Movement Zone Height.

Then, taking the values that define the tangent of the movement zone base; the angle of repose at the base is calculated as presented in Table 7.4.

Table 7.4. Estimation from the angle flow at the base for numerical and physical modeling

Model	IMZ H [m]	IMZ D [m]	φ [°]
Physical Model	32	14.80	61.94
Numerical Model	28	14.98	61.85

The angle of flow at the base obtained from the IMZ geometry for both – numerical and physical modeling – shows that the material is quite well characterized, validating the properties and the calibration of the software.

On the other hand, free surface rilling was pointed out as one of the main mechanisms governing flow. Once the IMZ reaches the top of stope, the initially horizontal surface becomes concave, ultimately reaching a constant slope at an angle equal to the material's angle of repose (see Figure 7.9); therefore following this logic the material movement at the surface will be highly dependent on the angle of repose and therefore it must be rigorously represented in the simulations.

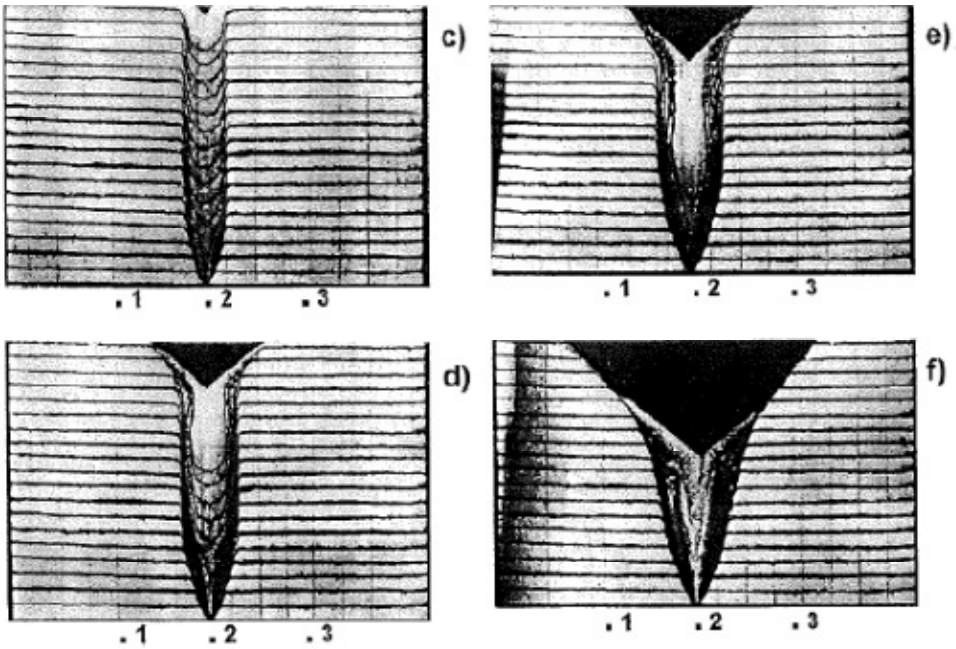

Figure 7.9.Development of a cone-shaped free surface above an isolated drawpoint (Kvapil 1965)

From the analysis conducted in the previous paragraphs, it can be established that IMZ maximum width and the main parameters (angle of repose and friction angle) affecting the movement zone shape are validated to be used in the next simulations to be conducted in REBOP for the other cases of study.

7.5.2. Case 1(Stable case; drawing from the main level)

In case 1, the extraction is performed by drawing only from the main extraction level (Level 76). This case doesn't include dilution. This simulation is equivalent to experiment 1 and the first part of experiment 3; the main results for case 1 are presented in Figure 7.10.

From the REBOP results, the recovered markers are very similar in both cases as presented in Figure 7.11. The results also show that on this condition the flow zone is not able to mobilize the footwall. From the analysis of the makers and through the REBOP results regarding to the particle movement, it is concluded that the flow velocity is higher in the axis of the moving body and decreases as we move vertically and as we move away from the center of flow mass generated due to extraction from the current level. Since the particle velocity is greater the closer to the vertical axis of the ellipsoid, and this movement zone does not cover the ore located outside the footprint of the current layout, the material located at the FW is not mobilized and the ore remain stagnant until is mobilized by the rilling mechanism. The displacements show the ability of the ore located at the limit between caved rock and the air gap, to move downwards by the rilling mechanism from the FW to the HW direction as observed in the physical model.

As can be seen from the comparison of the extracted markers (Figure 7.11), the main differences between the obtained results is the interaction of the extraction zones across the mayor apex. Through the inspection of the unrecovered markers, there is evidence that for the numerical modeling the extraction across the apex lower and the interaction height between extraction zones its located 120[m] above level 76, unlike the results from physical model, that locate the interaction height 60 [m] above level 76. A possible explanation of these phenomena is the fact that the physical model includes the presence of two smooth end walls- which mimic simultaneous draw along an infinitely long stope- encouraging interactive draw between the flow zones. This is related to the evidence that found Castro in his research, the author using gravel as a model media, found that when positioning the draw area in the center of the bin, far from the walls on two of the four sides, additional arching also can occur into the surrounding stagnant gravel during draw. This results in lower stagnant zone stresses than what has been measured in other models employing smooth walls. In addition, he also commented that in sands models stress arching does not occur , probably due to the use of a very low friction wall (plexiglass) where shear forces will be close to zero. This suggest that in sand models, the less arching and the use of a low shear strength material causes collapse of unmoved zones.

The reliability of the simulation is of a 68%, and it is presented in Table 7.5.

Table 7.5. Reliability of the simulation for Case 1

Recovered Markers Physical Model	#	470
Recovered Markers Numerical Model	#	282
Unrecovered Markers Physical Model	#	782
Unrecovered Markers Numerical Model	#	587
Reliability	%	68

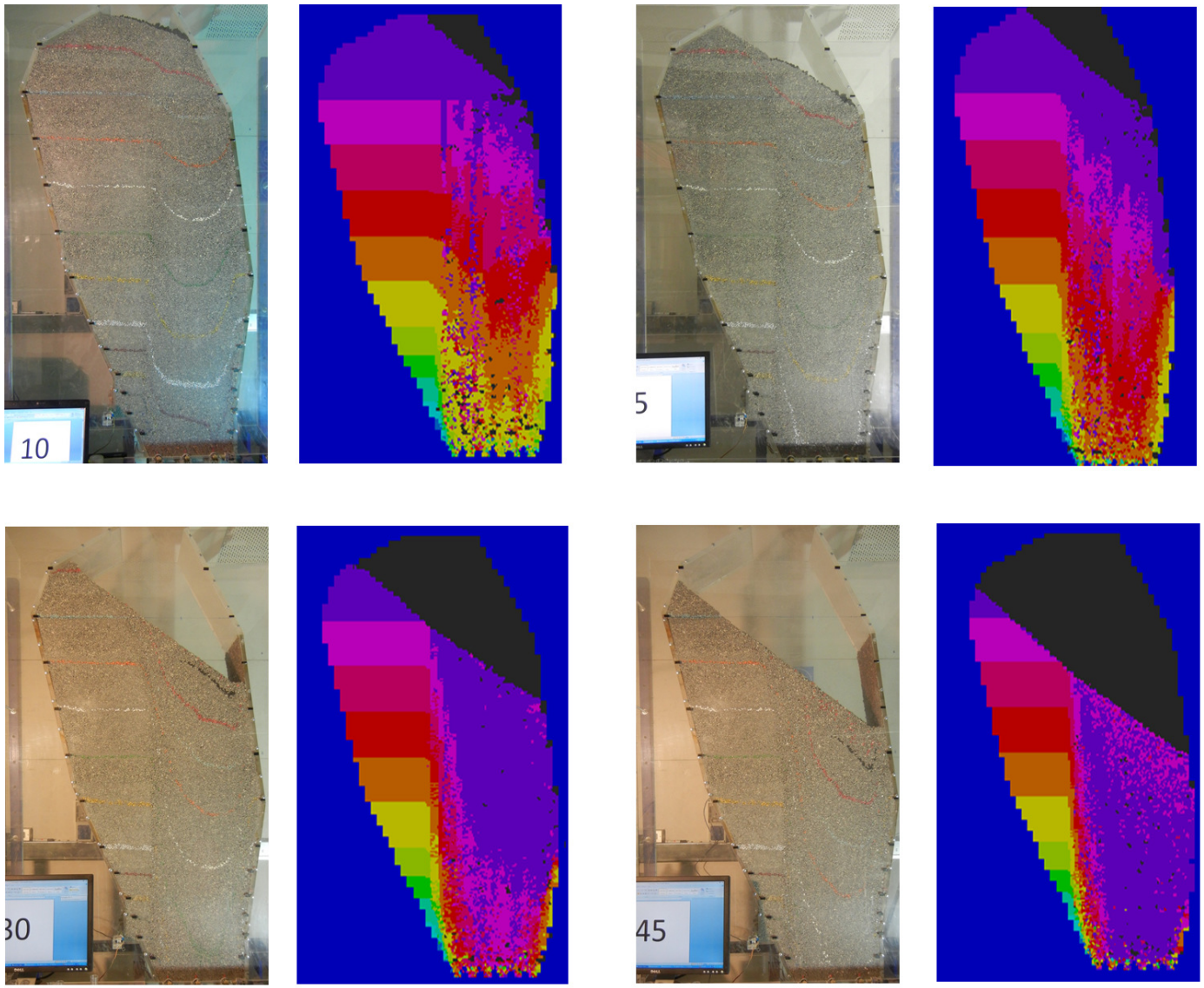

Figure 7.10. Visual comparison between numerical and physical modeling for Case 1.

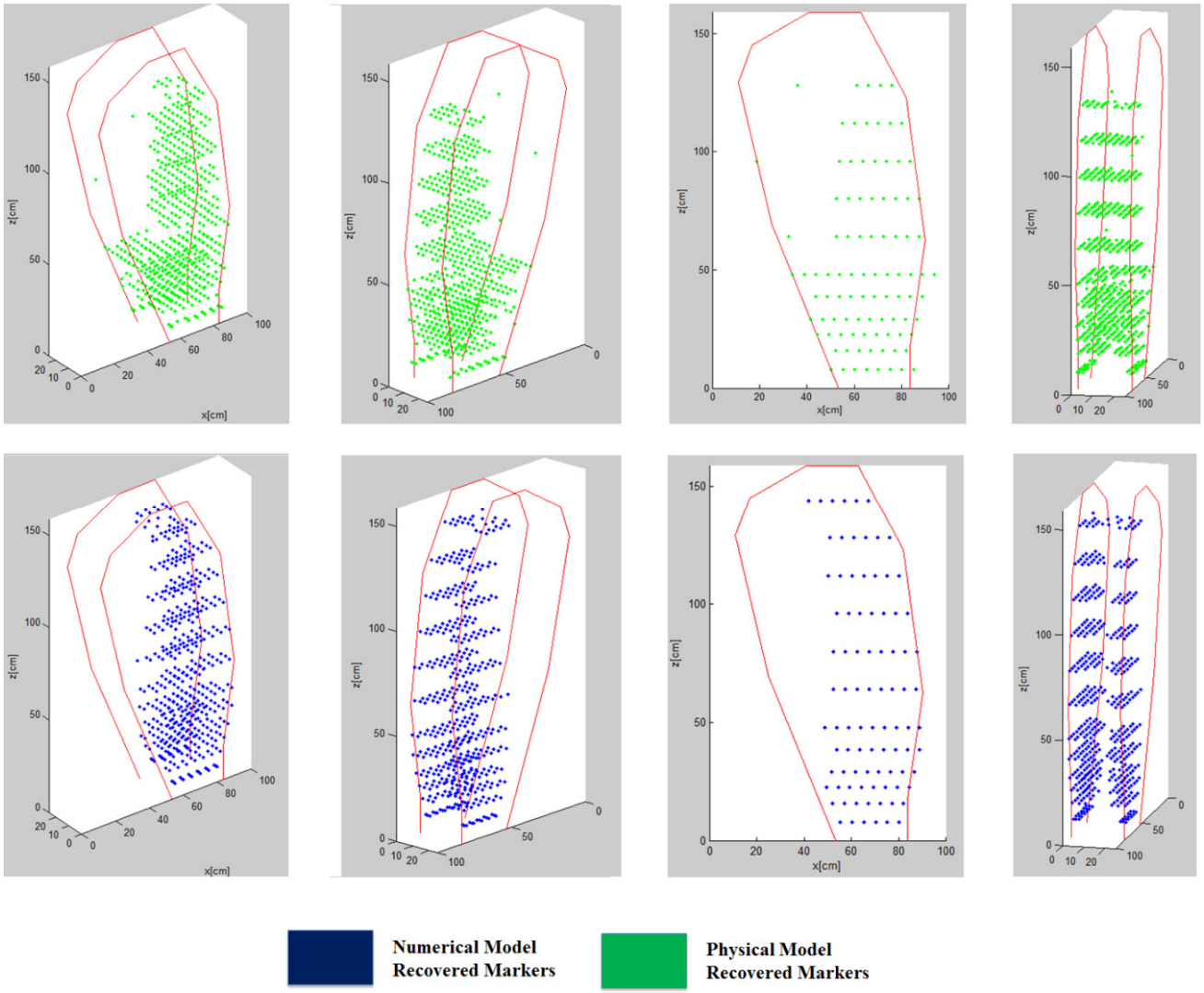

Figure 7.11. Comparison of the extracted markers of numerical and physical modeling for different views of the stope for Case 1 at same mass drawn.

7.5.3. Case 2 (Stable case; drawing from level 76 and 73)

Case 2 consist in the extraction drawing from the main extraction level (Level 76) until the programed extraction from this level is achieved; then the extraction is performed from level 76 and level 73 simultaneously. This case doesn't include dilution. The simulation is equivalent to experiment 3 and experiment 4.

From the comparison of the plotted extracted markers, the differences between the heights of interaction of the extracted zones are still significant, as commented previously for Case 1. The numerical model is not able to emulate the interaction zones, and therefore there are significant differences for the gravity flow mechanisms governing flow in this stagnant zone. The horizontal particle velocities at REBOP are insufficient to mobilize the zone across the apex as can be seen in Figure 7.12.

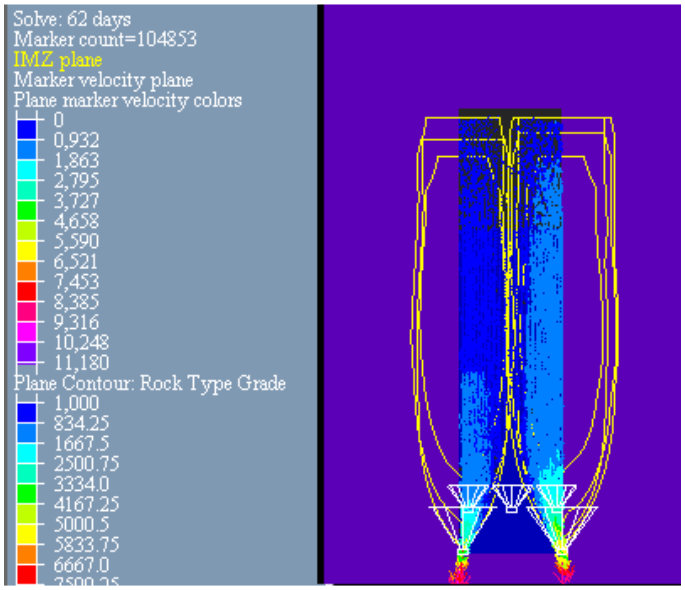

Figure 7.12.Velocity profile across the mayor apex

Figure 7.13 shows graphically the main results obtained from the simulation. From the REBOP results, the recovered markers are very similar in both cases. The recovered markers at the footwall wedge are mobilized due to the new mixing profile extraction generated by drawing from level 73. The generated mass flow mobilizes a fraction of the ore located at the footwall; this movement zone is determined by the IMZ geometry width as expected.

The displacements profiles evidence a vertical massive flow as wide as the footprint width of the extraction level due to extraction from level 76, and a ellipsoidal flow due to extraction from level 73. Still there is a passive zone located at the FW that is not mobilized by drawing from level 76. Yet, the displacements also show the ability of the ore located at the limit between caved rock and the air gap, to move downwards by the riling mechanism from the FW to the HW direction as observed in the physical model.

The reliability of the simulation is of a 69%.

Table 7.6. Reliability of the simulation for Case 2

Recovered Markers Physical Model	#	645
Recovered Markers Numerical Model	#	464
Unrecovered Markers Physical Model	#	583
Unrecovered Markers Numerical Model	#	388
Reliability	%	69

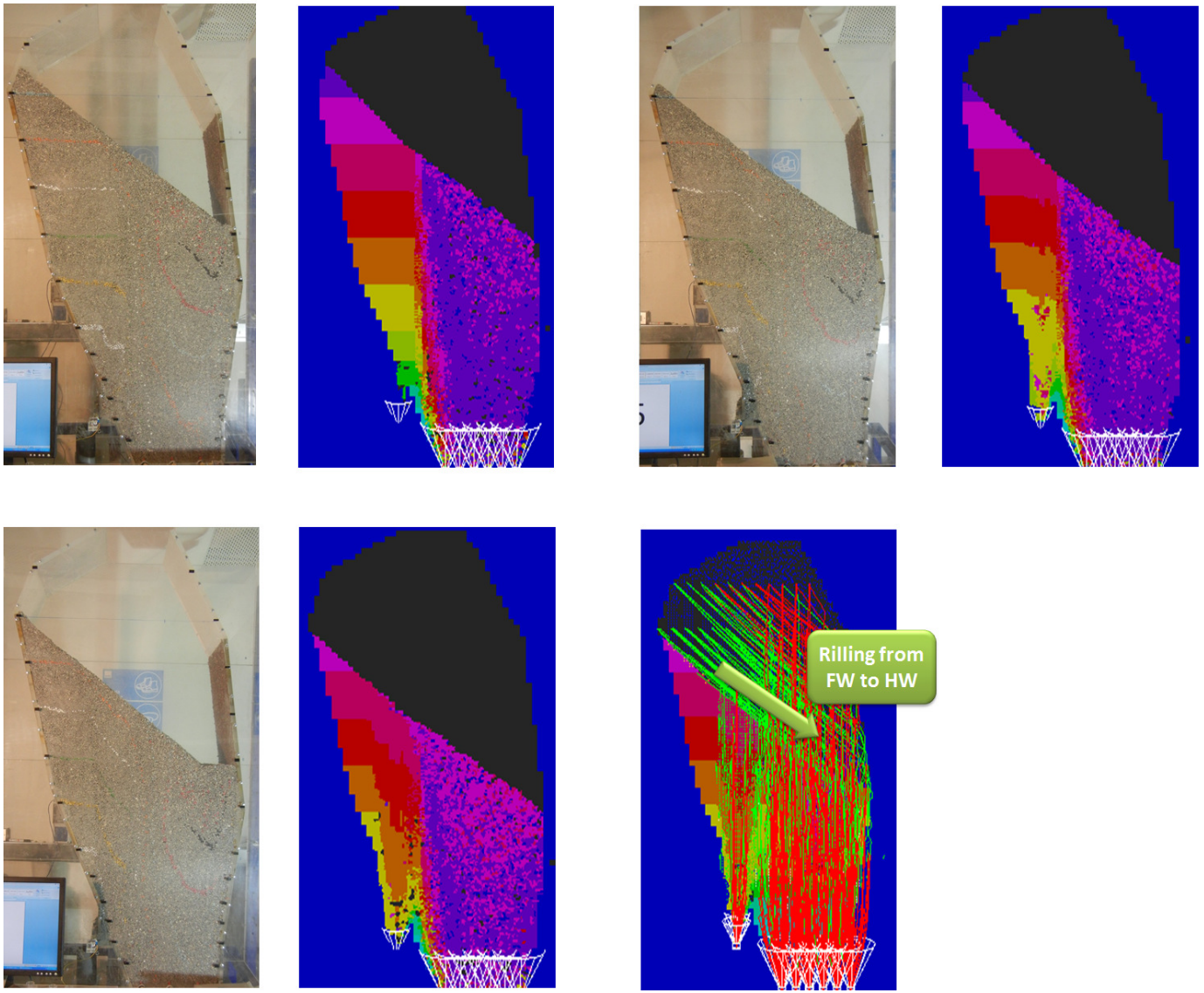

Figure 7.13. Visual comparison between numerical and physical modeling for Case 2.

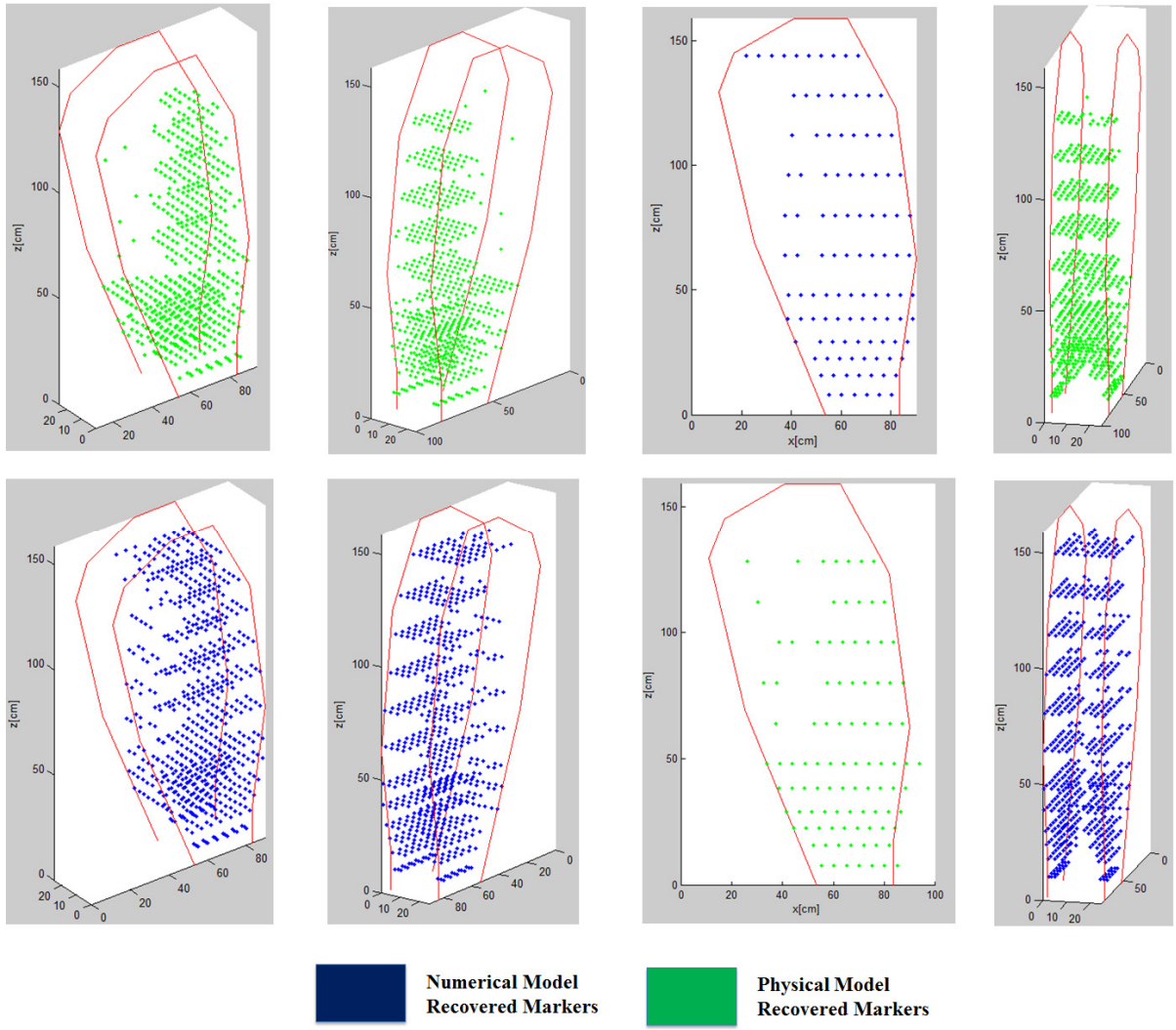

Figure 7.14. Comparison of the extracted markers of numerical and physical modeling for different views of the stope for Case 2

7.5.4. Case 4(Unstable case; drawing from level 76 and 73)

The main objective of this simulation is to replicate in the most accurate way the results from the physical model of the unstable case for the Eastern Stope, in order to evaluate the use of the flow simulator to predict dilution entry. For this purpose it will be determined the dilution entry at the drawpoints and then compared to the dilution entry tonnage obtained from the physical modeling in Experiment 5.

The analysis is carried out in accordance with the hypothesis detailed in Section 7.3. As described previously, the accuracy of the results will be quantified using the Root Mean Square Error RMSE (see Equation 28) and the Relative Error (see Equation 29).

$$Relative\ Error = \frac{V_{obs} - V_{sim}}{V_{obs}} \qquad \textbf{Equation 28}$$

$$RMSE = \sqrt[2]{\frac{\sum_{i=1}^{N}(V_{obs} - V_{sim})^2}{N}} \qquad \textbf{Equation 29}$$

Where:
V_{obs} : Value observed at the physical model.

V_{sim}: Value obtained from the REBOP simulation.

N: Number of values to be analyzed (drawpoints).

Based on the obtained results from the REBOP simulation, it can be calculated the RMSE for prediction of the dilution entry at the drawpoints.

Table 7.7.RMSE of the dilution entry at the drawpoints.

RMSE	[ton]	43,140
RMSE (Only drawpoints from level 76)	[ton]	22,840
RMSE 73 (Only drawpoints from level 73)	[ton]	97,410

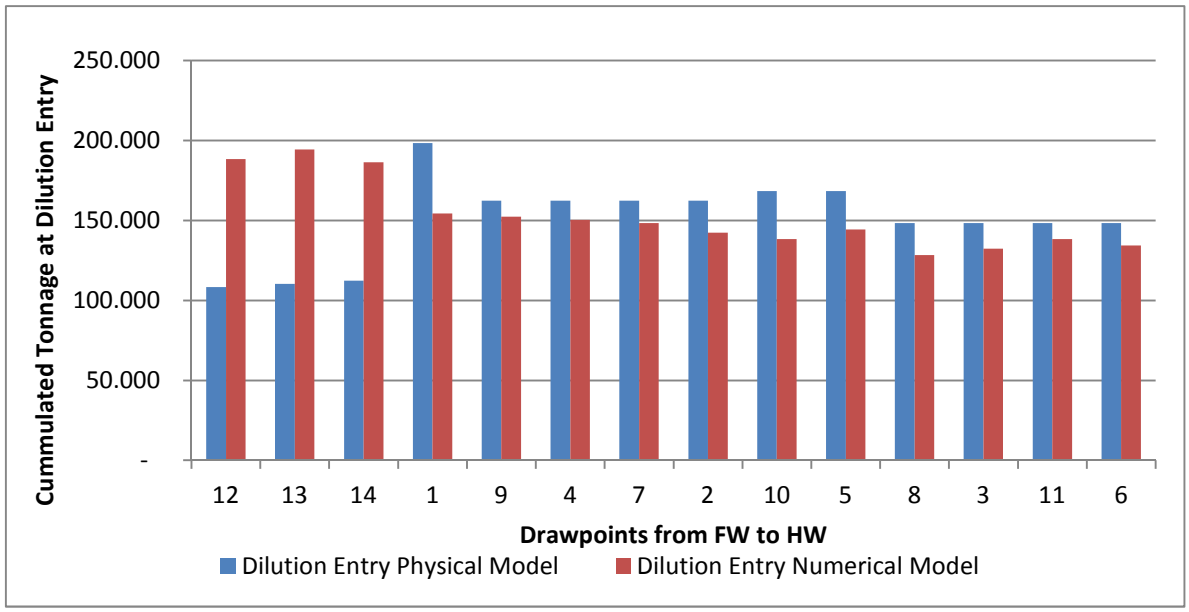

Figure 7.15. Dilution entry for the numerical and physical model

From the numerical simulation it can be concluded that the flow behavior emulated in REBOP for the drawpoints from level 76 (DP 1-11) follow the expected tendency obtained from the physical modeling, this is, the nearest the drawpoints are located to the HW, the earlier is the dilution entry, as presented in Figure 7.15.

On the other hand, for the drawpoints located at level 73 (12-13-14) dilution entry is reported later than at the physical model. As seen on Experiment 5, the flow mechanism due to extraction from level 73 generates lateral movement of the broken rock. The mobilized zone due to the extraction from level 73 generates an early connection with the low density zone due to extraction from level 76, resulting in a lateral dilution entry. There's evidence that the numerical model, REBOP, is not capable to represent this mechanism, and therefore dilution entry at the simulation occurs due to the waste lying above the drawpoints (horizontal dilution), as presented in Figure 7.16 and Figure 7.17.

The drawpoints located at level 76 show a RMSE of 22,840 [ton], and the drawpoints located at level 73 a RMSE of 97,410 [ton]. As summarized in Table 7.7, the overall RMSE is about 22,840 [ton] equivalents to a 9% of the total ore reserves per drawpoint. Another index of the accuracy of the simulation is the relative error of a -11.5 %, meaning that the REBOP simulation tends to underestimate the dilution entry at the drawpoints.

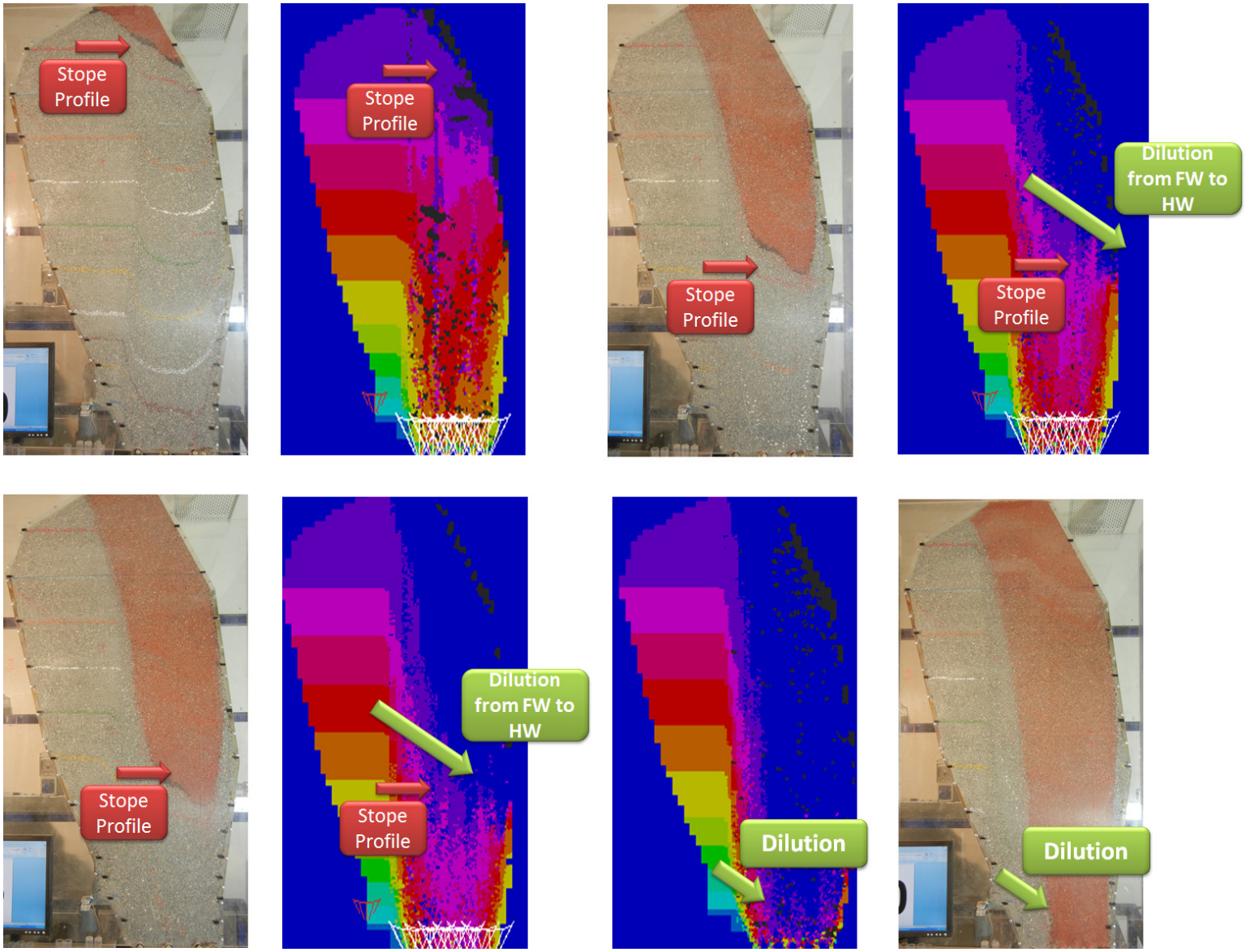

Figure 7.16. Visual comparison between numerical and physical modeling for Case 4 (with dilution) at same mass drawn.

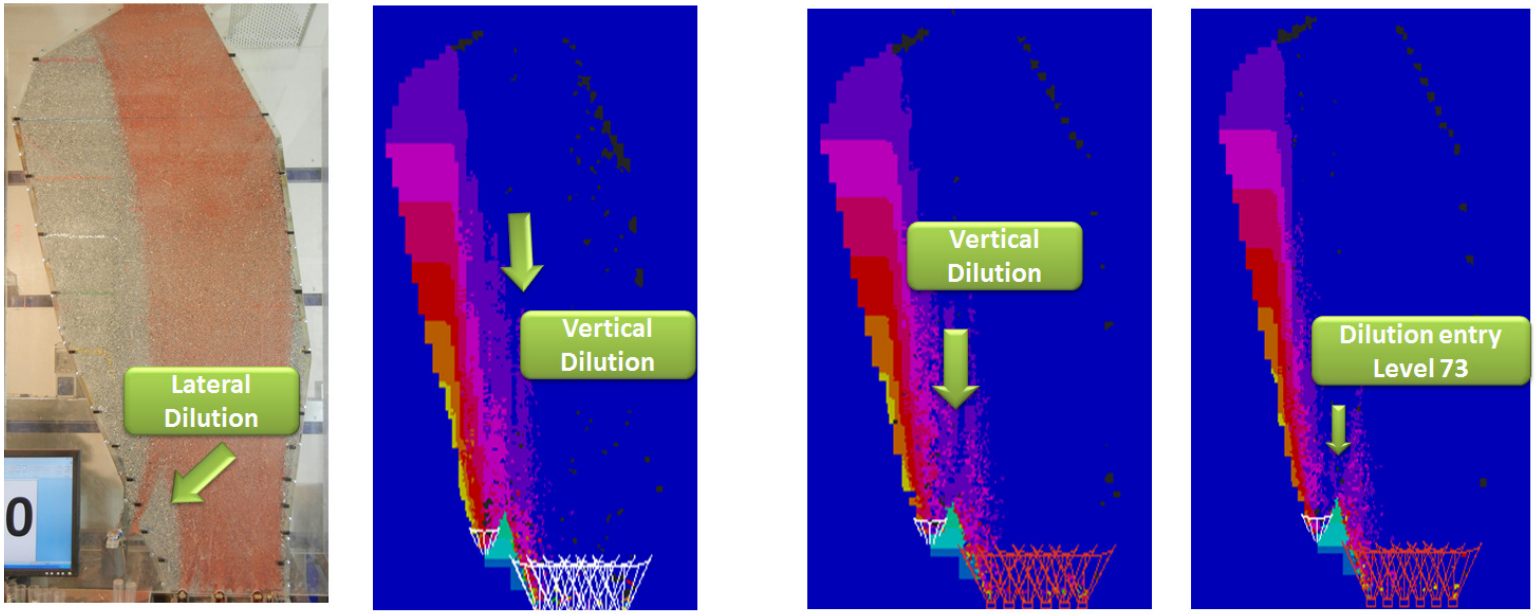

Figure 7.17.Visual comparison between numerical and physical modeling for Case 4 and dilution entry mechanisms.

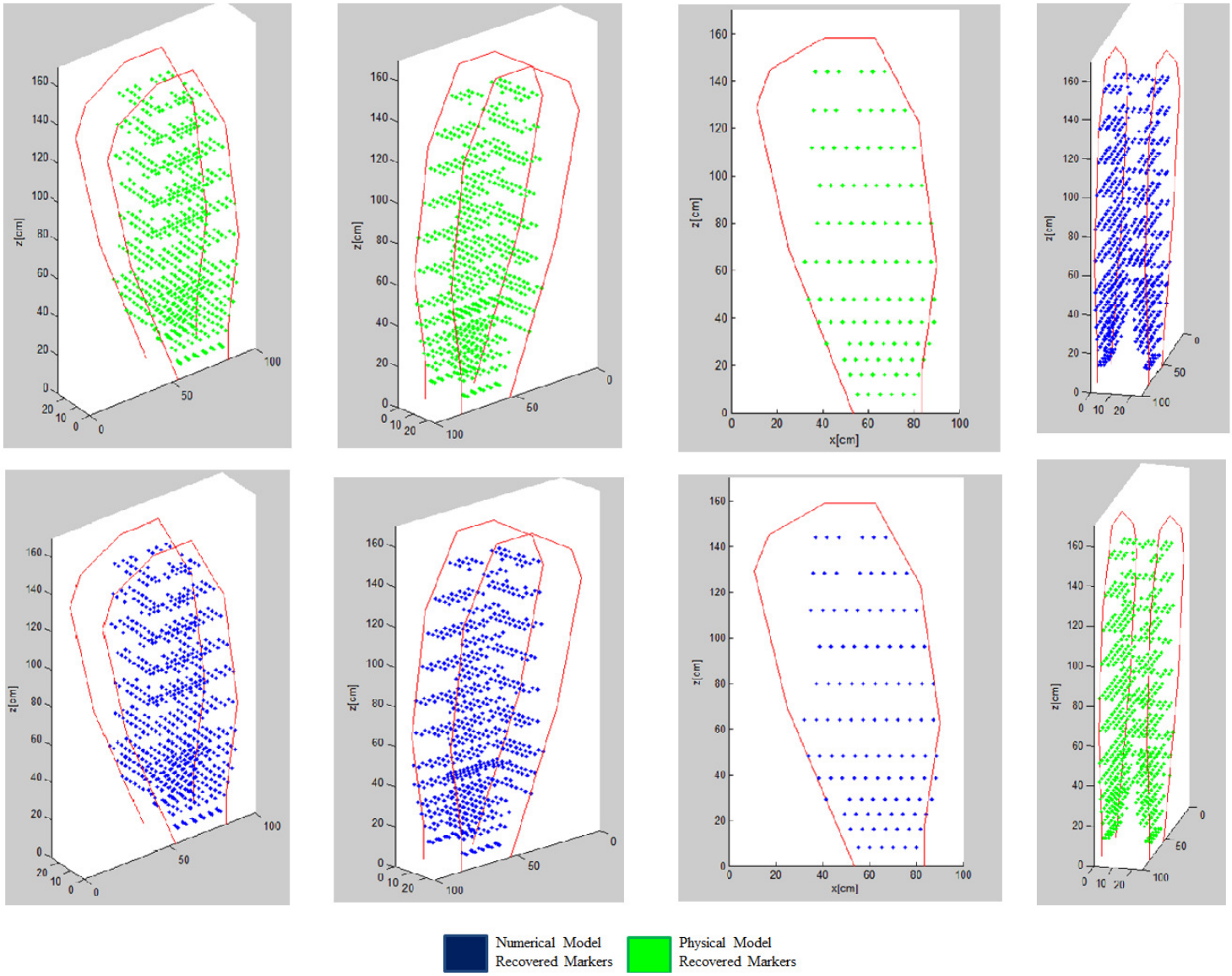
z[cm]
x[cm]
Numerical Model
Recovered Markers
Physical Model
Recovered Markers

The reliability of the simulation, in terms of ore recovery, is of a 64%.

Table 7.8. Reliability of the simulation for case 4.

Recovered Markers Physical Model	#	820
Recovered Markers Numerical Model	#	633
Unrecovered Markers Physical Model	#	408
Unrecovered Markers Numerical Model	#	227
Reliability	%	64

7.6. Main discussions and conclusions for the simulations

7.6.1. Case 0

i- The simulation is very accurate by estimating the maximum IMZ width, being obtained 30.4[m] versus the 30.8 [m] from the physical model.

7.6.2. Case 1

i- The draw mechanisms observed in the simulation respond to the ones observed at the physical model. The extraction from level 76 generates a vertical mass flow that develops preferentially towards de HW.

ii- The generated mass flow is not able to mobilize the material located outside the projection of the extraction level; however this material is capable to flow by the rilling mechanism.

iii- There is evidence that for the numerical modeling the extraction across the apex is lower than at the physical model. This can be explained by the fact that the physical model includes the presence of two smooth end walls- which mimic simultaneous draw along an infinitely long stope- encouraging interactive draw between the flow zones, since in sand models there's no stress arching.

7.6.3. Case 2

i- The extraction from level 73 generates a vertical massive flow that mobilizes a fraction of the ore located at the footwall based on the IMZ geometry width. Still remains a passive zone located at the FW that is not mobilized and that will be able to flow by rilling.

ii- From the simulations, displacements represent quite well the extraction, since they are more significant at the mobilized zone and show lower values outside the generated mass flow. The displacements also present the ability of the ore located at the limit between blasted rock and the stope walls (similar to the air gap in a caving method) to move downwards by the riling mechanism from the FW to the HW direction as observed in the physical model.

iii- As commented for Case 1, the numerical model shows lower interaction between flow zones across the mayor apex.

7.6.4. Case 4

i- For the drawpoints located at the current extraction level, REBOP replicates the tendency detected from the physical modeling governing dilution entry, this is, the nearest the drawpoints are located to the HW, the earlier is the dilution entry.

ii- For the drawpoints located at level 73 (12-13-14) dilution entry is reported later than at the physical model. There's evidence that the numerical model, is unable to represent lateral dilution, and therefore dilution entry at the simulation occurs due to the waste lying above the drawpoints (horizontal dilution).

iii- The overall RMSE is about 43,140 [ton] for the dilution entry point, this is equivalent to a 18% of the total ore reserves per drawpoint.

Table 7.9. Summary of results from the numerical simulation.

Case	Extraction	Dilution	Rilling	Mobility of the FW	Observations	Reliability
0	Level 76 (one drawpoint)	NO	√	-	IMZ Physical Model = 30.8 [m] IMZ Numerical Model = 30.4 [m]	Not Measured
1	Level 76	NO	√	Similar to the Physical Model Results Remains a passive zone at the FW	Lower interaction across the mayor apex at the Numerical Model. Displacements display the abe ability of the ore to move downwards by rilling	68%
2	Level 76 and Level 73	NO	√	Recovered markers at the FW due to the new mixing profile of level 73. Remains a passive zone at the FW	Lower interaction across the mayor apex at the Numerical Model. Displacements display the abe ability of the ore to move downwards by rilling	69%
4	Level 76 and Level 73	YES	x	Remains a passive zone at the FW	For drawpoints from level 73 the dilution entry is governed for the geometry of the stope (from HW to FW) For drawpoints from level 76 dilution entry is horizontal, unlike the physical model (lateral dilution)	64%

7.6.5. General Discussion

REBOP is a model for gravity flow of fragmented that relies on the properties of the fragmented rock to provide predictions of movement and extraction in block caving mines. The numerical model is used to test the results obtained from the experiments detailed in Chapter 6, in order to establish a match between numerical and physical gravity flow modeling.

During the analysis of results, it was tested that the numerical simulator is able to represent the flow behavior observed at the experiments such as the overlap and interaction of movement zones, the direction of the cave during the extraction from HW towards the FW and the free surface rilling phenomena at the top of the stope. Nevertheless, the software is not able to simulate the mechanisms governed by the lateral movement of the broken rock. As seen on the experimental phase, lateral dilution is key in order to understand the early contamination of the drawpoints located at the new level; therefore the use of REBOP is unsuitable for the analysis of recovery and dilution in cases where the possibility of lateral dilution exist.

In addition, the comparison of the measured air gaps between REBOP's simulations and the experimental results accomplish a good match, permitting to have a better idea of the behavior of the muck during draw. This is used to improve the calibration and validity of the results obtained with the flow simulator, as well as estimating the remnant ore after conducted the extraction.

CHAPTER 8
CONCLUSIONS AND RECOMMENDATIONS FOR FURTHER WORK

This chapter summarizes the main conclusions and discussions related to the experimental study conducted in order to improve the knowledge of the gravity flow mechanisms governing the movement of broken rock for Goldex Mine. The results of the experiments lead to a proposed design to be implemented at the mine in order to improve ore recovery and to delay dilution entry.

The purpose is to establish and validate a methodology that includes physical and numerical modeling to be used as an engineering design tool for future resolutions

8.1. Conclusions and recommendations

8.1.1. Limiting equilibrium analysis

Based on the experimental results it can be concluded that the limiting equilibrium analysis is not a proper tool in order to determine the mobility of the ore located at the wedge, using the analogy with a retaining wall by using the basic friction angle. The limitations of this analysis are mainly because of the enormous simplification of the problem to be solved. These limitations can be summarized as it follows:

i- The analysis is two-dimensional and therefore, neglects the three-dimensional distribution of stresses affecting the flow behaviour.

ii- The limiting equilibrium method satisfies force equilibrium but does not satisfy moment equilibrium.

iii- The analysis assumes that the failure surface is a plane. This is a common assumption but it does not necessarily correspond to the best representation of the actual failure surface.

iv- It is assumed that the normal and shear stresses acting on the failure plane have a uniform distribution, and the factor of safety, is calculated using these values.

v- The model does not take into account the stress-strain behaviour of the broken rock mass.

vi- It also it is assumed that the broken rock mass is homogeneous and isotropic, not representing the overall rock mass behaviour.

If there was available any information regarding to the roughness of the wall and the dilation angle at the surface, the limiting equilibrium analysis can be calibrated and used as an approximation of the mobility of the wedge.

Nevertheless, the method gives a first approach of the acting forces and it can be used by taking into consideration the limitations inherent to the method itself.

8.1.2. Physical Modeling

From the conducted literature review it can be summarized that the use of physical modeling with a single or multiple drawpoints has been useful in understanding the behavior of gravity flow of particulate materials. The physical modeling using gravel as a model media has been considered by some authors as the most suitable way for studying gravity flow of coarse granular materials. However other authors have stated that sand models have been validated for gravity flow operations that present fine fragmentation, as the case of study. For this purpose and using a rigorous approach defined by the conducted similitude analysis, the model media was adjusted and modified (dried and sieved) in order to represent the predominant forces- friction and gravity- neglecting the effect of other forces interacting for smaller particles.

The physical model can only satisfy geometrical and kinematical similitude. Dynamic similitude it's impossible to accomplish, since properties as resistance of the sand cannot be scaled. This fact must be considered when the analysis the experimental results is conducted.

The successful applicability of physical modeling is determined by the consideration of the distortions generated when scaling to the prototype.

It can be stated that the study of the gravity flow mechanisms at Goldex Mine through physical modeling was successful, since the experimental results allow determining the mechanism governing flow and the dilution entry mechanism for a given scenario. This gained knowledge has a fundamental role in the maximization of profits, by improving the information regarding to the mixing profile and the ore/waste behavior.

From the experimental results and their analysis were obtained the following conclusions regarding to the governing mechanisms due to extraction and are summarized below:

i- Considering the stable case, by drawing from the current extraction level, the flow zone quickly propagates vertically up to the stope surface. Since the drawpoints are sufficiently close together, there is an evident interaction between them and it results on a vertical massive flow as wide as the footprint width of the extraction level. This vertical flow develops preferentially towards the HW, since this represents the lowest strength path to develop (smaller height of column). The vertical massive flow doesn't mobilize the footwall on these conditions.

ii- Considering the stable case, when drawing both from level 76 and level 73, a fraction of the material located at the FW is mobilized by a different velocity profile. Still there is a passive zone located at the FW that is not mobilized by drawing from level 73 and that is be able to flow by rilling.

iii- Considering the unstable case, it can be concluded that dilution entry for the drawpoints it is mainly influenced by the flow profile during the first part of the

extraction. Since this profile develops faster towards the HW, dilution entry for the drawpoints located near the HW is reported earlier

iv- For the unstable case, by drawing from level 76 and 73 at the same time, it is observed that the flow mechanism due to extraction from level 73 generates lateral movement of the broken rock. As observed in many Panel Caving Mines, lateral dilution the phenomenon that determines the closure of the extraction for the drawpoints located at level 73. The addition of the new level increases ore recovery in a 14 %.

The results of the scaled model are compared to mine data provided by Agnico-Eagle management, which allowed the role of physical modeling to be quantified and qualified. These comments indicate that for engineering purposes physical modeling is a tool that could be confidently used for decisions making purposes, validating the proposed methodology.

8.1.3. Numerical Modeling

The numerical model conducted in REBOP V3.1.3 is used to test the results obtained from the experiments results in order to establish a match between numerical and physical gravity flow modeling. The results show that the software is able to represent the flow behavior observed at the experiments such as the mechanisms governing the size, overlap and interaction of movement zones, the direction of the profile during the extraction from HW towards the FW and the free surface rilling phenomena at the top of the stope.

The numerical simulations without dilution have the same behavior as the physical results and therefore REBOP can be used as a flow simulator, however a process of validation and calibration must be conducted previously in order to enhance the precision of the results, and with the purpose to understand the limitations of the simulations based on a better comprehension of the gravity flow governing mechanism. These tools are complementary and not substitutes for each other.

Nevertheless, the software is not able to simulate the mechanisms governed by the lateral movement of the broken rock and therefore the use of REBOP is inappropriate for the analysis of recovery and dilution in cases where the possibility of lateral dilution exist.

8.2. Further Work

It is essential to investigate stresses during flow as well as caved rock shear strength characteristics if interaction is to be used as part of the design criteria in operations based on gravity flow. Within the scope of this research it was not included the quantification of stresses, however and since they are an important component of the flow behavior it will be interest to implement load cells in the model in order to quantify their relation regarding to the dominant forces emulated at the model.

Although a considerable amount of experimental work in this research has been conducted towards an understanding of gravity flow principles under concurrent draw for the case of

study, it will interesting to conduct experiments under non concurrent draw, in order to improve the knowledge of the gravity flow behavior when the material is over pulled.

In addition, further research should regarding to the limiting equilibrium analysis conducted should be carried out including the limitations commented above. This with the purpose to improve the predictive capability of the limit equilibrium method as a predictive tool of the mobility for granular material.

CHAPTER 9

BIBLIOGRAPHY

[1] Agnico-Eagle Mines Limited, "http://www.agnico-eagle.com,"

[2] Alvial, J., 1992. *Analysis of Extraction at El Teniente 4 Sur LHD*. Proceedings of MassMin 92, Johannesburg, (Ed(s): H.W. Glen), The South African Institute of Mining and Metallurgy, pp 233-244.

[3] ASTM. *International Standard test method for measuring the angle of repose of free-flowing mold powders*. ASTM C1444-00, 2000.

[4] Brady, B.G.H and Brown, E.T., 2004. *Rock Mechanics for Underground Mining*, Kluwer Academic Publishers: Dordrecht, Netherlands.

[5] Brown, E.T., 2007. *Block caving geomechanics*, 2nd edn.. Julius Kruttschnitt Minerals Research Centre, The University of Queensland. Brisbane.

[6] Brunton, I., Sharrock, G. and Lett, J., 2012. *Full scale near field flow behavior at the Ridgeway Deeps Block Cave Mine*, Proceedings of MassMin 2012*,* Sudbury, Canada.

[7] Castellanos A., 2005. *The relationship between attractive interparticle forces and bulk behaviour in dry uncharged fine powders*, Advances in Physics. 2005. Vol. 54, pp. 263-376. Seville, Spain.

[8] Castro, R. and Whitten, W., 2007. *A new cellular automaton to model gravity flow in block caving based on physical modelling observations,* Proceedings of the 33th APCOM Conference, Santiago, Chile.

[9] Castro, R. *et al*., 2009. *Modelamiento Físico de la Minería Continua*, Technical Report prepared for IM2- Codelco, Santiago, Chile.

[10] Castro, R., 2001. *Escalamiento para modelo físico de flujo gravitacional*, Memoria para optar al título de Ingeniero Civil de Minas, Universidad de Chile, Santiago, pp. 49-62.

[11] Castro, R., 2006. *Study of the mechanisms of gravity flow for block caving*. PhD Thesis. University of Queensland, Brisbane, Australia.

[12] Castro, R., Trueman, R. and Halim, A., 2007. *A study of isolated draw zones in block caving mines by means of a large 3D physical model,* International Journal of Rock Mechanics and Mining Sciences, pp 860-870.

[13] Craig, R. F., 2004. *Soil Mechanics*, 7th, Spon Press: New York.

[14] Duquette, D., *et al*., 2005. *Feasibility Study- Goldex Mine- Agnico Eagle Ltd.*, Technical Report prepared for Agnico Eagle.

[15] Engineering and Mining Journal, www.e-mj.com

[16] Flores, G., 2005 . *Rock Mass response to the transition from open pit to undergrpund cave mining. Ph.D Thesis.* Australia: Julius Kruttschnitt Mineral Research Centre, The University of Queensland.

[17] Ghazavi, M., Hosseini, M. and Mollanouri, M., 2008. *A comparison between angle of repose and friction angle of sand, Geomechanics* in the emerging social & technological age (CD Proceedings, 12th IACMAG Conference, Goa, India, October 2008), X-CD Technologies Inc., Toronto, Paper No. M33.

[18] Halim A., 2004. *3D Large scale physical modelling for studying interactive drawing and drawpoint spacing in Block Caving Mines*. International Journal of Rock Mechanics and Mining Science.

[19] Heslop, T.G. and Laubscher, D., 1981. *Draw control in caving operations on Southern African Crysotile Asbestos Mines,* In D.R. Stewart (Ed.), Design and operation of caving and sublevel stoping mines: Society of Mining Engineers-AIME, New York, pp.715-728.

[20] Heslop, T.G., 1983. *The application of the interactive draw theory to draw control practice in large chrysotile asbestos mines,* Mining and Metallurgical Operations in Zimbawe, pp 290-313.

[21] Heslop, T.G., 2000. *Block Caving-Controllable risks and fatal flaws*. Proceedings of Massmin 2000, pp. 437-450, Brisbane, Australia.

[22] Hoek, E. and Brown, E.T., 1980. *Underground excavations in rock,* Institution of Mining and Metallurgy, London.

[23] Hoz, K., 2007. *Estimación de los parámetros al corte en suelos granulares,* Tesis de Magister, Universidad de Chile, Chile.

[24] Hudyma M., *et al*., 2010. *Monitoring open stope caving at Goldex Mine*, Second International Symposium on Block and Sublevel Caving, Perth, Australia.

[25] Itasca. 2008, *REBOP User Guide ver. 3.1*. Itasca Consulting Group, Inc., Minneapolis, Minnesota, USA.

[26] Janelid, J. and Kvapil R., 1966. *Sublevel Caving,* International Journal of Rock Mechanics and Mining Science & Geomechanical Abstracts, vol. 3, pp. 129-153.

[27] Kvapil R., 1965. *Gravity flow of granular Material on Hopper and Bin,* International Journal of Rock Mechanics and Mining Sciences Vol. 2, pp. 25-41.

[28] Kvapil R., 2004. *Gravity flow in sublevel and panel caving a common sense approach*, Proceedings of Massmin 2008, Lulea, Suecia, pp 35-81.

[29] Kvapil, R., *et al*., 1989. *Block Caving at El Teniente Mine*, Transactions of the Institution of Mining and Metallurgy Section A, pp.43-56, Chile.

[30] Langhaar, H., 1951. *Dimensional Analysis and Theory of Models*. New York: Wiley.

[31] Laubscher, D. H., 1994. *Cave Mining – the state of the art*, pp. 279-293, Journal of the South African Institute of Mining and Metallurgy, South Africa.

[32] Laubscher, D. H., 2000. *Block Cave Manual, Design Topic: drawpoint spacing*. Julius Kruttschnitt Mineral Research Centre, The University of Queensland, Brisbane, Australia.

[33] Mandel J., 1963. *Test on reduced scale models in soil mechanics and rock mechanics, a study of the conditions of similitude,* International Journal of Rock Mechanics and Mining Science, pp. 21-42.

[34] Marano G., 1980. *The interaction between adjoining drawpoints in free flowing materials and its application to mining*, pp. 25-32, Chamber of Mines Journal, Zimbawe.

[35] McCormick R., 1968. *How wide does a drawpoint draw?*. Engineering and Mining Journal, pp. 106-116.

[36] McNearney, R.L. and Abel, J.F., 1993. *Large Scale Two-Dimensional Block Caving Model Tests*. Int. J. Rock Mech. Min. Sci & Geomechan, 30:90-109.

[37] Nedderman, R.M. and Tüzün, U., 1979. *A kinematic model for the flow of granular materials*, Powder Technology, vol. 22, pp. 243-253.

[38] Nedderman, R.M., 1992. *Statics and Kinematics of Granular Materials*, 1,351 pp. Cambridge University Press: Cambridge.

[39] Orellana, M., 2011. *Modelación numérica de la minería continua*. Tesis de Magister. Universidad de Chile, Chile.

[40] Peters D., 1984. *Physical Modelling of the Draw Behaviour of Broken Rock in Caving*, Quaterly of the Colorado School of Mines, pp. 1-48, Colorado, USA.

[41] Peters D.C, 1984. *Physical Modeling of the draw behavior of broken rock in caving*, Colorado School of Mines, Colorado, USA.

[42] Pierce, M., 2009. *A model for gravity flow of fragmented rock in Block Caving Mines,* PhD Thesis, University of Queensland, Brisbane, Australia.

[43] Pöschel, T., Salueña, C., & Schwager, T., 2002. *Scaling properties of granular materials*, Physical Review E - Statistical, 64:011308, Nonlinear and Soft Matter Physics .

[44] Power, G.R., 2003. *Modelling granular flow in caving mines: Large scale physical modelling and full scale experiments*, PhD Thesis, University of Queensland, Brisbane, Australia.

[45] Raj, P., 2007. *Soil Mechanics & Foundation Engineering,* Pearson Education India.

[46] Richard G., *et al.,* 2011. *Technical Report on Restatement of the Mineral Resources at Goldex Mine*, Quebec, Canada.

[47] Rustan A., 2000. *Gravity flow of broken rock-What is known and unknown.* Proceedings of Massmin, Brisbane, Australia.

[48] Susaeta A., 2004. *Theory of gravity flow (Part I),* Proceedings of MassMin2004, pp. 167-172, Santiago, Chile.

[49] Susaeta A., 2004. *Theory of gravity flow (Part II),* Proceedings of MassMin2004, pp. 173-178, Santiago, Chile.

[50] Susaeta, A. and Diaz, H., 2000. *State of the art on the modelling of gravity flow in block caving mines (in Spanish)*, Minerales, vol. 55, pp. 17-26.

[51] Trueman, R., Castro, R. y Halim, A., 2007. *Study of multiple draw-zone interaction in block caving mines by means of a large 3D physical model*, International Journal of Rock Mechanics and Mining Science.

[52] Vargas, R., 2010. *Metodología de diseño de malla de extracción en block y panel caving incorporando back-analisis*, Tesis para optar al grado de Magister en Minería. Universidad de Chile, Chile.

[53] Visser, J., 1981. *An invited review Van der Waals and other cohesive forces affecting powder fluidization*, Powder Technology, Vol. 58, pp. 1-10.

[54] Whiteman, D.S., 2010. *Smart Marker system — A new tool for measuring underground ore body flow in block and sub-level mines*. Proceedings of the Second International Symposium on Block Caving and Sublevel Caving, Y.Potvin (Ed), 20-22 Abril 2010, Perth, Australia.

[55] Yenge L., 1980. *Analysis of Bulk Flow of Material Under Gravity Caving Process Part 1*, Colorado School of Mines, Colorado, USA.

[56] Yenge L., 1980. *Analysis of Bulk Flow of Material Under Gravity Caving Process Part 2*, Colorado School of Mines, Colorado, USA.

APPENDIX A

FORCES AFFECTING GRAVITY FLOW

A.1. Introduction

As stated in Chapter 3, besides gravity and friction other kinds of forces may develop, affecting granular flow. In order to comprehend the phenomena at a reduced scale, they will be studied to evaluate how these interparticle forces could affect gravity flow and the experimental results.

The scope of this review is related to attractive forces that may generate among particles and their quantification.

A.1.1.Van der Waals forces

Van der Waals forces between particles have their origin in the forces between their constituent molecules, and it is well known that molecules attract each other even if they are totally neutral.

Their origin can be understood as follows: in any molecule, the instantaneous positions of the electrons around the nuclear protons give rise to a finite electric dipole, which in turn originates an electric field that polarizes a nearby molecule inducing a dipole on it. (Castellanos, 2005).The Van der Waals forces (or Van der Waals interaction) are the sum of the attractive or repulsive forces between molecules. It is also a sometimes used loosely as a synonym for the totality of intermolecular forces.

Lifshitz (1956) developed the macroscopic theory of van der Waals forces between and within continuous materials. Based on the Lifshitz theory, it was developed a method to estimate Van der Waals forces for a specific material. Van der Waals forces can be calculated as it follows:

$$F_{VdW} = \frac{h_W R}{8\pi\delta_0^2}\left[1 + \frac{h_W}{8\pi\delta_0^3 D}\right] \qquad \textbf{Equation 30}$$

Where:

δ_0 : Distance between molecules[m]

h_W: Lifshitz- Van der Waals constant

D: Measure of the stiffness of the material [Pa]

R: Measure of the roughness of the material [m]

Using the values proposed below to quantify the effect of the Van der Waal Force, for silica:

δ_0 =4x10^{-10} [m]

h_W= 7 [eV]

D= 10^8 [Pa]

R: 10^{-7} [m]

It is obtained the estimated value for the Van der Walls force among particles for the model media.

$$F_{VdW} = 8{,}76 \times 10^{-10}[N] \qquad \textbf{Equation 31}$$

Therefore the Bond Number associated to the Van der Waals Forces will be defined as:

$$F_{B\_VdW} = \frac{F_{VdW}}{F_G} \qquad \textbf{Equation 32}$$

A.1.2.Capillary forces

Capillary forces are caused by condensed moisture on the surface of the particle. For dry granular materials these forces may be negligible compared to the other gravity and Van der Waals forces, though in some circumstances special precautions need to be taken to avoid ambient humidity if the purpose is to minimize the action of capillary forces.

When moisture is beyond 65%, capillary condensation of the fluids between particles generates a contact that develops an extra attraction between them, resulting in a component additional to the Van der Waals attraction. For two smooth, spherical particles of radius R and a fluid of surface tension γ, this contribution is:

$$F_H = 2\pi\gamma R \qquad \textbf{Equation 33}$$

Where:

γ: Surface tension [N/m]

R: Particle radius [m]

Therefore the Bond Number associated to the Capillary Forces will be defined as:

$$F_{B\_H} = \frac{F_H}{F_G} \qquad \textbf{Equation 34}$$

A.1.3.Electrostatic forces

Electromagnetism is the interaction of particles with an electrical charge; when charged particles at rest interact they interrelate through electrostatic force. The interaction force between a spherical particle of radius R, having a particle charge of W, interacting with an uncharged particle at a separation distance H due to its own charge, is given by the classical Coulomb equation:

$$F_c = \frac{Q^2\left[1 - \frac{H}{(R^2 + H^2)^{1/2}}\right]}{16\pi\varepsilon_0 H^2} \qquad \textbf{Equation 35}$$

Where:

ε_0: Permittivity of vacuum [F/m]

It's been found that for fine particles, electrostatic charging invariably arises due to the tribo-electric charging phenomena. Nevertheless Van der Waals forces are still dominant, and therefore the effect of electrostatic forces can be neglected

Therefore the Bond Number associated to the Electrostatic Forces will be defined as:

$$F_{B\_C} = \frac{F_C}{F_G} \qquad \textbf{Equation 36}$$

A.1.4.Magnetic Forces:

The magnetic force is the total electromagnetic force or Lorentz force measured by an observer on a moving charge distribution. Magnetic forces are produced by the motion of charged particles such as electrons, indicating the close relationship between electricity and magnetism. A rather specific additional attraction may arise when the particles can be magnetized. Depending on the degree of magnetization, very high attraction forces can be achieved.

This magnetic force is given by:

$$F_M = \frac{p^2}{6\pi\mu H^2} \qquad \textbf{Equation 37}$$

Where:

p: Degree of magnetization

μ : Conductivity of the medium

H : Separation distance between particles

Therefore the Bond Number associated to the Electrostatic Forces will be defined as:

$$F_{B\_M} = \frac{F_M}{F_G}$$ **Equation 38**

APPENDIX B

NUMERICAL MODELING REBOP FORMULATION

B.1.Introduction for predictive flow models.

Quite a few numerical, mathematical and empirical models have been developed for predicting flow behavior and stresses during the discharge of materials from silos and bins, while other models have been developed specifically for flow prediction in block/panel caving mines. In many cases, they have been validated with observations of flow in controlled laboratory-scaled physical experiments (Pierce, 2010). These models however present several issues due to the lack of understanding of the physical rules that govern the gravity flow phenomena.

Through several years experimentalists have noted that when granular material is drawn through an orifice, a roughly ellipsoidal-shaped volume of material above the orifice moves downward and dilates. This volume of moving material is named Isolated Movement Zone (IMZ); the stationary material surrounding the movement zone is referred as the stagnant zone (Pierce, 2010).While there is evidence to suggest that the mean particle size diameter exerts a significant influence on IMZ shape, the impacts of very wide, non-symmetric or bimodal distributions on far-field IMZ shape have not been investigated in most experiments.

In order to improve the conditions of simulations for gravity flow, it was developed REBOP, which is a relatively simple mathematical model for of the upward propagation and widening of IMZs, and the corresponding internal movements of material (Pierce, 2010). The gravity flow simulator REBOP was developed in the International Caving Study by Cundall *et al*. (2000) based on observations of flow in PFC3D. The model was similar to the kinematic models proposed by Nedderman (1995) and Ferjani (2004) -which consider only the IMZ limits and internal velocities-, but differs in several respects. The main difference lies in the fact than instead of relying on fitting functions of the observed IMZ shapes, the IMZs are comprised in a number of disk-shaped layers, and IMZ growth results from incremental laws enforced at the layer level. Growth of the IMZ occurs either through the expansion (i.e. increase in radius) of an existing layer or through the addition of new layers on top. The material movements associated with IMZ growth are tracked by trace markers that are established on a fixed lattice at the start of the simulation. When a marker becomes engulfed by an IMZ, its position is updated based on its location inside the IMZ (distance from the centreline and layer number) and an incremental law (derived from PFC3D) that controls how material moves downward from one layer to the next. Unlike stochastic simulations, markers are not forced to move to fixed lattice sites. They are considered drawn when they exit the lowermost layer, providing a way to trace the material drawn and outline the extraction zone (IEZ).

The incremental laws governing local IMZ expansion and material movement in REBOP were originally derived on the basis of flow patterns observed in PFC3D and FLAC

simulations of draw conducted by Lorig and Cundall (2000). Most of the simulations incorporated a single isolated drawpoint. Based on the observation of particle movements and displacement profiles within the resulting movement zone, three main mechanisms were postulated to govern upward and outward growth of an isolated movement zone: porosity jump (or dilation), collapse and erosion. Incremental rules were developed to describe how each of these mechanisms controls the growth of discrete layers within the movement zone. Draw was simulated by extracting a small mass from the lowermost layer and moving up through the overlying layers, growing each layer in sequence as necessary to conform to the incremental laws while ensuring continuity and mass balance.

Pierce's actualization of the code embraces a new understanding for the IMZ growth ; the new logic was tested through back-analysis of scaled physical experiments conducted by Castro (2006) and a comparison to the results of DEM -Discrete Element Methods- simulations conducted as part of his doctoral thesis (Pierce, 2010). REBOP's new formulation exhibits a sensitivity to fragment size, drawpoint width, friction angle and porosity jump that is consistent with the conclusions drawn from the range of physical and numerical models analyzed, and with the results of additional DEM and continuum simulations conducted as part of Pierce's research.

By basing the IMZ growth on mechanistically based laws at the layer scale, rather than empirically based shapes at the IMZ scale, REBOP offers an opportunity to be predictive in situations that have not been studied previously in physical or numerical experiments. In addition, it is possible for IMZ shapes to deviate from ideal when spatial variations in material properties (e.g. porosity, density, fragmentation) are expected. The REBOP approach is also appealing because it allows the fundamental behaviours examined in DEM simulations to be represented at mine scale. As suggested by Lorig and Cundall (2000), the lower-level approach employed in REBOP is potentially much closer to reality, and allows local mechanisms and interactions to be reproduced.

B.2. REBOP Model Formulation and theoretical basis of the flow simulator.

In order to achieve a better understanding of the rules governing flow prediction conducted by REBOP, the simulator will be characterized with the purpose to comprehend the main inputs influencing gravity flow. The gravity flow kinematics is based on the following main principles:

1. The medium is discretized and the corresponding mass of a determined layer will flow from one layer to the layer below. The movement of material is governed by mass balance equations between layers.
2. The material moves from a low porosity zone that remains stagnant, to a higher porosity zone due to extraction. The mechanisms of the growth of the IMZ are controlled mainly by differences in the near and far fields.

    - In the near field –IMZ heights below 100-200 mean particle diameters- the shape of the IMZ appears to be controlled more strongly by the drawpoint geometry. Above a wide drawpoint (i.e., > 10 mean particle diameters), the near-field shape of the IMZ is

generally ellipsoidal and is wider than predicted by kinematic theory, which assumes a point sink of zero width.

- In the far field- IMZ heights over 100-200 mean particle diameters -the IMZ assumes a cylindrical shape with a width that is a function of IMZ height and the mean particle size. The results of experiments on a range of materials (including rock) at several different scales suggest that the far-field width is predicted well by the kinematic theory developed by Nedderman (1995).

3. When the movement zone reaches surface, porosity will remain constant and the mass balance will satisfy a reduction and variation at the topography and a lateral expansion of the extraction zone.
4. The calculation mechanism is a discretization of the medium by markers; each marker has a determined volume and position. By tracing these markers the flow can be characterized.

In the following section the concepts submitted above are going to be reviewed in major detail for improving the understanding and the mechanism of the flow simulator.

B.2.1.REBOP Mathematical Formulation

As described by Pierce (2010) "*it is assumed that the IMZ can be represented by a series of horizontal disk-shaped layers. Material inside the disks has moved and is characterized by a dilated final porosity, n_1 , while the material outside the disk is stagnant and has a porosity, n_0, that is less than or equal to the porosity inside the disk*". Pierce added "*the goal is to establish the change in IMZ size and shape resulting from extracting a given mass, Δm, from the drawpoint*".

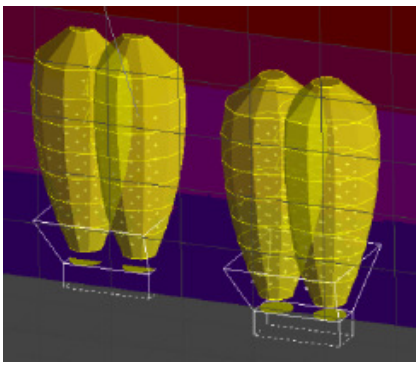

Figure B. 1. Discretization of the IMZ in layers by REBOP.

The algorithm can be explained considering a representative layer i (see Figure B.1). The layer i presents a void volume which moves upward the lower layer i-1. This void can be filled by two different mechanisms:

- Downward flow of material from the disk above, i +1 (In this case, no volume change accompanies flow, because the material moving downward from inside disk i +1 already has dilated to the maximum porosity); and
- Dilation and inward flow of stagnant material from the perimeter of disk i . (In this case, the stagnant material is assumed to dilate from its initial porosity to the maximum porosity, resulting in an increase in volume and an increase the radius of disk i . The void volume, controlling the IMZ growth mechanism, is calculated from the extracted mass, and the rock mass density and porosity.

In a first stage, REBOP calculates the volume used by dilation. To this end, its defined volume ratio between the stagnant material incorporated to the flowing zone from the perimeter of the layer v_i^d and the void volume coming from the lower layer v_i. The ratio is defined as:

$$r = \frac{v_i^d}{v_i} \qquad \textbf{Equation 39}$$

Stability considerations suggest that r is a function of the local slope at the limit of the IMZ β_i, given by Equation 40:

$$\beta_i = \frac{R_i - R_{i-1}}{h} \qquad \textbf{Equation 40}$$

Where:

R_i: Radius of layer i

R_{i-1}: Radiuous of layer i-1

h: layer height

In the upper part of the IMZ, β_i is negative, due to $R_i :< R_{i-1} :$, therefore the main mechanism for the growth of the IMZ is erosion, since the stagnant material around layer i is predisposed to move due to extraction of layer i-1, as can be seen in Figure B.2.

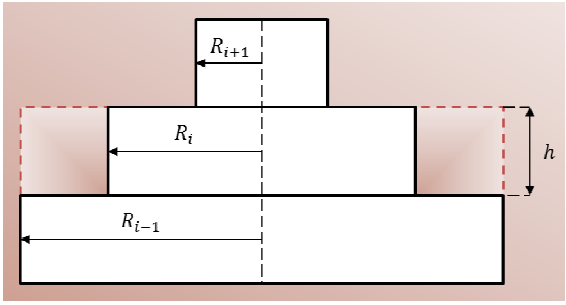

Figure B. 2. Representative layer of the case $R_i < R_{i-1}$

On the other hand, when, β_i becomes positive, the stagnant material rounding layer i is more stable, and therefore the erosion mechanism is less important. Experimental studies have indicated the existence of a minimal critical slope β_{min} for dilation to occur. This minimal slope is function of the friction angle of the stagnant material (ϕ), as specified in Equation 14.

$$\beta_{min} = \tan\left(45 + \frac{\phi}{2}\right) \qquad \textbf{Equation 41}$$

Therefore, if β_i is higher than or equal to β_{min}, there will be no erosion and r will be equal to cero, and all the void volume will be occupied by the upper layer.

Considering the two cases mentioned above, it can be determined r , as a function of the average diameter of the material (d), the friction angle (ϕ),the height of the layers (h) and a growth control parameter of lateral expansion (q). The radio is therefore expressed as shown in Equation 42.

$$r = \frac{10 \cdot \overline{d} \cdot h}{\pi \cdot R_i^2}\left(max\left(0{,}1 - \frac{(R_i - R_{i-1}) \cdot \tan\left(45 + \frac{\phi}{2}\right)}{h}\right)\right)^q \qquad \textbf{Equation 42}$$

Using the calculated value for r, it can be obtained the new radious R_i' of the layer i, since due to the dilation of the material increases its volume, filling completely the volume v_i^d (Equation 43).

$$R_i' = \sqrt{R_i^2 + \frac{r \cdot v_i}{\pi \cdot h \cdot (n_1 - n_0)}} \qquad \textbf{Equation 43}$$

Where:

n_1 : Porosity of the stagnant material within the IMZ

n_0: Porosity of the material within the IMZ:

At a final stage of the algorithm its calculated the remaining void volume occupied by material coming from the upper layer i+1 as shown in Equation 44.

$$v_{i+1} = (1 - r) \cdot v_i \qquad \textbf{Equation 44}$$

This calculation is conducted for the layer i+a and so on in ascending order until the void volume decreases to zero.

In the case that the IMZ reaches surface, the porosity will remain constant and the mass balance will be satisfied by diminishing the topography and by expanding laterally the geometry of the IMZ, resulting in an increasing of the initial porosity and its volume.

For the estimation of the IEZ limits, this are characterized drawing the contour of the original location of the extracted material at each drawpoint.

B.2.2.REBOP Inputs

The inputs of the flow simulator REBOP are the block model, the drawpoints, and a draw schedule. Calculation results provides the user a range of data that includes IMZ and IEZ limits, movement of caved material in the IMZ displayed as vectors, contours of grade and other caved rock properties from each drawpoint.

i- Block Model

The block model is a 3D representation in regular blocks of the information at a specific location. This representation corresponds to the ore deposit or the model to be characterized. The block model contains all of the grade and material properties required for flow calculations in REBOP. The inputs needed are listed below:

1. **Easting, Northing, Elevation:** Position of the block center in Cartesian coordinates.
2. **CavePeriod:** is the period number in the draw schedule at which the block is capable of flowing. The block is made available for flow at the start of the specified Period. The choice of whether to specify cave limits in a simulation through the CavePeriod property depends on two factors: (1) whether cave stalling and associated free-surface development and rilling is to be simulated; and (2) whether cave stresses are of interest to the user.
3. **BlockID :** A unique integer ID for the block. This is used for internal tracking and for reporting which blocks have material reporting to each drawpoint.
4. **Grade:** grade of the block.
5. **SolidsDen:** Specific gravity of the block material.

6. **InSituPor:** In-situ porosity of the block material. This is the porosity that the block material exhibits before it starts flowing. Porosity, n, is related to the void volume is related to the void volume, *Vv*, and the total volume, *Vt*, as follows: n= Vv /Vt.
7. **MaxPor:** Maximum porosity of the material. This is the porosity that the block material exhibits once it has dilated fully (bulked) during flow (i.e., it is the porosity inside the IMZs).
8. **FricAng:** Friction angle of the material, controls the minimum angle that the base of the IMZ makes with the horizontal, the angle of repose at the free surface, and the stresses inside the IMZ. Generally 35-50 degrees.
9. **MeanDia/SDDia**: Mean and standard deviation in diameter of the primary fragmented block (assuming Gaussian distribution).
10. **SDDia**: Laboratory intact UCS of the block material (for 5cm diameter core); units in [kPa] if SolidsDen in [t/m3].

Both InSituPor and MaxPor will control the bulking of the material, on the other hand FricAng and MeanDia will regulate the growth of the IMZ as the UCS and the SDDia will determine the secondary fragmentation in case is included in the analysis.

ii- Drawpoints

The drawpoints are characterized by the following properties:

1. **DPName**: A unique name for the drawpoint.
2. **Easting, Northing, Elevation**: Position of the drawpoint; this is defined as a point on the floor of the draw drift immediately below the brow (2-DP drawbell) or the center of the drawbell on the floor (1-DP drawbell).
3. **DBID**: The ID number of the drawbell to which the drawpoint belongs.
4. **DBType**: The type of drawbell associated with DBID; each drawbell can be of the same type or of a different type; the geometry of each drawbell type listed in this column must be defined in the next input file related to drawbell geometry

iii- Drawbell

There are two types of drawbells in block caving: conical, and rectangular.

1. **NumDP:** Number of drawpoints in the drawbell; if set to 1, a conical drawbell is assumed; if set to 2, a rectangular drawbell is assumed.
2. **BellName:** a unique identifier for the drawbell type.
3. **NumDP:** number of drawpoints: for a conical drawbell, this must be one; for a rectangular drawbell, this must be two.
4. **DDWidth**: the draw-drift width.
5. **DDHeight:** the draw-drift height.
6. **BellHeight**: is the drawbell height.
7. **SideAngl**e: is the wall angle (conical) or sidewall angle (rectangular).
8. **EndAngle :** the end wall angle (rectangular); it is not used for conical drawbells.

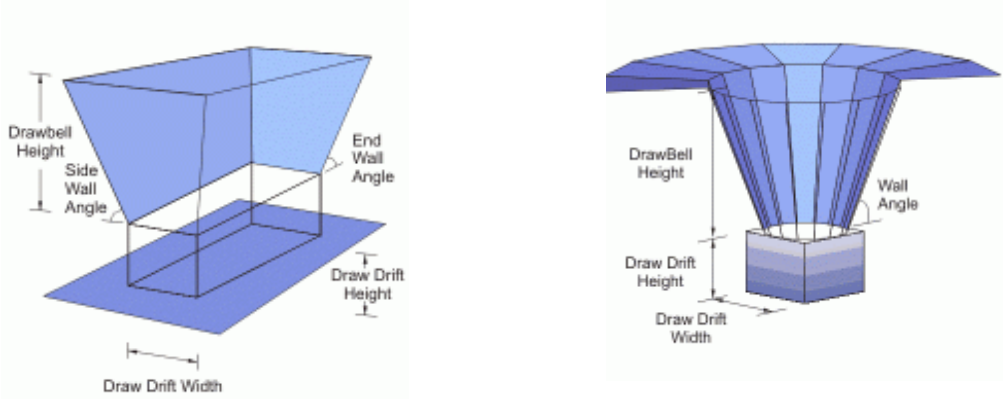

Figure B.3. (Left) Drawbell with two drawpoints.(Right) Drawbell with one drawpoint

The only quantities affecting the solution here are the draw drift width (controls width of IMZ base) and draw drift height (controls elevation of IMZ base) (Pierce, 2010).

iv- Draw Schedule

The draw schedule is referred to the amount of material to be extracted at a certain period of time.

v- Trace Markers

Tracer markers are optional and may be added to a block cave model in REBOP to represent markers that will be placed in situ or to track the movement of material from a specific location. Trace markers differ from the regular markers automatically generated within REBOP for tracking material movement. Tracer markers have zero mass and do not carry any information on grade or material properties.

B.2.3.REBOP Solution Properties

i- Resolution properties

The Resolution settings control how finely the IMZ surface is discretized into disk-shaped layers and the block material into markers. Experience suggests that the marker spacing should not exceed the draw width or block height (whichever is smaller), and the layer thickness should not exceed twice the draw width.

ii- Mechanisms

The software allows activating 3 functions that may influence the behavior of flow such as:

1. **Fines Migration**: This mechanism allows emulating different velocity rates for the markers within the IMZ, based in their diameter. A marker can flow preferentially to lower zones if the diameter of the marker is smaller than the mean diameter of the markers within its own layer and if its located in a shear zone within the IMZ:
2. **Stress calculation**: For calculation of stresses, REBOP uses analytical solutions and numerical modeling solutions that depend directly from the cave back, rock mass properties, the spacing between drawpoints and the draw strategy. This stress calculation is of great interest due to the influence of stresses in gravity flow and secondary fragmentation. In order to include this mechanism is needed the gravity acceleration ant the friction angle at the limits of the block model.
3. **Secondary Fragmentation:** Simulates the fragmentation and rounding of rock fragments within the IMZ due to extraction, and therefore emulates by decreasing the average diameter of the elements within the IMZ. The degree of fragmentation for the markers will depend on the stresses within the IMZ and the rock mass properties related to the UCS and the shear strength resistance.

It's important to remark that the flow mechanisms mentioned above are still in a test period and they must be validated with in situ tests. Accordingly, they will not be included in the simulations to be conducted in this research.

APPENDIX C

MODEL MEDIA CHARACTERIZATION

C.1. Particle Size Distribution

The particle size distribution to be used in the physical model was calculated by scaling (1:200) the particle size distribution at Goldex Mine. The data to be used was provided by a blasthole fragmentation analysis carried out using WipFrag.

Size	Size	Fu(x) 21-06-10	Fu(x) 15-09-10	Fu(x) 23-06-10	Fu(x) Avg
[']	[µm]	%	%	%	%
64	1625600	100	77.87	72.82	83.56
32	812800	83.96	70.12	66.43	73.50
16	406400	63.63	62.99	55.37	60.66
8	203200	36.01	47.81	35.74	39.85
4	101600	17.17	27.26	19.32	21.25
3	76200	12.97	19.41	14.98	15.78
2.5	63500	10.82	15.94	13.24	13.33
2	50800	8.9	12.61	11.47	10.99
1.5	38100	6.91	9.12	9.26	8.43
1	25400	4.3	5.8	7.1	5.73
3/4	19050	2.92	4.37	6.07	4.45
1/2	12700	1.64	3.19	4.69	3.17
3/8	9525	1.19	2.91	4.4	2.83
1/4	6350	0.88	2.66	4.21	2.58
#4	4750	0.78	2.58	4.15	2.50
#8	2360	0.38	2.49	4.09	2.32
#10	1180	0.37	2.47	4.09	2.31

Table C. 1. Particle size distribution at Goldex Mine

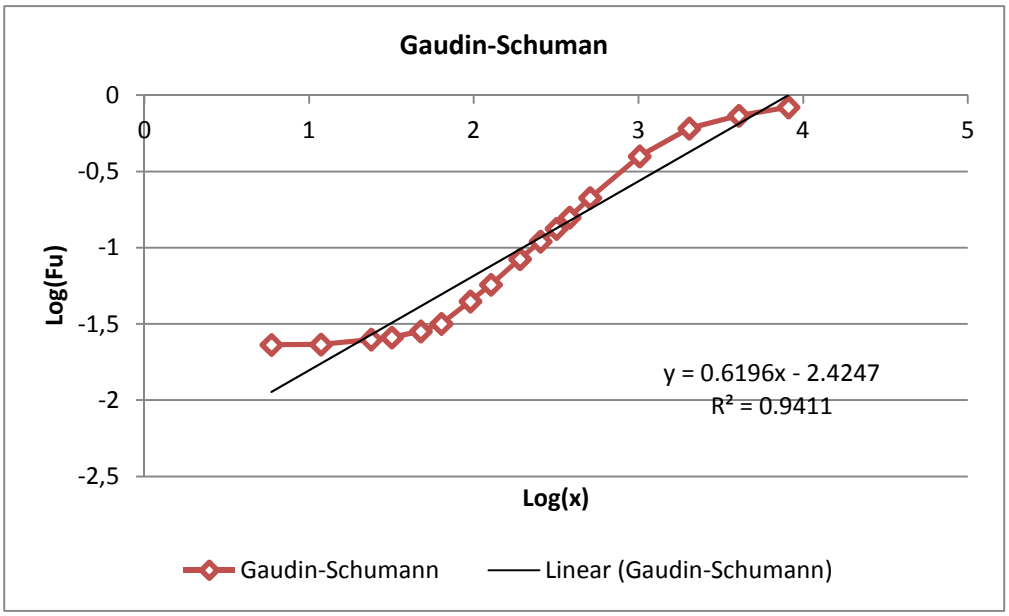

Figure C. 1. Gaudin Schuman equation for Goldex Mine particle size distribution

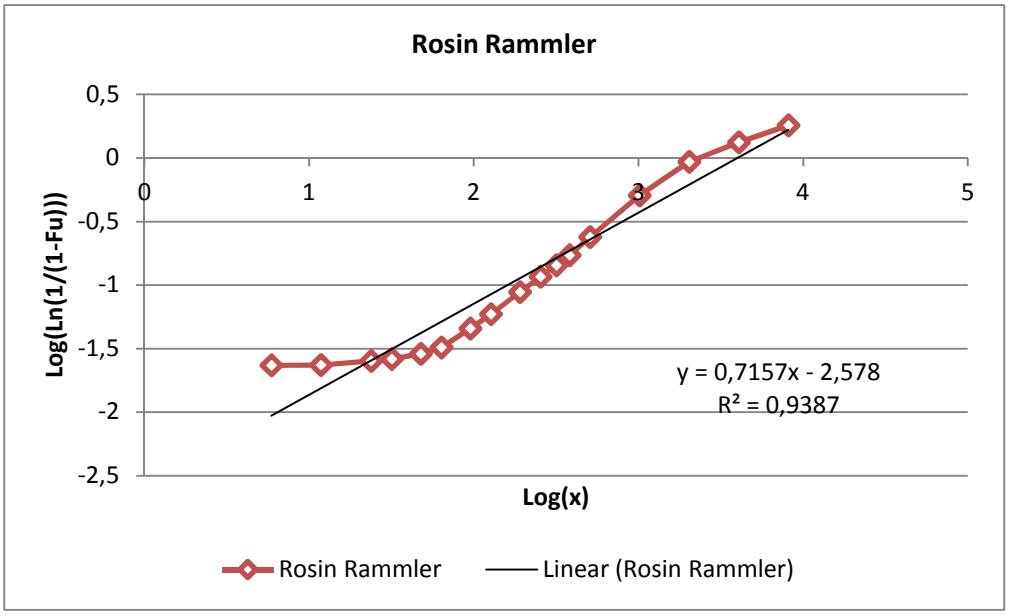

Figure C. 2. Rosin Rammler equation for Goldex Mine particle size distribution

C.2. Bulk Density

Bulk density is a property of granular material. It is defined as the mass of many particles of the material divided by the total volume they occupy. The total volume includes particle volume, inter-particle void volume and internal pore volume. Bulk density is not an intrinsic property of a material; it can change depending on how the material is handled.

The bulk density at Goldex Mine is 1.9[t/m3], as in the model media to be used in the physical model.

C.3. Shear Strength Characteristics

A granular material is an assembly of particles; its mechanical behavior depends on the size and shape of the particles, their arrangement, particle-to-particle friction, associated pore spaces, and the degree of saturation. When deformations occur in granular materials, the external forces may cause internal fabric changes, caused by particles sliding, rolling, and interlocking. Those changes will produce a different response of the material behavior.

Sand is a cohesionless media, that it is, a free-running type of soil, whose strength depends on friction between particles. Therefore, the characterization of the model media, will only considerate the friction angle, since cohesion is zero.

In the following sections, it will be calculated the angle of repose as the friction angle in order to characterize the model media shear strength behavior.

C.3.1. Determination of the angle of repose

The angel between the soil cone and the horizontal direction obviously depends on the soil parameters such as the internal friction angle, grain size distribution, grain shape, unit weight, moisture content, stratification, segregation.

The angle of repose is measured using the Standard Test Method for Measuring the Angle of Repose (ASTM C 1444 –00).

The angle of repose can be calculated using the following equation:

$$\varphi(Angle\ of\ repose) \quad = tan^{-1}\left(\frac{2H}{D_A}\right) \qquad \textbf{Equation 45}$$

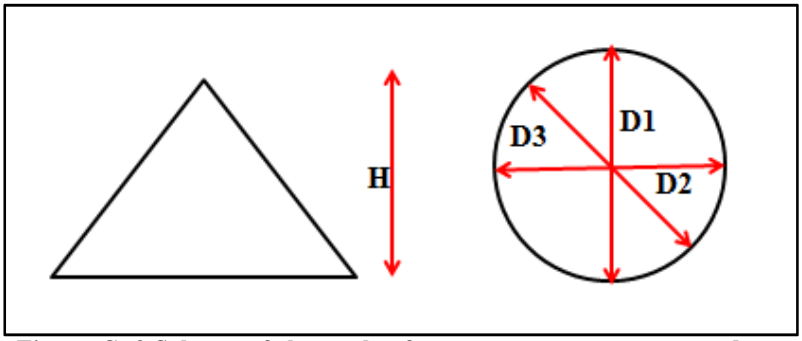

Figure C. 3.Scheme of the angle of repose measurement procedure

Where:

H = height of the cone

D_A = average of the three test determinations, D_1, D_2, and D_3 diameters measured

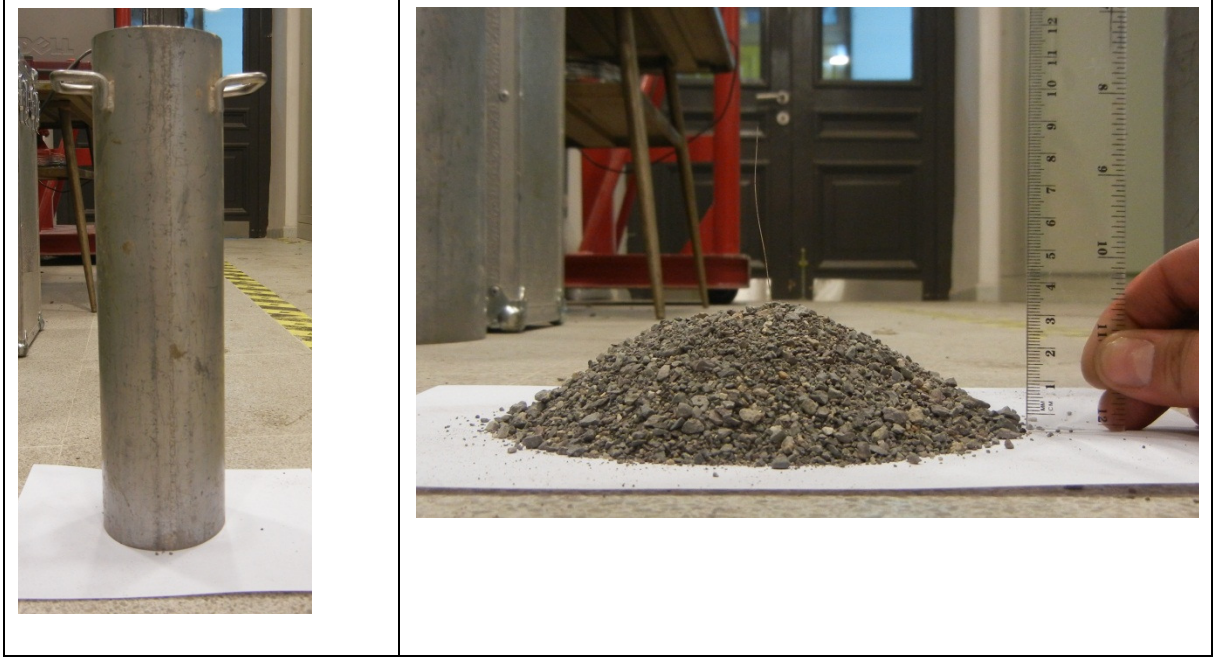

Figure C. 4. (Left) Apparatus for determining sand repose angle. (Right) Measurement of the cone height.

The results are shown in Table C.2.

Table C. 2. Angle of repose for the model media.

Test	H	D1	D2	D3	r	φ
[#]	[m]	[m]	[m]	[m]	[m]	[°]
1	4.3	16.2	16.3	16.5	8.17	28.1
2	4.2	16.3	16.1	16.5	8.15	27.6
3	4.5	16.1	16.6	16.6	8.22	29.1

C.3.2. Determination of friction angle

Friction angle can be correlated to the angle of repose (Ghazavi, y otros, 2008)

$$\phi = 0.36\ \varphi + 21.2 \qquad \textbf{Equation 46}$$

where :
ϕ: Friction angle
φ: Angle of repose

This expression shows that when the sand is deposited in a loose state, the friction angle is almost smaller that the repose angle. However, the compaction density of the deposited sand increases, the friction angle is greater than the repose angle.

Using Equation 46, the friction angle is calculated as it follows.

Table C. 3. Friction Angle for the model media.

Test	ϕ
[#]	[°]
1	31.4
2	32.2
3	31.5
Average	32

APPENDIX D

MATLAB CODES

D.1. Data analysis code for unrecovered markers

At the time of conducting the experiments and given the large amount of markers placed at the physical model, and with the purpose to optimize the accuracy of the calculation of ore recovery, it was we generated a code to determine the unrecovered markers from the experience. The algorithm is outlined below

```
%xls=Sheet.xls, Example xls='Markers.xlsx'
%sheet1=Excel Sheet


function binario=BuscarIndices(xls,sheet1,sheet2)
 [num,txt]=xlsread(xls,sheet1);
[num2,txt2]=xlsread(xls,sheet2);

for i=1:size(txt,1)
nombre=txt{i};
a=find(strcmp(txt2,nombre));
if(size(a,1)==0)
binario(i)=0;
else
binario(i)=1;
end
end
binario=binario';
```

D.2. Interpolation code for the calculation of ore recovery.

With the objective to calculate ore recovery for each experiment it was conducted a linear interpolation within the volume of the stope. The Interpolation Mode is set to Linear, i.e, the block interpolates data values by assuming that the data varies linearly between samples taken at adjacent sample times. The values to be used are 1 if the marker is recovered and 0 it the marker is not recovered. The algorithm result is a volume value that represents the recovered volume at the stope.

```
% Interpolates cumulated mass and if the volume is recovered or not
% Requires the markers extracted per drawpoint x_exp, markers initial position, drawpoint
location and drawbell geometry.
```

```
%x_exp=cell(1,11); % 11 puntos de extracción

%interpolation of raw_data
% scale 1 cm
x_step=1;
y_step=1;
z_step=1;

%Initializes cell for calculation

w=cell(1,14);
w_bin=cell(1,14);

%Discretization and interpolation of markers
[XI,YI,ZI]=meshgrid(min(x_tot_bin(:,1)):x_step:max(x_tot_bin(:,1)),min(x_tot_bin(:,2)):y
_step:max(x_tot_bin(:,2)),0:z_step:max(x_tot_bin(:,3)));

% Interpolates for each drawpoint, w is mass and w_bin is a binary term for each marker

for i=1:14
w{i}=griddata3(x_exp{i}(:,1),x_exp{i}(:,2),x_exp{i}(:,3),x_exp{i}(:,4),XI,YI,ZI,'linear');

w_bin{i}=griddata3(x_exp{i}(:,1),x_exp{i}(:,2),x_exp{i}(:,3),x_exp{i}(:,5),XI,YI,ZI,'line
ar');
   if i>1
      wt=min(wt,w{i});
      wt_bin=min(wt_bin,w_bin{i});
   end
   if i==1
      wt=w{1};
      wt_bin=w_bin{1};
   end
end

% graphics the results in 3D
slice(XI,YI,ZI,wt_bin,[70],[5 20],[50]); hold on;
hold on;

% graphics the results in 3D
plot3(dp(:,1),dp(:,2),dp(:,3),'.b');
axis equal;

%plots the stope
plot3(caseron(:,1),caseron(:,2),caseron(:,3),'-r');
```

```
plot3(caseron2(:,1),caseron2(:,2),caseron2(:,3),'-r');

%plots apex
plot3(drawbell(:,1),drawbell(:,2),drawbell(:,3),'-b');
plot3(drawbell2(:,1),drawbell2(:,2),drawbell2(:,3),'-b');

%Calculates ore recovery based on the interpolation
rec=sum(sum(sum(wt_bin(:,:,19:96)>=0)));
```